

# POLITECNICO DI TORINO

DIPARTIMENTO DI INGEGNERIA MECCANICA E AEROSPAZIALE



Master's Degree Thesis

## DEVELOPMENT AND VALIDATION OF PHYSICAL BASED MODEL OF HEAT EXCHANGERS FOR AN ORC POWER PLANT

SUPERVISORS

Prof.ssa Daniela Anna Misul

Prof. Mirko Baratta

Ing. Giovanni Giardiello

Ing. Alberto Bertone

Ing. Francesco de Nola

CANDIDATE

Alessandro Salvemini

Academic Year 2020/2021

# INDEX

INTRODUCTION-----	8
<b>1 ORGANIC RANKINE CYCLE (ORC)-----</b>	<b>10</b>
1.1 HISTORY AND IMPLEMENTATION OF ORC-----	10
1.2 OPERATION OF THE ORGANIC RANKINE CYCLE (ORC)-----	12
1.3 ORGANIC FLUIDS PROPRIETIES-----	15
1.4 PROPRIETY OF R245FA -----	18
<b>2 PHYSICAL MODELS AT THE BASE OF HEAT EXCHANGERS-----</b>	<b>19</b>
2.1 TYPE OF HEAT EXCHANGERS -----	19
2.2 DIFFERENT POSSIBLE PHYSICAL APPROACHES-----	22
2.3 CONVECTION PHENOMENON IN THE HEAT EXCHANGER-----	24
2.3.1 CONVECTIVE HEAT TRANSFER COEFFICIENT -----	28
2.4 CONDUCTION PHENOMENON -----	29
2.5 OVERALL EXCHANGED THERMAL POWER-----	30
2.5.1 CO-CURRENT CASE-----	33
2.5.2 COUNTER-CURRENT CASE -----	33
<b>3 MAP-BASED MODEL-----</b>	<b>38</b>
3.1 PLANT DESCRIPTION -----	38
3.1.1 PUMP-----	38
3.1.2 EXPANDER-----	39
3.1.3 HEAT EXCHANGERS -----	40
3.2 OVERALL EXPERIMENTAL PLANT-----	42
3.3 MAP-BASED MODEL BUILDING-----	43
3.4 SINGLE COMPONENTS BUILDING PROCESS -----	43
3.4.1 STEP 1 -----	43
3.4.2 STEP 2 -----	45
3.5 BUILT MODEL SIMULATION-----	47
3.6 MAP-BASED SIMULATION RESULTS-----	48
3.6.1 TEMPERATURE, PRESSURE AND GAS FRACTION RELATIVE PERCENTAGE ERROR AT THE EVAPORATOR OUTLET-----	49
3.6.2 POWER TO THE SHAFT PRODUCED BY THE EXPANDER -----	52
3.7 BRIEF CONCLUSIONS ON THE RESULTS OF THE MAP-BASED MODEL -----	53
<b>4 PHYSICAL MODELLING OF EVAPORATOR -----</b>	<b>54</b>
4.1 CONSTRUCTION OF THE FIRST MODEL -----	54
4.1.1 GEOMETRY CONSTRUCTION -----	54
4.1.2 CONSTRUCTION OF THE CONVECTIVE HEAT EXCHANGE -----	59
4.1.3 PLATE THERMAL MASS-----	60
4.1.4 BOUNDARY AND INITIAL CONDITIONS -----	61
4.1.5 STUDY OF THE INITIAL DENSITY OF REFRIGERANT R245FA-----	62
4.1.6 FIRST ASSEMBLED MODEL-----	64
4.1.7 CONCLUSION ON THE FIRST MODEL ATTEMPT -----	64
4.2 COUNTERCURRENT EXCHANGE IMPLEMENTATION -----	65
4.3 TWO SEGMENT PHYSICAL-BASED MODEL -----	66
4.3.1 SIMULATION AND RESULTS -----	67
4.3.2 CONCLUSIONS ON THE TWO SEGMENTS MODEL -----	72
4.4 THREE SEGMENT PHYSICAL-BASED MODEL -----	73
4.4.1 SIMULATION AND RESULTS -----	74

4.4.2	CONCLUSIONS ON THE THREE SEGMENTS MODEL	79
4.5	FOUR SEGMENTS PHYSICAL-BASED MODEL	80
4.5.1	CONCLUSION ON THE FOUR SEGMENTS MODEL	84
<b>5</b>	<b>HEAT TRANSFER MULTIPLIER STUDY</b>	<b>85</b>
5.1	MODEL CONSIDERED FOR THE HTM STUDY	85
5.2	FIRST ATTEMPT WITH HTM = 2	86
5.2.1	CONCLUSIONS ON THE FIRST ATTEMPT OF HTM = 2	90
5.3	PARAMETRIC ANALYSIS OF THE HTM	91
5.3.1	TEMPERATURE	91
5.3.2	PRESSURE	92
5.3.3	GAS FRACTION	93
5.4	RESULTS AND GRAPHS	93
<b>6</b>	<b>HYBRID PLANT: PHYSICAL-BASED EVAPORATOR IN MAP-BASED PLANT</b>	<b>97</b>
6.1	PREPARATION OF THE MODEL FOR SIMULATION	97
6.2	STUDY OF THE HEAT TRANSFER MULTIPLIER VALUE	98
6.2.1	TEMPERATURE	99
6.2.2	PRESSURE	100
6.2.3	GAS FRACTION	101
6.2.4	POWER	102
6.3	RESULTS AND GRAPHS	103
<b>7</b>	<b>HYBRID PLANT: PHYSICAL-BASED EVAPORATOR AND CONDENSER IN MAP-BASED PLANT</b>	<b>106</b>
7.1	PHYSICAL-BASED CONDENSER	106
7.1.1	RESULT OF VERIFICATION OF THE HTMS OF EVAPORATOR AND CONDENSER INFLUENCE	108
7.2	MULTI-OBJECT MULTI-OBJECTIVE OPTIMIZATION	110
7.2.1	INPUT PARAMETERS	110
7.2.2	OUTPUT PARAMETERS	110
7.2.3	OPTIMIZATION MODEL	111
7.2.4	OPTIMIZATION SETTINGS	112
7.3	OPTIMIZATION RESULTS	113
7.4	CONCLUSIONS ABOUT OPTIMIZATION	121
<b>8</b>	<b>FINAL CONCLUSIONS AND FUTURE IMPLEMENTATIONS</b>	<b>122</b>
<b>9</b>	<b>APPENDIX</b>	<b>124</b>
	<b>BIBLIOGRAPHY</b>	<b>127</b>

# INDEX OF FIGURES

Figure 1.1 – Motor qualitative power balance-----	8
Fig. 1.1-1 – Rankine cycle schematization-----	10
Fig. 1.2-1 - The simple schematization of ideal Rankine Cycle-----	12
Fig. 1.2-2 - T-S diagram for ideal Rankine Cycle -----	12
Fig. 1.2-3 - Rankine cycle with high and low pressure turbines -----	14
Fig. 1.3-1 - T-s curve for the three types of fluids -----	16
Fig. 1.3-2 - Comparison between some organic fluids and water -----	17
Fig. 1.4-1 - R245fa chemical-physical properties table -----	18
Fig. 1.4-2 - R245fa T-s diagram -----	18
Fig. 2.1-1 - Shell and tube heat exchanger with two pipes -----	20
Fig. 2.1-2 - Shell and tube heat exchanger with multiple pipes -----	20
Fig. 2.1-3 - External view of a BPHE-----	21
Fig. 2.1-4 - Exploded view of a BPHE and its operation -----	21
Fig. 2.3-1 - control volume for an heat exchanger -----	24
Fig. 2.3-2 – C.V. in two pipes heat exchanger -----	25
Fig. 2.3-3 - Convection resistance scheme -----	27
Fig. 2.4-1 - Conduction resistance scheme -----	29
Fig. 2.5-1 - Co-current (left) and counter-current (right) flow temperatures trend-----	30
Fig. 2.5-2 - Counter-current flow with $C_h = C_c$ -----	34
Fig. 2.5-3 - Counter-current flow with $C_h > C_c$ -----	35
Fig. 2.5-4 - Counter-current flow with $C_h < C_c$ -----	35
Fig. 3.1-1 – Cat Pump® model 1051CM -----	39
Fig. 3.1-2- Scroll expander functioning -----	40
Fig. 3.1-3 - Air Squared® model E22H038B-L-SH-----	40
Fig. 3.1-4 - BPHE internal functioning scheme-----	41
Fig. 3.1-5 - SWEP model B80Hx70/1P-SC-S 4x24U -----	42
Fig. 3.2-1 - General scheme of the experimental reference plant -----	42
Fig. 3.4-1 - Template of Receiver -----	44
Fig. 3.4-2 - “Help” function of Receiver, page 1 -----	44
Fig. 3.4-3 - “Help” function of Receiver, page 2 -----	45
Fig. 3.4-4 - Case setup for case from 1 to 8 -----	46
Fig. 3.4-5 – Assembled map-based model-----	46
Fig. 3.5-1 – Simulation setting template -----	47
Fig. 3.5-2 - "Help" for Time Control Flag and Maximum Simulation Duration (Time) -----	48
Fig. 3.6-1 – Error trend of R245fa temperature at the evaporator outlet, full map-based model-----	50
Fig. 3.6-2 – Error trend of R245fa pressure at the evaporator outlet, full map-based model-----	51
Fig. 3.6-3 - Error trend of the produced power to the shaft, full map-based model-----	53
Fig. 4.1-1 – Extract from the SWEP catalog for the B80Hx70/1P-SC-S 4x24U model-----	55
Fig. 4.1-2 - Different types of functional blocks for pipes -----	55
Fig. 4.1-3 - Reconstruction (not to scale) of the exchanger using the PipeRectangle functional blocks-----	56
Fig. 4.1-4 - Geometric data set on the program -----	57
Fig. 4.1-5 – Geometry section of functional block PipeRectangle-----	58
Fig. 4.1-6 - Thermal section of functional block PipeRectangle -----	58
Fig. 4.1-7 - Different functional blocks for thermal connections -----	59
Fig. 4.1-8 - General components for thermal exchange -----	60
Fig. 4.1-9 - "Help" function for the initial density value of R245fa -----	62
Fig. 4.1-10 -First attempt of physical-based model of evaporator -----	64

Fig. 4.2-1 - Countercurrent flow -----	65
Fig. 4.3-1 – Two segments physical-based evaporator model -----	67
Fig. 4.3-2 - Temperature trend of three models, 2 segments evaporator -----	68
Fig. 4.3-3 – 61 cases temperature error trend, 2 segments evaporator -----	69
Fig. 4.3-4 - Pressure trend of three models, 2 segments evaporator -----	70
Fig. 4.3-5 - 61 cases pressure error trend, 2 segments evaporator -----	71
Fig. 4.3-6 – 61 case average gas fraction trend, 2 segments evaporator -----	72
Fig. 4.4-1 - Three segments physical-based evaporator model -----	73
Fig. 4.4-2 - Temperature trend of three models, 3 segments evaporator -----	74
Fig. 4.4-3 - 61 cases temperature error trend, 3 segments evaporator -----	75
Fig. 4.4-4 - Pressure trend of three models, 3 segments evaporator -----	76
Fig. 4.4-5 - 61 cases pressure error trend, 3 segments evaporator -----	77
Fig. 4.4-6 - 61 case average gas fraction trend, 3 segments evaporator -----	78
Fig. 4.5-1 - Four segments physical-based evaporator model -----	80
Fig. 4.5-2 - Temperature trend of three models, 4 segments evaporator -----	81
Fig. 4.5-3 - 61 cases temperature error trend, 4 segments evaporator -----	82
Fig. 4.5-4 - Pressure trend of three models, 4 segments evaporator -----	82
Fig. 4.5-5 - 61 cases pressure error trend, 4 segments evaporator -----	83
Fig. 4.5-6 - 61 case average gas fraction trend, 4 segments evaporator -----	84
Figure 5.1 - View of the internal wavy exchange surface of BPHE -----	85
Fig. 5.2-1 – 61 cases temperature error trend, 4 segments evaporator, HTM = 2 -----	87
Fig. 5.2-2 - 61 cases pressure error trend, 4 segments evaporator, HTM = 2 -----	89
Fig. 5.4-1 - 61 cases temperature error trend, 4 segments evaporator, HTM = 50 -----	95
Fig. 5.4-2 - 61 cases pressure error trend, 4 segments evaporator, HTM = 50 -----	95
Fig. 5.4-3 – Gas fraction for 61 cases, 4 segments evaporator, HTM = 50 -----	96
Fig. 6.1-1 – Hybrid plant with physical-based 4 segments evaporator -----	97
Fig. 6.3-1 - 61 cases temperature error trend, hybrid plant with physical-based evaporator, HTM = 50 -----	104
Fig. 6.3-2 - 61 cases pressure error trend, hybrid plant with physical-based evaporator, HTM = 50 -----	104
Fig. 6.3-3 – 61 cases power error trend, hybrid plant with physical-based evaporator, HTM = 50 -----	105
Fig. 6.3-4 - 61 cases gas fraction trend, hybrid plant with physical-based evaporator, HTM = 50 -----	105
Fig. 7.1-1 – Hybrid map-based plant with physical-based condenser and evaporator -----	107
Fig. 7.2-1 – modeFRONTIER optimization model -----	111
Fig. 7.2-2 – Pareto Front example curve -----	112
Fig. 7.3-1 - Temperature evaporator inlet hybrid plant error trend: left->not optimized , right->optimized --	115
Fig. 7.3-2 - Temperature evaporator outlet hybrid plant error trend: left->not optimized , right->optimized-	116
Fig. 7.3-3 - Pressure evaporator outlet hybrid plant error trend: left->not optimized , right->optimized -----	117
Fig. 7.3-4 – Gas fraction comparison between experimental, full map-based, hybrid not optimized and hybrid optimized -----	117
Fig. 7.3-5 - Temperature condenser inlet hybrid plant error trend: left->not optimized , right->optimized ---	118
Fig. 7.3-6 - Temperature condenser outlet hybrid plant error trend: left->not optimized , right->optimized--	119
Fig. 7.3-7 – Power produced by expander hybrid plant error trend: left->not optimized , right->optimized--	120

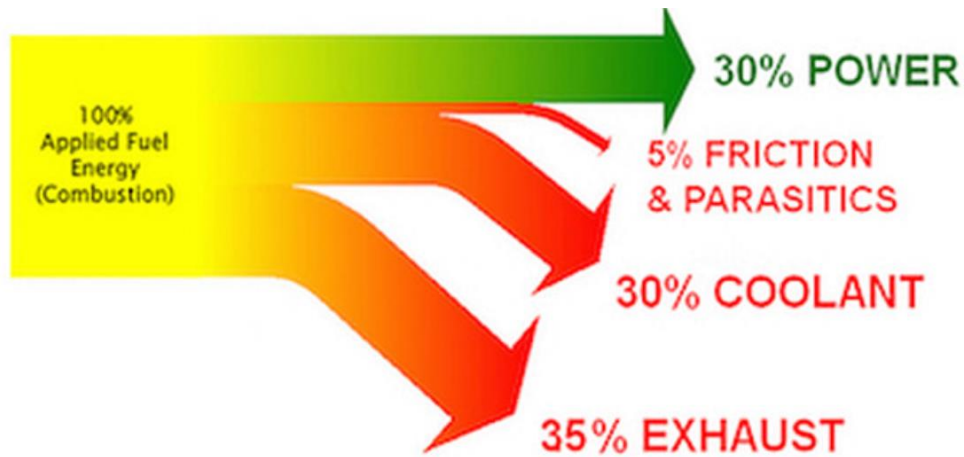
# INDEX OF TABLES

Table 3.1-1 – Cat Pump® model 1051CM characteristics-----	38
Table 3.1-2 – Air Squared® model E22H038B-L-SH main characteristics-----	39
Table 3.1-3 - SWEP model B80Hx70/1P-SC-S 4x24U (left) and B10THx16/1P-SC-M (right) characteristics -----	41
Table 3.6-1 – R245fa temperature at the evaporator outlet, full map-based model -----	49
Table 3.6-2 - R245fa pressure at the evaporator outlet, full map-based model-----	50
Table 3.6-3 – R245fa gas fraction at the evaporator outlet, full map-based model -----	51
Table 3.6-4 – Power to the shaft produced by the expander, full map-based model -----	52
Table 4.1-1 – Chemical-physical proprieties for StainlessSteel material presents in the software library -----	61
Table 4.1-2 - Comparison between relative percentage error of map-based model with set initial charge and set initial density -----	63
Table 4.3-1 - Temperature average comparison, 2 segments evaporator -----	68
Table 4.3-2 – Temperature mean relative percentage error, 2 segments evaporator-----	68
Table 4.3-3 - Pressure average comparison, 2 segments evaporator-----	70
Table 4.3-4 - Pressure mean relative percentage error, 2 segments evaporator -----	70
Table 4.3-5 – Refrigerant gas percentage comparison, 2 segments evaporator-----	71
Table 4.3-6 – Refrigerant gas fraction mean relative percentage error, 2 segments evaporator -----	72
Table 4.4-1 - Temperature average comparison, 3 segments evaporator -----	74
Table 4.4-2 - Temperature mean relative percentage error, 3 segments evaporator -----	75
Table 4.4-3 - Pressure average comparison, 3 segments evaporator-----	76
Table 4.4-4 – Pressure mean relative percentage error, 3 segments evaporator-----	77
Table 4.4-5 - Refrigerant gas percentage comparison, 3 segments evaporator -----	78
Table 4.4-6 - Refrigerant gas fraction mean relative percentage error, 3 segments evaporator -----	78
Table 4.5-1 - Temperature average comparison, 4 segments evaporator -----	81
Table 4.5-2 – Temperature mean relative percentage error, 4 segments evaporator-----	81
Table 4.5-3 - Pressure average comparison, 4 segments evaporator-----	82
Table 4.5-4 - Pressure mean relative percentage error, 4 segments evaporator -----	83
Table 4.5-5 - Refrigerant gas percentage comparison, 4 segments evaporator -----	83
Table 4.5-6 - Refrigerant gas fraction mean relative percentage error, 4 segments evaporator -----	84
Table 5.2-1 – Temperature average, 4 segments evaporator, HTM = 2-----	86
Table 5.2-2 – Temperature mean relative percentage error, 4 segments evaporator, HTM = 2-----	87
Table 5.2-3 - Pressure average, 4 segments evaporator, HTM = 2 -----	88
Table 5.2-4 – Pressure mean relative percentage error, 4 segments evaporator, HTM = 2 -----	88
Table 5.2-5 – Gas fraction average, 4 segments evaporator, HTM = 2 -----	90
Table 5.2-6 – Gas fraction mean relative percentage error, 4 segments evaporator, HTM = 2-----	90
Table 5.3-1 – Temperature average, 4 segments evaporator, HTM parametric analysis-----	91
Table 5.3-2 – Temperature mean relative percentage error, 4 segments evaporator, HTM parametric analysis-----	92
Table 5.3-3 - Pressure average, 4 segments evaporator, HTM parametric analysis -----	92
Table 5.3-4 – Pressure mean relative percentage error, 4 segments evaporator, HTM parametric analysis-----	92
Table 5.3-5 – Gas fraction average, 4 segments evaporator, HTM parametric analysis -----	93
Table 5.3-6 – Gas fraction mean relative percentage error, 4 segments evaporator, HTM parametric analysis -----	93
Table 5.4-1 – Comparison between map-based and physical-based evaporator 4 segments model for the average <sub>MRPE</sub> -----	94
Table 6.2-1 - Temperature average, hybrid plant with physical-based evaporator, HTM analysis -----	99
Table 6.2-2 - Temperature mean relative percentage error, hybrid plant with physical-based evaporator, HTM analysis -----	99
Table 6.2-3 - Pressure average, hybrid plant with physical-based evaporator, HTM analysis -----	100

Table 6.2-4 - Pressure mean relative percentage error, hybrid plant with physical-based evaporator, HTM analysis -----	100
Table 6.2-5 - Gas fraction average, hybrid plant with physical-based evaporator, HTM analysis -----	101
Table 6.2-6 - Gas fraction mean relative percentage error, hybrid plant with physical-based evaporator, HTM analysis -----	101
Table 6.2-7 - Power average, hybrid plant with physical-based evaporator, HTM analysis -----	102
Table 6.2-8 - Power mean relative percentage error, hybrid plant with physical-based evaporator, HTM analysis -----	102
Table 6.3-1 - Comparison between full map-based plant and hybrid plant with physical-based evaporator for the average <sub>MRPE</sub> -----	103
Table 7.1-1 - Chosen value for verification of HTM values influence -----	108
Table 7.1-2 - Values average, hybrid plant with physical-based evaporator and condenser, HTM analysis --	108
Table 7.1-3 - Mean relative percentage error, hybrid plant with physical-based evaporator and condenser, HTM analysis -----	109
Table 7.3-1 - Hybrid map-based plant with physical-based condenser and evaporator optimization results	114
Table 7.3-2 - Temperature evaporator inlet comparison between experimental, map-based, hybrid not optimized and hybrid optimized plants -----	115
Table 7.3-3 - Temperature evaporator outlet comparison between experimental, map-based, hybrid not optimized and hybrid optimized plants -----	115
Table 7.3-4 - Pressure evaporator outlet comparison between experimental, map-based, hybrid not optimized and hybrid optimized plants -----	116
Table 7.3-5 - Gas fraction evaporator outlet comparison between experimental, map-based, hybrid not optimized and hybrid optimized plants -----	117
Table 7.3-6 - Temperature condenser inlet comparison between experimental, map-based, hybrid not optimized and hybrid optimized plants -----	118
Table 7.3-7 - Temperature condenser outlet comparison between experimental, map-based, hybrid not optimized and hybrid optimized plants -----	118
Table 7.3-8 - Power produced by the expander comparison between experimental, map-based, hybrid not optimized and hybrid optimized plants -----	120
Table 7.3-9 - <i>averageMRPE</i> comparison between experimental, map-based, hybrid not optimized and hybrid optimized plants -----	120
Table 9-1 - <i>SpaceFiller</i> multi-objective multi-object optimization -----	124
Table 9-2 - Experimental collected data -----	126

## Introduction

The purpose of this thesis work was to develop a virtual validated physical-based model of heat exchangers for an Organic Rankine Cycle power plant. The idea behind the necessity to have a physical-based model of exchangers inside the plant, was to couple the ORC plant with an internal combustion engine to increase its efficiency using the exhaust gases to feed the hot side of the evaporator. The exhaust gases are expelled, in conditions of engine thermal regime, at temperatures that are still quite high, of the order of hundreds of degrees. In fact, if a power balance of modern thermal engines is carried out, most of the power loss, which turns into a signifying reduction in efficiency, is given by the thermal power dispersed in the environment by the exhaust gases.



*Figure 1.1 – Motor qualitative power balance*

Furthermore, focusing the attention on the general thermal losses, given by the union of the dissipation during cooling and the exhaust gases, only these, constitute about 65% of the total power produced by initial combustion, which is lost in the environment.

It is immediately evident that if this power could be recovered even only partially, the efficiency of internal combustion engines could increase considerably. This would result in lower fuel consumption with an impact on both vehicle handling costs and a reduction in the pollution produced, a topic that is also much discussed today.

To try to satisfy this purpose, it has been decided to try to couple with engine a Rankine cycle, with organic fluid circulating inside it and for this reason called Organic Rankine Cycle (ORC), which can partially recover the heat of the exhaust gases to convert it into available power produced by an

expander, eventually coupled with an alternator, and thus increase the overall efficiency of the internal combustion engine.

One of the main problems in inserting this ORC cycle is related to its size. In fact, the initial idea, was to increase the efficiency of car engines for private transport and this involved a very limited capacity of the engine compartment.

However, as demonstrated in the thesis *"Modellazione e calibrazione di un sistema ORC per il recupero del calore dei gas di scarico di un motore a combustion interna"* written by the student Michelangelo D'Amborgio, the maximum effectiveness of the ORC occurs especially at constant engine revolutions. In private cars, especially in areas of urban use, the engine revolutions vary often and rapidly, making the increase in engine efficiency due to the ORC, less effective. For this reason, it has been imagined that a greater efficiency of the ORC component could be had in the engines of trucks or ships, where the engine revolutions are kept constant for long distances and, moreover, the space necessary for its installation, no longer represents such a stringent constraint as for private cars.

For this reason, a physical development of the components of the ORC virtual model was necessary, initially based on a map-based model, to validate a model that is independent from the specific components and their geometrical and material proprieties and, therefore, can find applications in motors of different power respect those for which it was originally intended.

In this thesis the work was concentrated on the development and validation of the physical-based model of heat exchangers and on their substitution inside the map-based power plant. The purpose, in order to validate the final model, was to obtain a physical-based models whose behavior could reflect the trend of both map-based components and the experimental one, taken from the thesis *"Experimental characterization of scroll expander for small-scale power generation in an Organic Rankine Cycle"* written by the student Felipe Airoidi, who built an experimental model from which the collected data were used to model the map-based plant and which will be used as reference in this thesis work.

# 1 Organic Rankine Cycle (ORC)

## 1.1 History and implementation of ORC

The Organic Rankine Cycle (ORC), as its name suggest, is a Rankine Cycle in which flows an organic fluid. The Rankine Cycle took its name from the Scottish engineer William John Macquorn Rankine who developed a complete theory of the steam engine, approximately between 1850 and 1860. The Rankine Cycle is a thermodynamical closed cycle to convert heat into work. Initially it was developed to work with steam and also nowadays the Rankine Cycle, based on water as working fluid, provides approximately the 85% of worldwide electricity production.

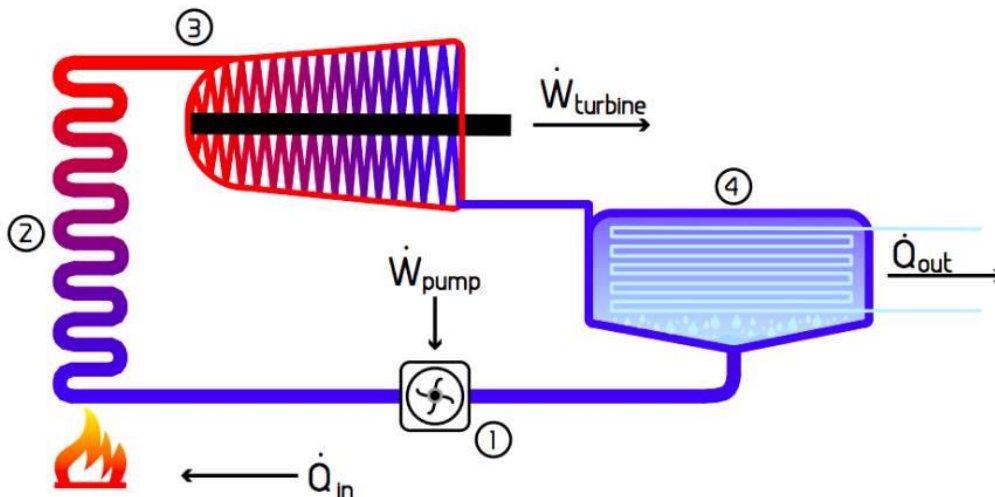


Fig. 1.1-1 – Rankine cycle schematization

However, for some applications, working with steam can lead to condensation problem and to the formation of water drops that impact on the turbine blades creating mechanical damage on them. To overcome this problem, the solution was found having superheated steam at evaporator outlet, brought to several hundred degrees centigrade and several bars of pressure, to prevent this condensation phenomenon in the expansion phase inside the turbine, but this requires a lot of heat power to bring the steam to that condition. Using a lot of thermal power means generally producing a quite high useful power from turbine, but also having system of rather large dimensions.

## Organic Rankine Cycle (ORC)

To overcome the problem when it is impossible to bring the steam into superheated condition, to try to find the method to miniaturize the plants and in order to be able to use the cycle in various areas, toward the end of the 1800s, it began to experiment to use organic fluids instead of steam as working fluids.

The first attempts were made by the engineer Frank Ofeldt, in 1883, who invented a unique boat engine, which boiled naphtha, without burn it, to power a cylinder, in place of turbine conventionally installed classic Rankine Cycles.

Using organic fluids, the cycle took the name of Organic Rankine Cycle (ORC) to distinguish it from the classic Rankine Cycle using water.

The ORC technology was seriously develop only during the 20<sup>th</sup> century and which Italy, thanks to research carried out at the Politecnico of Milan, played a fundamental role.

## Organic Rankine Cycle (ORC)

### 1.2 Operation of the Organic Rankine Cycle (ORC)

It wanted to analyze in detail the functioning of Organic Rankine Cycle.

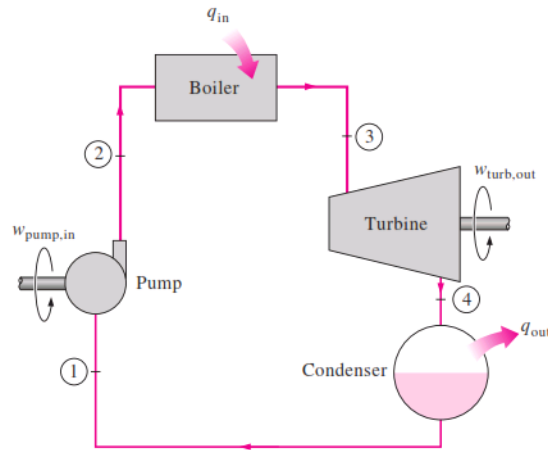


Fig. 1.2-1 - The simple schematization of ideal Rankine Cycle

In this cycle, four main components can be identified:

- Pump
- Boiler (also called Evaporator)
- Turbine (or in general Expander)
- Condenser

Before analyzing in detail the above mentioned component, can be useful to introduce the thermodynamic cycle<sup>1</sup>, to understand better their purpose:

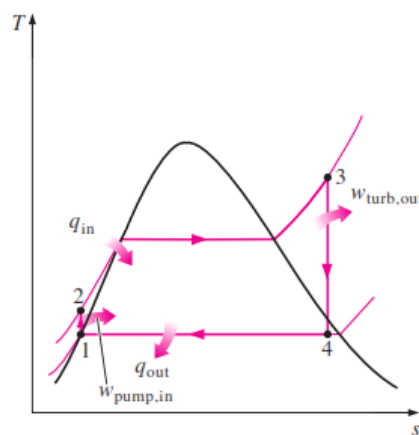


Fig. 1.2-2 - T-S diagram for ideal Rankine Cycle

<sup>1</sup> It refers to the ideal cycle with a single high pressure turbine and a single overheating phase.

## Organic Rankine Cycle (ORC)

It is possible to identify four main phases:

- 1-2: Isentropic compression given by the pump
- 2-3: Isobaric heat addition given by the boiler
- 3-4: Isentropic expansion in the expander
- 4-1: Isobaric heat extraction in the condenser

The fluid enters inside the pump in the point 1 (starting point of the cycle) as saturated liquid. Then it is compressed by the pump until the operating boiler pressure. It is important that point 1 is on the saturation curve, because it is useful to compress the fluid in the liquid phase as its compressibility is less, if not approximate to zero, compared to the gaseous phase and so it is possible, therefore, to use a small power, to greatly increase the pressure of the fluid. Inside the pump a quite low amount of heat is released for the compression, so the temperature of the fluid increases a little, but the pressure increases a lot, so the fluid passes from the condition of saturated liquid to that of subcooled liquid. The fluid is brought to the point 2 of the cycle and the subcooled liquid enters in the boiler or evaporator. Here a large amount of heat is transferred by means of an exchanger. Generally, for large plants for the production of electricity, using water as working fluid, the heat is produced by the combustion of natural gas or organic waste and in this type of plants the most commonly used geometries for evaporator are shell and tubes exchanger.

In the plants examined in this thesis, the operating fluid was organic and it is vaporized through hot water at just over a hundred degrees centigrade, and even when the final purpose is achieved coupling it with an internal combustion engine, the organic fluid will be vaporized from the exhaust of engine itself at some hundreds degrees centigrade. Furthermore, since the powers involved are significantly lower than the system described above, a Brazed Plate Heat Exchanger (BPHE) is used to maximize the heat exchange.

Regardless of the type of system and the dimensions of the exchanger, the purpose of the evaporator is to transform the fluid from a subcooled to a completely gaseous state and, once the saturation point on the curve is reached, increase more the temperature, transforming it into superheated steam. This operation is fundamental, as mentioned in the previous chapter, to avoid that in the last part of subsequent expansion phase, a coexistence of liquid and gaseous phase can be created. In addition to this, the purpose of overheating is to increase thermal efficiency of the system, trying to absorb most heat as possible. At this point the point 3 of the cycle is reached and the superheated vapor enters in the expander. Inside this component the vapor is expanded,

## Organic Rankine Cycle (ORC)

creating a thrust pressure on the turbine blades which turn, transmitting the rotary motion to the output shaft. Through the shaft it is possible to extract useful power from the system which can be used for various purposes: the greatest use occurs through coupling it with an alternator for the conversion of mechanical power into electric one.

Obviously, due to mechanical coupling and internal dissipation of the alternator, part of the useful power produced by shaft is lost during the conversion into electric current. Once the expansion phase was over, point 4 of the curve is reached. During the design, the superheating operation is calculated so that this point remains on the saturation curve (vapor phase) to avoid that during the last part of the expansion can occur a partial fluid condensation and the creation of small liquid drops which impact on the turbine blades, creating stress and possibly mechanical damage on them.

Starting from the saturated vapor condition, the fluid enters in the condenser, in which there is a heat extraction to bring it back to the condition of saturated liquid. The extraction can take place in different ways: by means of a fluid-water exchanger or in some cases directly in the environment by means of fluid-air exchanger. In the plant considered in this thesis, the fluid is condensed with cold water, but, in the idea of coupling it with the internal combustion engine, the condensation of the working fluid should take place directly through the engine cooling radiator. During the heat extraction phase there is the coexistence of liquid and gas and at the end of it, the starting point 1, in saturated liquid condition, is reached and the cycle can start over.

The cycle described until now is an idealization of the real one, for which, as the most important assumption, for example, it is impossible to have the compression and the expansion phases as perfectly isentropic. Another example in reality, for medium and large plants, there is a double stage of expansion thanks to high and low pressure turbines and between them a further heating phase, in order to exploit the heat still residual in the fluid at the end of the first expansion, to produce more useful work and increase the plant efficiency.

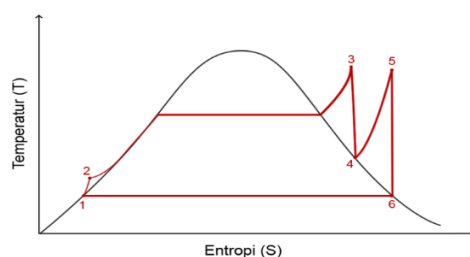


Fig. 1.2-3 - Rankine cycle with high and low pressure turbines

### 1.3 Organic fluids proprieties

As already mentioned several times in the previous paragraphs, the fluids used in the ORC systems are organic. The choice to use organic fluids, instead of conventional water, as working fluid in the Rankine Cycle, derives from the necessity to use a lower thermal power in the evaporation phase, in order also to be able to reduce the size of the plants.

Some of the main characteristics of the organic fluids are the low boiling point and a low latent heat of evaporation. The low boiling temperature is perfect for bringing the fluid to complete vaporization at temperature, often, below 100 °C. By doing a reverse reasoning, for example applying directly to the case examined, the exhaust gases coming out from the engine of a car, are at temperate between 300 °C and 400 °C. In general, Rankine Cycles working with organic fluids are highly recommended for situations in which heat is released from source at temperatures between 100 °C and 400 °C and for powers lower than 1 MW, cases in which traditional Rankine Cycle with water steam, would have too low efficiency and, on the other hand, ORCs maintain a sufficiently high efficiency that justify the investment cost and use. Further examples of applications of ORCs are coupling with renewable sources for production of “green” electricity, such as biomasses, geothermal, solar and ocean heat.

Going back to the final purpose, the exhaust gases can be used to vaporize an organic fluid and, using its, it is sure to obtain, even for a relatively low pressure (of the order of few bars), a superheated vapor and even exploiting a high expansion in the turbine, it is quite safe to not fall inside the saturation curve with the possible coexistence of two phases.

The low latent heat allows to use a small-sized exchanger, because not much thermal power is required to bring the fluid from the liquid to the gaseous phase and the other way around. This translates, in addition to a net decrease in the geometrical dimensions of the evaporator, to a lower cost and lower weight on board the vehicle which involves less consumption of fuel and therefore less pollution produced.

Organic fluids consist of light hydrocarbons and chlorofluorocarbons (freons).

Now it is necessary to make some clarifications on the possible type of organic fluids to understand if the affirmation, made earlier, that is impossible to have a fraction of liquid during the expansion, is completely correct.

## Organic Rankine Cycle (ORC)

Organic fluids can be classified in three categories, according to the slope of the vapor saturation curve in the T-s diagram:

- Dry organic fluids: they have a positive slope of the vapor saturation curve and, in general, have a quite high molecular weight.
- Isentropic organic fluids: they have a quite vertical saturated vapor curve.
- Wet organic fluids: they have a negative slope of the vapor saturation curve and, in general, have a quite low molecular weight.

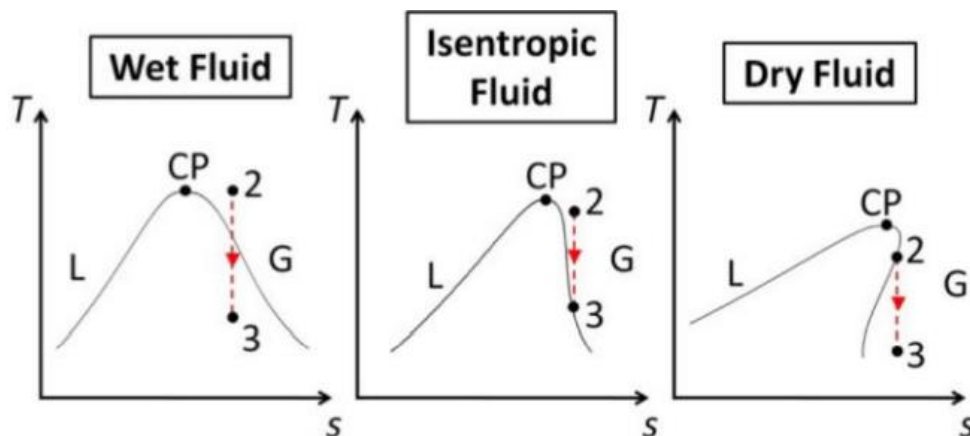


Fig. 1.3-1 - T-s curve for the three types of fluids

In order to avoid confusion with the previous chapter, phase 2-3, in this description, identifies the expansion phase of the fluid.

As it is possible to immediately see from the above figure Fig. 1.3-1, the main influence that the type of fluid has on the cycle, is due to the presence or not of a second phase during the expansion. For a wet fluid, in the case of the figure where overheating doesn't lead to very high temperature and pressure, as occurs in most applications of use of an ORC, the expansion ends in a region characterized by the coexistence of a liquid and vapor phases, therefore there will be partial condensation of the fluid in the expander with bad effects on its wear and erosion. For isentropic fluid, it moves almost vertically on the curve and it will maintain a saturated vapor for all expansion phase. In this case it is not necessary a real overheating since, once the totality of vapor fraction has been reached (crossed the vapor saturation curve), it is certain, for the slope of the curve, that during the expansion there will be no liquid presence. For dry fluid, it remains in a state of overheating even after expansion. In this case is possible to use the minimum amount of thermal energy to transform the fluid into superheated vapor, or even just saturated vapor, and, during the

## Organic Rankine Cycle (ORC)

expansion, the alter will tend to become superheated vapor. This brings to the same considerations made for isentropic fluids. The greatest problem in using dry organic fluids, is their extreme difficulty in condensing, which often requires and additional exchanger to start to extract heat, by bringing the fluid closer to the vapor saturation curve and then bring the fluid back to saturated liquid through the condenser. In addition to often adding an additional exchanger, called recuperator, which increase the weight and the cost of building and maintenance of the plant, it is also necessary to pay attention to how the fluid exits from the expander, because it is possible an excessive degree of overheating and this can lead to problems for components connected downstream of the expander. If it is possible to find a solution to the problems mentioned, dry fluids are ideal for ORCs because it is possible to completely avoid the formation of condensation in the final phase of expansion, limiting the problems on the efficiency of the cycle and, in case of a turbine as expander, problems related to damage of the blades due to condensation.

The fluid that was used in this thesis work, was the R245fa, which can be classified between the isentropic and dry organic fluids.

To conclude this paragraph on the organic fluid's proprieties, a comparative graph is proposed between the various type of fluids used in ORC and the water, traditionally used for big Rankine steam plants, in order to be able to appreciate, again, the difference between the types of organic fluids, but also the difference between organic fluids and water for low temperature vaporization.

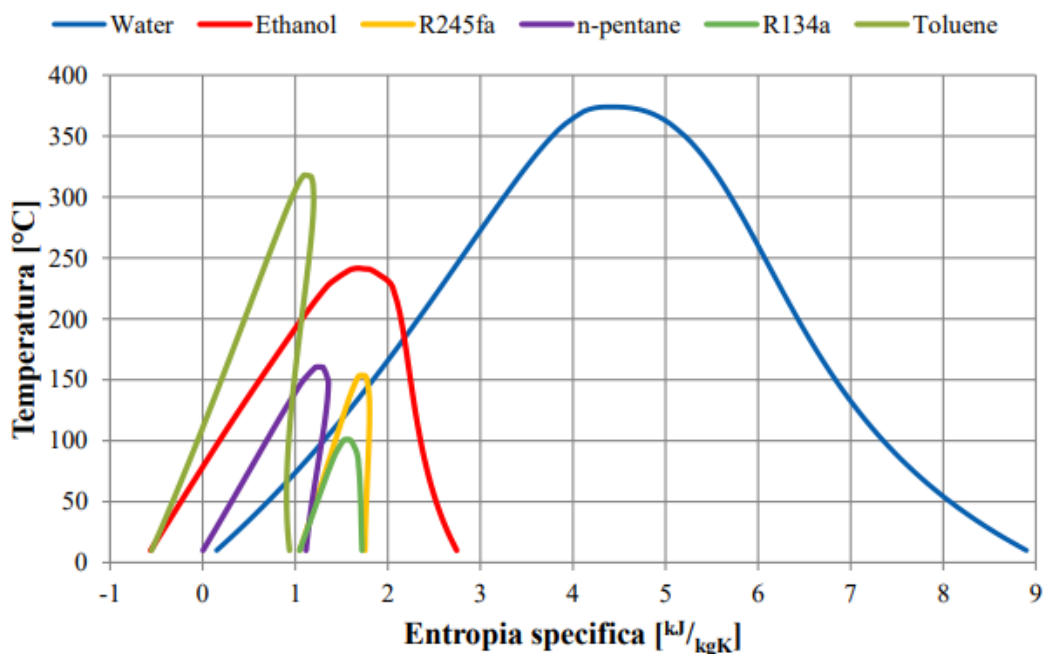


Fig. 1.3-2 - Comparison between some organic fluids and water

### 1.4 Propriety of R245fa

As already mentioned in the previous paragraph, the fluid that was used in the ORC cycle of this thesis was the pentafluoropropane R245fa, also called in commercial field Genetron® 245fa, produced by ©Honeywell refrigerants. This one can be classified as dry organic fluid, even if it is very close to the characteristic of an isentropic fluid. However, what is relevant is that, once the vapor saturation curve has been reached, during the expansion phase it remains completely vapor, possibly superheated, without condensation.

The main chemical-physical proprieties of this organic fluid are summarized in the figures below:

Maximum $p_{ev}$	Maximum $T_{ev}$	Minimum $p_{con}$	Minimum $T_{con}$
2,8MPa	140°C	149,4kPa	20°C

Properties of HFC-245fa			
Chemical Name	1,1,1,3,3-pentafluoropropane		
Molecular Formula	CF <sub>3</sub> CH <sub>2</sub> CHF <sub>2</sub>		
Molecular Weight	134		
Flammability Limits in Air @ 1atm** (vol.%)	None		
Flash Point *	None		
Water Solubility in HFC-245fa	1600 ppm		
ASHRAE Safety Group Classification	B1		

\*Flashpoint by ASTM D 3829-87; ASTM D1310-86  
\*\*Flame Limits measured at ambient temperature and pressure using ASTM E681-85 with electrically heated match ignition, spark ignition and fused wire ignition; ambient air.

Standard International Units*		English Units*	
Boiling Point °C @ 1.01 bar	15.3	Boiling Point (°F) @ 1atm	59.5
Freezing Point °C @ 1.01 bar	<-107	Freezing Point (°F)	<-160
Critical Temperature** (°C)	154.05	Critical Temperature** (°F)	309.29
Critical Pressure** (bar)	36.4	Critical Pressure** (psia)	527.9
Critical Density** (m <sup>3</sup> /kg)	517	Critical Density** (lb/ft <sup>3</sup> )	32.28
Vapor Density @ Boiling Point (lb/ft <sup>3</sup> )	5.921	Vapor Density @ Boiling Point (lb/ft <sup>3</sup> )	0.3697
Liquid Density (kg/m <sup>3</sup> )	1339	Liquid Density (lb/ft <sup>3</sup> )	83.58
Liquid Heat Capacity (kJ/kg K)	1.36	Liquid Heat Capacity (Btu/lb °F)	0.33
Vapor Heat Capacity @ constant pressure, 1.01 bar (kJ/kg K)	0.8931	Vapor Heat Capacity @ constant pressure, 1atm (Btu/lb °F)	0.218
Heat of Vaporization at Boiling Point (kJ/kg)	196.7	Heat of Vaporization at Boiling Point (Btu/lb)	84.62
Liquid Thermal Conductivity (W/m K)	0.081	Liquid Thermal Conductivity (Btu/hr ft °F)	0.0468
Vapor Thermal Conductivity (W/m K)	0.0125	Vapor Thermal Conductivity (Btu/hr ft °F)	0.0072
Liquid Viscosity (mPa s)	402.7	Liquid Viscosity (lb/ft hr)	0.9744
Vapor Viscosity (mPa s)	10.3	Vapor Viscosity (lb/ft hr)	0.025

\*Properties at 77 °F / 25 °C unless noted otherwise  
\*\*NIST Refprop v 7.6

Fig. 1.4-1 - R245fa chemical-physical properties table

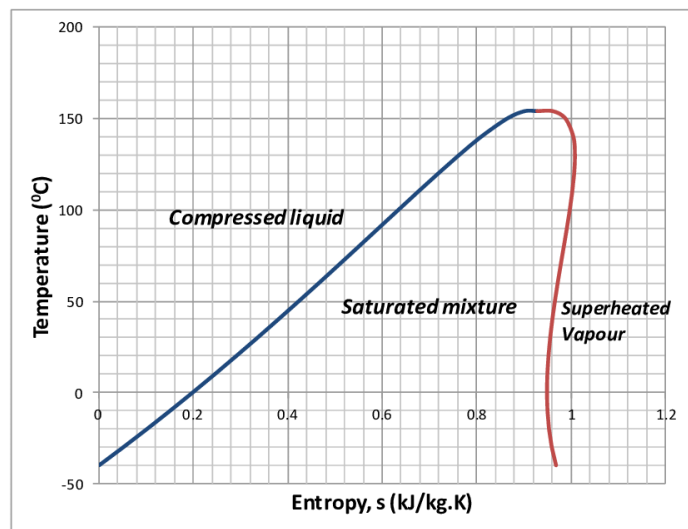


Fig. 1.4-2 - R245fa T-s diagram

## 2 Physical models at the base of heat exchangers

### 2.1 Type of heat exchangers

A heat exchanger has the purpose to transfer thermal energy between two fluids.

Nowadays, the possible models of heat exchanger are many, with differences in type, size, material, physical principle of heat exchange, direction of fluid and this implies that they can find applications in a very large range of use that varies from thermal energy values of few watts to a ten of Megawatts. From point of view of physical classification, it is possible to distinguish two main types:

- For mixture: in this case the fluids mix. The temperature of the final fluid depends from the two initial fluids and the composition of the final fluid is different from the beginning and always depends from the two initial fluids. In practice, the two initial fluids come into contact, generating a final fluid with thermodynamic and chemical-physical proprieties intermediate respect to the initial values if the individuals. Generally the fluids used for this type of heat exchanger are homogeneous.
- By surface: in this case the fluids remain separated without never coming into contact during all heat exchange. The fluids interact only at energetic level, maintaining the initial chemical proprieties and varying only their temperature. In this case the fluids may not be homogeneous.

What is generally done is to try to isolate, for example by means of glass wool, the exchanger from the external environment in order to ensure that there is a lower dissipation as possible and that largest amount of heat is only exchanged between fluids. For this reason, the hypothesis of adiabaticity is often made during the study of heat exchangers.

One of the most common types of heat exchangers are the shell and tubes ones: this belongs to the category of surface heat exchangers and them consist in two concentric pipes in which the fluids can move in co-current or counter-current.



*Fig. 2.1-1 - Shell and tube heat exchanger with two pipes*

Given that, in some cases, to obtain a heat exchange sufficient to reach a certain temperature, this type would require a very large exchange surfaces and this implies a very long length of pipes, a shell and tube with many tubes inside a larger diameter tube can be created and in this case is possible to increase the heat exchange maintaining smaller dimensions.

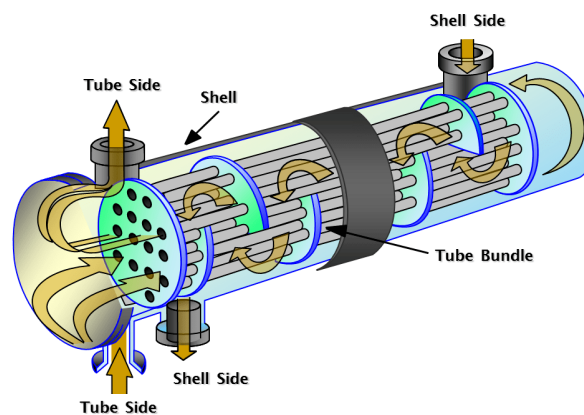


*Fig. 2.1-2 - Shell and tube heat exchanger with multiple pipes*

The main characteristics of this type of shell and tube heat exchanger are the diameter of the internal and external tubes, the material and the number of internal tubes.

## Physical models at the base of heat exchangers

A further evolution is the brazed plate heat exchanger (BPHE), which was the type present the plant analyzed in this thesis.



*Fig. 2.1-3 - External view of a BPHE*

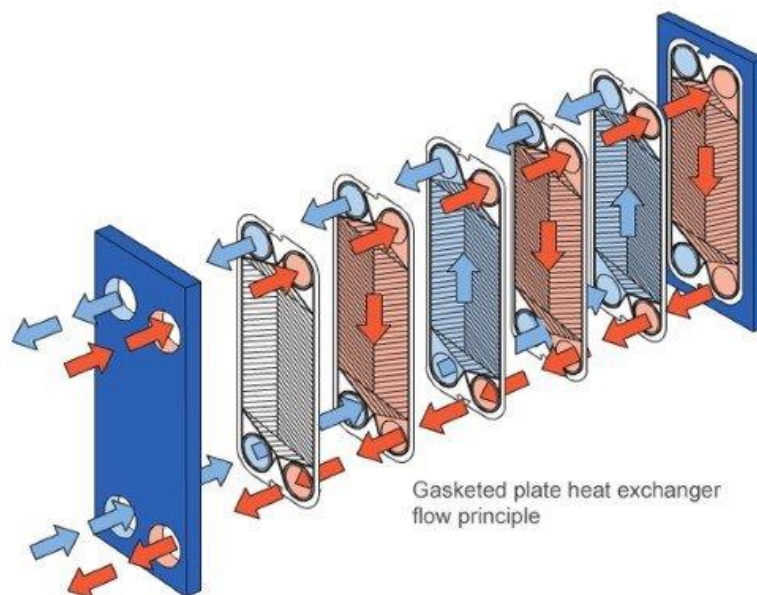


*Fig. 2.1-4 - Exploded view of a BPHE and its operation*

Although the exchange no longer takes place through circular, but flat surfaces, it is always a surface exchanger, without mix, whose operating physics is absolutely identical to the simpler case of shell and tube heat exchanger. The only real difference occurs in the study of the flow, because are often present ripples on the surfaces to maximize heat exchange and this can cause a turbulent flow. From the point of view of heat exchange and, therefore, of thermodynamic analysis it can be considered as a shell and tube exchanger without making significant errors.

## 2.2 Different possible physical approaches

There are different possibilities to consider the heat exchange inside the heat exchangers.

The main three are:

- Pure thermodynamical models (0-D)
- One dimensional simplified models or Mixed models (1-D)
- Three dimensional models (3-D)

Pure thermodynamical models (0-D) are the easiest and simplest. They represent lumped-parameter in which, therefore, the only variable is time. In this type of model, it is neglected every phenomenon directly related to the motion of the fluid, without considering any eventual phenomenon of turbulence, and all attention is focus only on the heat exchange. For this reason, it is call thermodynamic system and not thermofluidodynamic system. This model is widely used for exchanges in which the heat exchange phenomenon is largely preponderant with respect to fluidodynamic phenomenon, such as a hot fluid at rest in a container that exchange heat with the environment, or to consider ideal cases of heat exchange. However, the results obtained from these models often do not faithfully describe the real phenomenon. In this case the only possible discretization is on time, because space is not considered, and depending on the time step chosen, the simulation will be faster or will require higher computational time. Obviously, also if the case is idealized, to start the simulation it is necessary to set the initial conditions.

One dimensional model (1-D) is an implementation of the purely thermodynamic model. In this case, in addition to the heat exchange phenomenon, the kinematic phenomenon is also considered, through a one-dimensional simplification of the flow. Even if it is a model that simplifies the reality a lot, especially in presence of turbulence and eddies in the flow, it represents, with an excellent degree of precision the flows that occurs in pipes, far from the junctions. Compared to the pure thermodynamical, for this analysis, which can be defined thermofluidodynamic as the spatial variable with velocity also comes into play, the discretization will be both temporal and spatial. As in the previous case, decreasing the time step, the precision increases at the expense of computational time and the same reasoning can be applied to spatial discretization: refining the computational grid, the number of nodes in which the velocity is evaluated increase, so it is possible to have a greater precision in the description of the phenomenon, but also simulation time can extend a lot. In the one dimensional model the only relevant geometric quantity is the axial coordinate of the duct to which the flow velocity along that direction is correlated. Exactly as for the

## Physical models at the base of heat exchangers

pure thermodynamic model (0-D), to solve the problem it is necessary to set the initial conditions, but in addition it should also necessary to set the boundaries conditions at least for pressure and temperature.

The last type of possible approach is the three dimensional model (3-D). This one turns out to be the most complex, but also the most complete and realistic and, sometimes, its adoption is necessary when, in some cases, the phenomena of turbulence, eddies and flow mixing are fundamental, as for example in a junction of several ducts. The 3-D model starts with a geometric CAD model of the component and setting on it the spatial computational mesh, obviously in three dimensions. Once the mesh has been set, it is necessary to also set a solver for the turbulence, possibly adopting more or less complex methods, depending on how much turbulence represents a relevant phenomenon for the motion of the fluid, for example as occurs during combustion inside the cylinders of internal combustion engine. Having a three dimensional grid and having to consider the phenomenon of turbulence, which can be extremely complex, greatly increases the complexity of the problem and this require a lot of computational power and a significant time dilation for simulation.

What often happens, in order to find the right compromise between simulation times/costs and precision of the results, is to divide the problem into different areas and use, where the phenomena of turbulence and eddies are small, a one dimensional (1-D) model and only for the parts in which eddies and turbulence are truly preponderant, the three dimensional model.

The model that will be used to implement a physical model of the heat exchangers of the ORC in this thesis, was the one dimensional (1-D). This choice was made for two main reasons: first to simplify the modeling and reduce the simulation time, consider however the kinematic phenomena of the flow, and second because having a closed (loop) cycle, without junctions to external ducts, neglect the turbulence phenomenon can be an acceptable simplification, since the latter does not play an important role, at steady-state, in the cycle.

### 2.3 Convection phenomenon in the heat exchanger

Considering the heat exchange involving fluids circulating in a plant by means of external organs, such as pumps or fans, it is possible to speak of forced convection.

Before writing the equations that regulate the heat exchange in the exchangers without mixing, it is good to put forward some hypothesis to simplify the problem.

The first is to consider a steady-state state, neglecting all changes during the evolution and starting to study the phenomena only when is fully evolved. The second to consider a one dimensional model (1-D), so considering the influence of time and of only one spatial dimension, that corresponds to the fluid direction one. The third to have a perfect adiabatic exchanger, without any heat losses in external environment.

To simplify the writing, it is possible to identify with "1" the first fluid and with "2" the other one. If there is not mixing, so addition or extraction of fluid, it is possible to write a mass balance equation for a control volume around the heat exchanger.

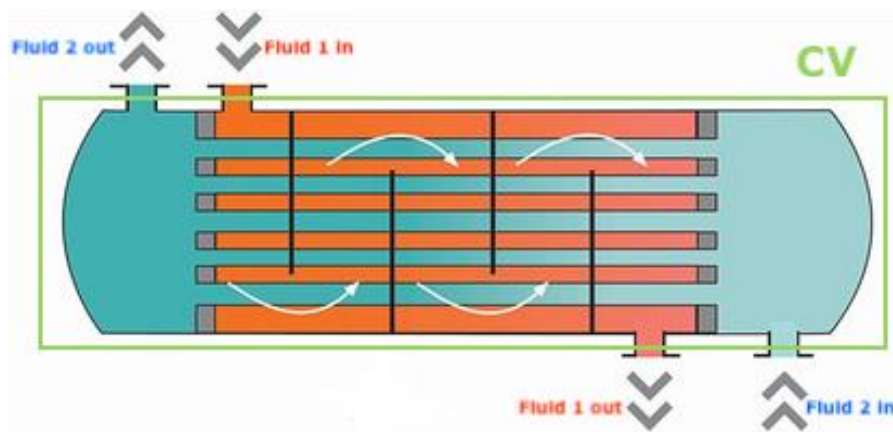


Fig. 2.3-1 - control volume for an heat exchanger

The mass balance equation is:

$$\dot{m}_{1in} = \dot{m}_{1out} \quad \text{Equation 1}$$

$$\dot{m}_{2in} = \dot{m}_{2out} \quad \text{Equation 2}$$

So that the exchanger can work, it is necessary to have a temperature difference, it is possible to speak of hot fluid and cold fluid.

## Physical models at the base of heat exchangers

The balance equations can be rewritten with the different subscripts:

$$\dot{m}_{c_{in}} = \dot{m}_{c_{out}} = \dot{m}_c \quad \text{Equation 3}$$

$$\dot{m}_{h_{in}} = \dot{m}_{h_{out}} = \dot{m}_h \quad \text{Equation 4}$$

Now is possible to write the energy balance equation, considering the adiabatic hypothesis, in which all heat is exchanged only between fluids. In this case the system is open, so it is possible to write the balance in terms of unit of mass enthalpy.

$$\dot{Q}_{cold} = \dot{Q}_{hot} \quad \text{Equation 5}$$

$$\dot{m}_h h_{h_{in}} + \dot{m}_c h_{c_{in}} = \dot{m}_h h_{h_{out}} + \dot{m}_c h_{c_{out}} \quad \text{Equation 6}$$

$$\dot{m}_h (h_{h_{in}} - h_{h_{out}}) = \dot{m}_c (h_{c_{in}} - h_{c_{out}}) \quad \text{Equation 7}$$

However, the control volume considered is not the only possible one. There is, in fact, another interesting possibility of choosing a control volume and it corresponds to center it between the hot and cold fluid. For comprehensive and visual simplicity, let's consider a two pipes shell and tube heat exchanger and to build the control volume at the interface between the two fluids:

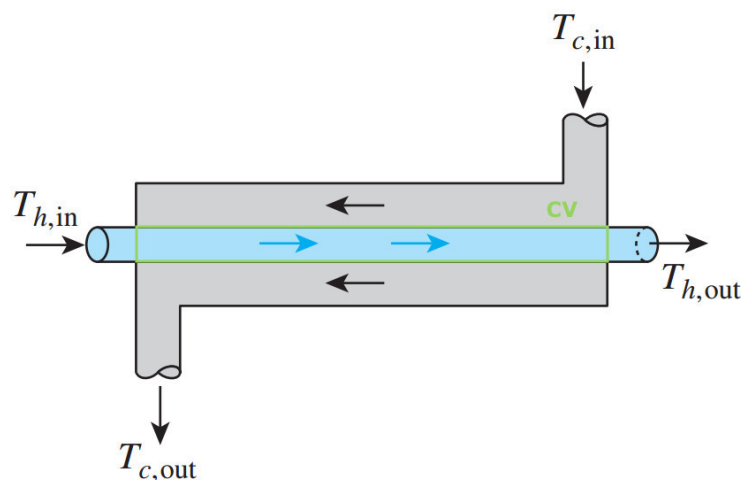


Fig. 2.3-2 – C.V. in two pipes heat exchanger

In this case, by writing the energy balance equation respect to this new control volume for both cold and hot side, there is a thermal flow which exit from this one.

## Physical models at the base of heat exchangers

In particular it is considered the case in which is possible to neglect the kinetic and potential energy:

$$\dot{m}_h h_{h_{in}} = \dot{Q}_t + \dot{m}_h h_{h_{out}} \Rightarrow \dot{Q}_t = \dot{m}_h (h_{h_{in}} - h_{h_{out}}) \quad \text{Equation 8}$$

$$\dot{m}_c h_{c_{in}} = \dot{Q}_t + \dot{m}_c h_{c_{out}} \Rightarrow \dot{Q}_t = \dot{m}_c (h_{c_{in}} - h_{c_{out}}) \quad \text{Equation 9}$$

Obviously, it is immediately possible to see that, if the hypothesis of an adiabatic exchanger is valid, the outgoing or incoming thermal power in the control volume for cold and hot side is the same.

To find the mass enthalpy value, it is possible to use state diagrams, if the fluid contains a double phase, such as during the vaporization or condensation phase of an organic fluid in a ORC, or by multiplying the specific heat at constant pressure and the temperature, if the fluid consist of a single phase, as for water. If the last case is considered, the thermal power in the control volume is equal to:

$$\dot{Q}_t = C_h (T_{h_{in}} - T_{h_{out}}) = C_c (T_{c_{in}} - T_{c_{out}}) \quad \text{Equation 10}$$

With:

- $C_h = \dot{m}_h c_{p_h}$  : for hot fluid
- $C_c = \dot{m}_c c_{p_c}$  : for cold fluid

Furthermore, if the fluid is completely in the liquid phase, as for water, it can be considered as incompressible and the specific heat evaluated at constant pressure is equal to the specific heat evaluated at constant volume:

$$c_p = c_v$$

If, on the other hand, the fluid is in gaseous phase only, such as completely vaporized organic fluid, is possible to consider it as ideal, finding that the specific heat at constant pressure is:

$$c_p = \frac{dh}{dT}$$

Which depends only by the temperature.

## Physical models at the base of heat exchangers

To obtain an equation that allows to describe in the most realistic way possible, the heat flux within the type of exchanger analyzed, it is also necessary to take into account the phenomenon of convective resistance.

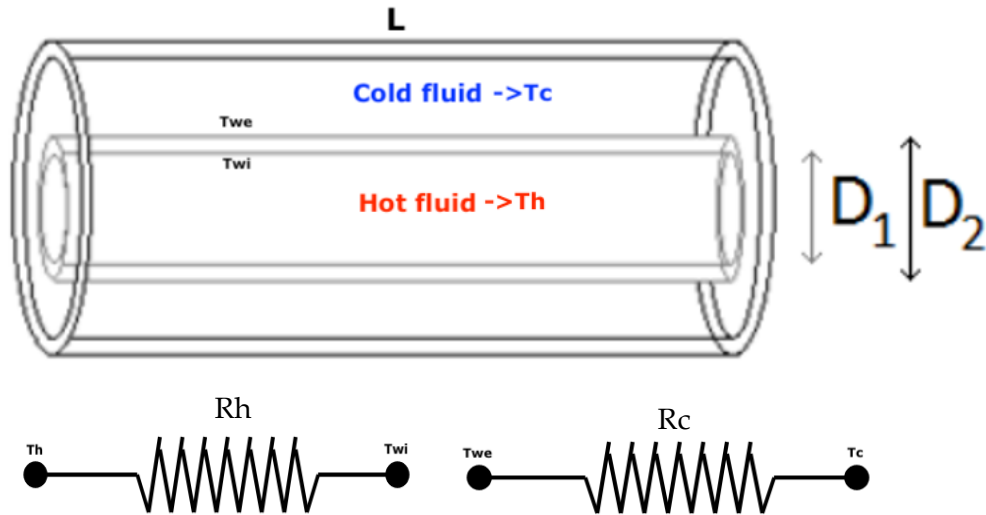


Fig. 2.3-3 - Convection resistance scheme

$$R_h = \frac{1}{h_h A_h} = \frac{1}{h_h \pi D_1 L}$$

Equation 11

$$R_c = \frac{1}{h_c A_c} = \frac{1}{h_c \pi D_2 L}$$

Equation 12

With:

- $h_h$  and  $h_c$  are respectively the hot and cold convective heat transfer coefficient (and not the mass enthalpies).
- $A_h$  and  $A_c$  are respectively the hot and cold transfer areas.
- $D_1$  is the internal diameter where the temperature is  $T_{wi}$ <sup>2</sup>.
- $D_2$  is the internal diameter where the temperature is  $T_{we}$ <sup>2</sup>.

<sup>2</sup> Practically the difference between  $D_1$  and  $D_2$  gives twice the thickness of the inner tube:  $D_2 - D_1 = 2s$ .

### 2.3.1 Convective heat transfer coefficient

The convective heat transfer coefficient in smooth pipes is calculated using the Colburn analogy.

$$h = \frac{1}{2} C_f \rho U_{eff} C_p Pr^{(-2/3)} \quad \text{Equation 13}$$

With:

- $C_f$ : friction coefficient of smooth pipe
- $\rho$ : density
- $U_{eff}$ : effective fluid speed out from the boundary layer
- $C_p$ : specific heat
- $Pr$ : Prandtl number

The Colburn analogy is used for all types of flux: turbulent, laminar and mixed.

When the flow is surely laminar<sup>3</sup>, it is possible to evaluate the convective heat transfer coefficient in this way:

$$h = \frac{Nu \cdot k}{d} \quad \text{Equation 14}$$

With:

- $Nu$ : Nusselt number
- $k$ : thermal conductivity coefficient
- $d$ : pipe diameter

For the laminar case  $Nu$  is imposed equal to 3,66.

For mix flow<sup>4</sup>, the convective heat transfer coefficient is calculated using the *Equation 14*, interpolating the Nusselt number.

For turbulent flow<sup>5</sup> is directly used the Colburn relation in the *Equation 13*.

---

<sup>3</sup> Reynold number lower than 2000.

<sup>4</sup> Reynold number between 2000 and 4000.

<sup>5</sup> Reynold number higher than 4000.

## Physical models at the base of heat exchangers

The Equation 13 is used to evaluate the convective heat transfer coefficient, is valid for circular section and smooth pipes. In case of other type of section, as for rectangular, or if the pipe is not smooth, but has a certain surface roughness, as happens in the exchanger model used in this thesis, is necessary to introduce some correction factors.

In the program GT-Suite, which was used in this thesis, all this correction factors were considered thanks a coefficient called “*Heat transfer multiplier*”, which will be analyzed in depth in the following chapters.

### 2.4 Conduction phenomenon

To correctly complete the description of the heat exchange phenomenon inside the exchanger, it is also necessary to consider the conduction phenomenon that occurs between the two faces of the plate that separates the hot and cold fluids. Specifically, it is important to consider the conductive resistance that is generated when the heat flux passes through the plate.

The conductive resistance scheme turns out to be:

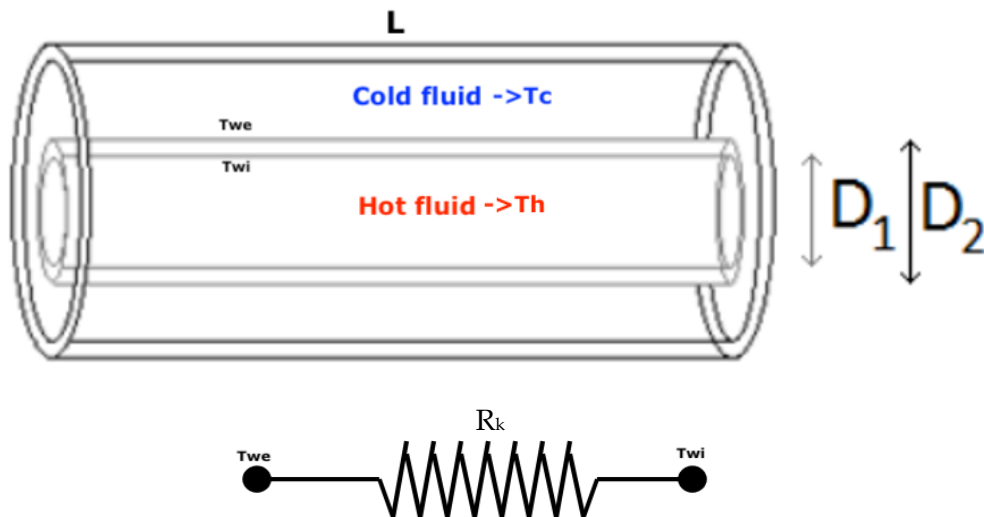


Fig. 2.4-1 - Conduction resistance scheme

$$R_k = \frac{\ln\left(\frac{D_2}{D_1}\right)}{2\pi kL}$$

Equation 15

With:

- $k$  is the conductive heat transfer coefficient.

## 2.5 Overall exchanged thermal power

To conclude the discussion, considering now all the listed thermal resistances, it is possible to write the total exchanged thermal power.

Before writing the final equation, it is good to specify that also the contribution of thermal radiation resistance should also be considered. However, this last one, is neglected because is much lower than the convective and conduction contributions. Take care because this not imply that the radiation does not take part in the heat transfer, its contribution is automatically calculated by the program in order to evaluate the temperature at the plate wall , but only the contribution of resistance for the calculation of the exchanged thermal power is not considered.

Then, having made the previous precision, it is possible to proceed with the writing of the exchanged thermal power equation between the two fluids:

$$\dot{Q}_t = \frac{(T_h - T_c)}{R_h + R_c + R_k} = UA(T_h - T_c) \quad \text{Equation 16}$$

With:

- U is the global unitary conductance.
- A is the exchange surface between the two fluids and is the surface on which the calculation of U is based.
- $T_h$  and  $T_c$  are the temperatures of the hot and cold fluids respectively.

The main problem that arises is to identify the value of  $T_h$  and  $T_c$ , since they vary along the exchanger.

To solve this problem, it is first necessary to display the temperature trend as a function of the axial direction, choosing the exchange area as the independent variable.

At this point it is possible to distinguish the cases of co-current and counter-current flow.

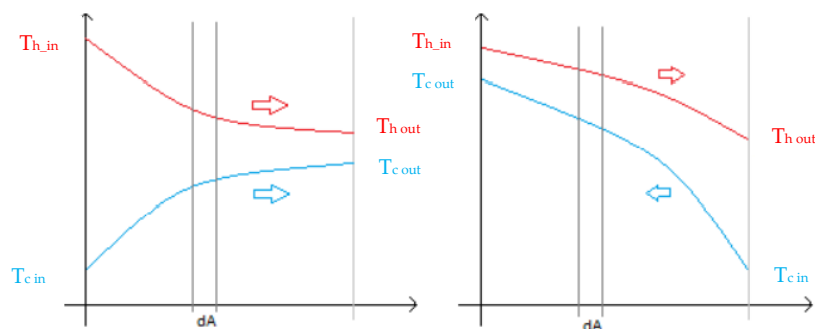


Fig. 2.5-1 - Co-current (left) and counter-current (right) flow temperatures trend

## Physical models at the base of heat exchangers

Considering an infinitesimal exchange length  $dL$ , which gives an infinitesimal exchange area  $dA$ , it is possible to write the heat power balance equation for hot fluid:

$$\partial\dot{Q} = -\dot{m}_h c_h dT_h \quad \text{Equation 17}$$

The minus sign is always present, regardless the type of flow, for the hot fluid since, due the sign convention, the thermal power yielded is positive, but  $dT_h$  is negative because the temperature of hot fluid decrease along the axial direction, so the initial minus sign is necessary to have sign concordance with the convention.

For cold fluid the heat power balance equation is:

$$\partial\dot{Q} = \pm\dot{m}_c c_c dT_c \quad \text{Equation 18}$$

The case of the cold fluid is different because the balance *Equation 18* can be both positive and negative. The sign convection states that the received thermal power is negative, but for the co-current flow the  $dT_c$  is positive, because the cold fluid flow agrees with the positive axial direction, so the its temperature increase, so the right initial sign is minus, which gives the negative sign in the balance equation, while for the counter-current flow the  $dT_c$  is negative, because the flow direction is opposite to the positive axial direction (assumed the hot fluid direction) and there is, in fact, a decrease of cold temperature between inlet and outlet and so the right initial sign is plus, which this give, also in this case, to the balance equation a negative sign.

Isolating the infinitesimal temperature variation:

$$dT_h = -\frac{\partial\dot{Q}}{c_h} \quad \text{Equation 19}$$

$$dT_c = \pm\frac{\partial\dot{Q}}{c_c} \quad \text{Equation 20}$$

By subtracting member by member to obtain the infinitesimal temperature difference between hot fluid and cold fluid, it is possible to obtain:

$$d(T_h - T_c) = -\partial\dot{Q} \left( \frac{1}{c_h} \pm \frac{1}{c_c} \right) \quad \text{Equation 21}$$

## Physical models at the base of heat exchangers

Now it is possible to define the coefficient:

$$M \stackrel{\text{def}}{=} \frac{1}{c_h} \pm \frac{1}{c_c} \quad \text{Equation 22}$$

The sign inside the coefficient depends on the type of flow that is present.

Now it is possible to make some simple mathematical steps:

$$d\Delta T = -M\delta\dot{Q} = -MU\Delta T dA \quad \text{Equation 23}$$

$$\frac{d\Delta T}{\Delta T} = -MU dA \quad \text{Equation 24}$$

$$\int_{\Delta T_a}^{\Delta T_b} \frac{d\Delta T}{\Delta T} = - \int_0^{A_{tot}} U M dA \quad \text{Equation 25}$$

With:

- $\Delta T_a$  that is the temperature difference for  $A = 0$ <sup>6</sup>
- $\Delta T_b$  that is the temperature difference for  $A = A_{tot}$ <sup>7</sup>

From the integration operation is obtained:

$$\ln \frac{\Delta T_b}{\Delta T_a} = -UM A_{tot} \quad \text{Equation 26}$$

$$\Delta T_b = \Delta T_a e^{-UM A_{tot}} \quad \text{Equation 27}$$

Isolating the coefficient  $M$ :

$$M = \frac{\ln \frac{\Delta T_b}{\Delta T_a}}{U A_{tot}} \quad \text{Equation 28}$$

---

<sup>6</sup> The area  $A = 0$  corresponds to the length  $L = 0$ , therefore, is possible to identify it, if was chosen the positive direction the hot fluid direction one, as inlet.

<sup>7</sup> The area  $A = A_{tot}$  corresponds to the length  $L = L_{tot}$ , therefore, is possible to identify it, if was chosen the positive direction the hot fluid direction one, as outlet.

### 2.5.1 Co-current case

$$M \stackrel{\text{def}}{=} \frac{1}{C_h} + \frac{1}{C_c}$$

$$dT_h = -\frac{\partial \dot{Q}}{C_h} = -\frac{U dA \Delta T}{C_h}$$

$$dT_c = -\frac{\partial \dot{Q}}{C_c} = \frac{U dA \Delta T}{C_c}$$

It is possible to write:

$$\frac{dT_h}{dA} = -\frac{U \Delta T}{C_h}$$

$$\frac{dT_c}{dA} = \frac{U \Delta T}{C_c}$$

Making the second derivatives it is possible to obtain:

$$\frac{d^2 T_h}{dA^2} > 0$$

$$\frac{d^2 T_c}{dA^2} < 0$$

Going back to review the *Fig.2.5-1*, for co-current (left image), it is possible to see that  $T_h(A)$  is described by a decreasing curve with downward concavity, while  $T_c(A)$  is described by an increasing curve with upward concavity.

### 2.5.2 Counter-current case

$$M \stackrel{\text{def}}{=} \frac{1}{C_h} - \frac{1}{C_c}$$

In this case, depending on the relation between  $C_h$  and  $C_c$ , three different cases are possible:

1.  $C_h = C_c$

In this case:

$$M = 0 \Rightarrow \Delta T_b = \Delta T_a = \text{cost}$$

## Physical models at the base of heat exchangers

This case describes, for example, the case in which both hot fluid and cold fluid are exactly the same fluid, with the same identical properties.

$$\frac{dT_h}{dA} = -\frac{U\Delta T}{C_h} = \text{const}$$

$$\frac{dT_c}{dA} = -\frac{U\Delta T}{C_h} = \text{const}$$

Graphically:

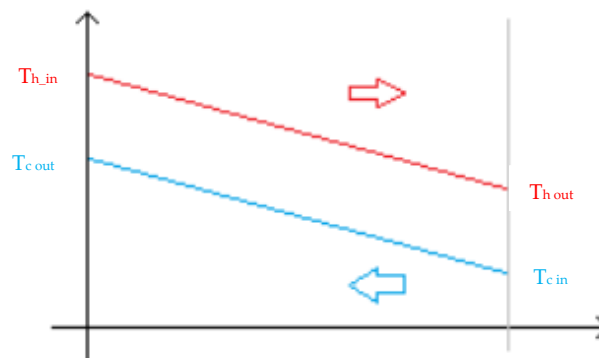


Fig. 2.5-2 - Counter-current flow with  $C_h = C_c$

### 2. $C_h > C_c$

In this case:

$$M < 0 \Rightarrow \Delta T \text{ increases along the axial direction}$$

So:

$$\frac{dT_h}{dA} = -\frac{U\Delta T}{C_h} \Rightarrow \Delta T \text{ that decreases} \Rightarrow \frac{d^2T_h}{dA^2} < 0$$

$$\frac{dT_c}{dA} = -\frac{U\Delta T}{C_c} \Rightarrow \Delta T \text{ that decreases} \Rightarrow \frac{d^2T_c}{dA^2} < 0$$

Physical models at the base of heat exchangers

Graphically:

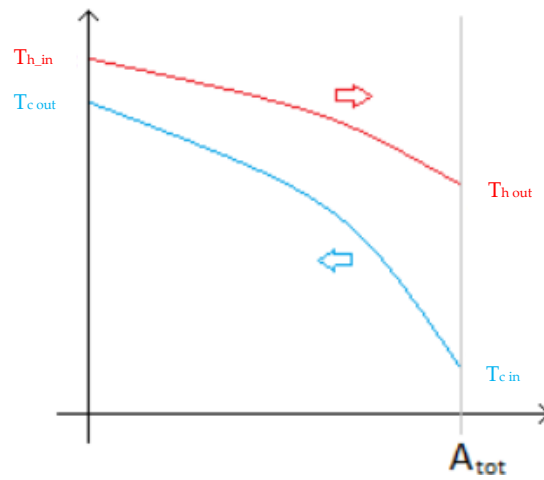


Fig. 2.5-3 - Counter-current flow with  $C_h > C_c$

3.  $C_h < C_c$

In this case:

$M > 0 \Rightarrow \Delta T$  decreases along the axial direction

$$\frac{d^2 T_h}{dA^2} > 0$$

$$\frac{d^2 T_c}{dA^2} > 0$$

Graphically:

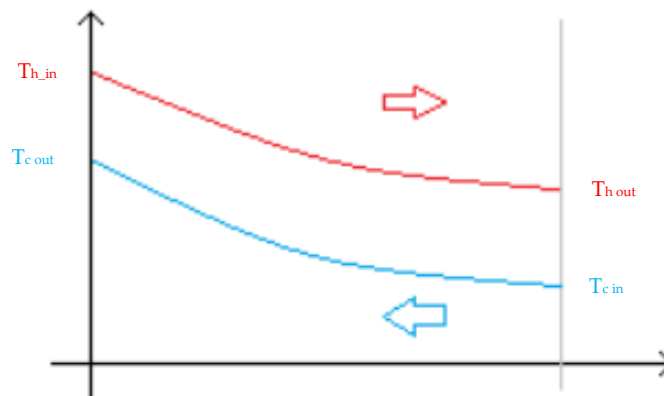


Fig. 2.5-4 - Counter-current flow with  $C_h < C_c$

Physical models at the base of heat exchangers

Now going back to the *Equation 23*, reworking can be achieved:

$$\partial \dot{Q} = U dA \Delta T \quad \text{Equation 29}$$

Not considering  $A_{tot}$ , but only a generic exchange area  $A$ , the temperature difference, for this generic area, can be written starting from the *Equation 27*:

$$\Delta T = \Delta T_a e^{-UMA} \quad \text{Equation 30}$$

Substituting *Equation 30* in the *Equation 29* and integrating it on the total exchange area  $A_{tot}$ , it ends up with:

$$\int_0^{A_{tot}} \partial \dot{Q} = \int_0^{A_{tot}} U dA \Delta T_a e^{-UMA} \quad \text{Equation 31}$$

$$\dot{Q} = -\frac{\Delta T_a}{M} (e^{-UMA_{tot}} - 1) \quad \text{Equation 32}$$

Substituting the definition of  $M$  in *Equation 28* inside the *Equation 32*, it is possible to obtain:

$$\dot{Q} = -\frac{\Delta T_a}{\frac{\ln \frac{\Delta T_b}{\Delta T_a}}{UA_{tot}}} (e^{-UMA_{tot}} - 1) = -\frac{UA_{tot} \Delta T_a}{\ln \frac{\Delta T_b}{\Delta T_a}} (e^{-UMA_{tot}} - 1) \quad \text{Equation 33}$$

And substituting the *Equation 27* inside this last *Equation 33*:

$$\dot{Q} = UA_{tot} \frac{\Delta T_b - \Delta T_a}{\ln \frac{\Delta T_b}{\Delta T_a}} \quad \text{Equation 34}$$

Calling the logarithmic mean temperature:

$$\Delta T_{ml} = \frac{\Delta T_b - \Delta T_a}{\ln \frac{\Delta T_b}{\Delta T_a}} \quad \text{Equation 35}$$

With:

- $\Delta T_a$  represents the temperature difference at the inlet of the exchanger
- $\Delta T_b$  represents the temperature difference at the outlet of the exchanger

## Physical models at the base of heat exchangers

It ends up by substituting *Equation 35* into *Equation 34*:

$$\dot{Q} = UA_{tot}\Delta T_{ml} \quad \text{Equation 36}$$

*Equation 36* ends the discussion of the description of the thermal power exchanged inside shell and tube heat exchanger, between the hot and cold flows, for both cases of co-current or counter-current flow directions.

It can be summarized by saying that the thermal power is influenced by three factors:

- $U$ : conductance per unit of area, closely related to the conductive and convective resistances.
- $A_{tot}$ : overall heat exchange area between the two flows.
- $\Delta T_{ml}$ : directly related to the boundary conditions of inlet and outlet temperatures of hot and cold fluids.

## 3 Map-based model

### 3.1 Plant description

An Organic Rankine Cycle power plant consists, in general, of several components:

- A compressor or pump: it has the function of increasing the pressure of operating fluid, generally in the liquid state in this phase, and for its operation it is necessary to supply it with external power.
- A turbine or expander: inside it the fluid expands, generally passing from the liquid phase to gaseous or fraction phase, generating useful power. This component works in conjunction, typically, with an alternator, to convert mechanical power into electrical power.
- Two or more heat exchangers: one acting as an evaporator and the other as a condenser. They have the task to change the phase of the working fluid, extracting its heat.

#### 3.1.1 Pump

In the plant considered, the pump was a volumetric piston pump. The brand was *Cat Pumps*® and the specific model was *1051CM*. In this case a volumetric piston pump was an excellent choice as it allows to work with low flow rate, but with high pressure jumps. Furthermore, the considered model of pump had the characteristic of having a quite almost linear relationship between its rotational speed and the moved mass flow rate.

The technical characteristics of the pump used are summarized in the table below:

<b>MAX SPEED [RPM]</b>	450
<b>BORE [mm]</b>	25
<b>STROKE [mm]</b>	30
<b>MAXIMUM WORKING PRESSURE [bar]</b>	152

*Table 3.1-1 – Cat Pump® model 1051CM characteristics*



Fig. 3.1-1 – Cat Pump® model 1051CM

### 3.1.2 Expander

The expander used was of scroll type. The use of this particular type of expander was very innovative, because it is generally used as a compressor, in particular in the air conditioning systems, and not as expander. Its design is of the new generation and its operation is exactly the same, but with opposite purpose, compared to the more common use as compressor. In particular, the brand of the expander used in the plant analyzed was *Air Squared*® and the specific model is *E22H038B-L-SH*. The main characteristics are summarized in the following table:

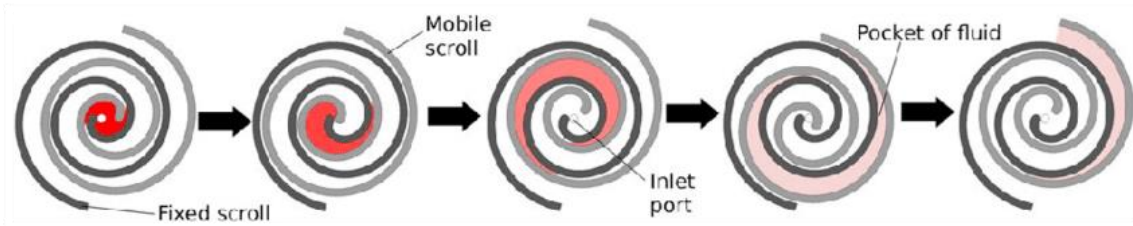
<b>NOMINAL POWER [Kw]</b>	5
<b>BUILT-IN VOLUME RATIO</b>	3,5
<b>DISPLACEMENT VOLUME [cm<sup>3</sup>]</b>	73,6
<b>MAXIMUM INLET PRESSURE [kPa]</b>	1380
<b>MAXIMUM WORKING TEMPERATURE [°C]</b>	175
<b>SPEED WORKING RANGE [RPM]</b>	500-3600

Table 3.1-2 – Air Squared® model E22H038B-L-SH main characteristics

It is possible to immediately make an interesting observation: this specific component can be used only in systems with low boiling temperature operating fluids, such as organic fluids. This because, by analyzing the maximum working temperature, it turns out to be only 175 °C, if it is used within a classic Rankine cycle with steam as operating fluid, generally entering in the expander at several

## Map-based model

hundred degrees centigrade, there would be a structural failure of the component or, perhaps, its major damage.



*Fig. 3.1-2- Scroll expander functioning*



*Fig. 3.1-3 - Air Squared® model E22H038B-L-SH*

### 3.1.3 Heat exchangers

In the specific plant considered there were not two, but three heat exchangers. One performs the function of evaporator to bring the operating fluid from liquid to gaseous phase, one the function of condenser, to bring the fluid from gaseous phase to the liquid phase and the third, called sub-cooler, to further subcooling the liquid. This last one had smaller dimensions respect the previous two, was placed immediately before the suction of the pump and had a safety function, in order to prevent that biphasic fluid enters in the pump.

All the exchangers present in the plant considered were made of AISI 304 stainless steel and were of the brazed plate type. For this reason, were called brazed plate heat exchangers (BPHE).

It was decided to opt for these exchangers because, as for this application with fluids at low temperatures and pressures, they can guarantee a better heat exchange, in a smaller volume,

Map-based model

compared to the classical shell and tube exchangers. However, all the theory seen so far for shell and tube, is perfectly valid also for BPHE.

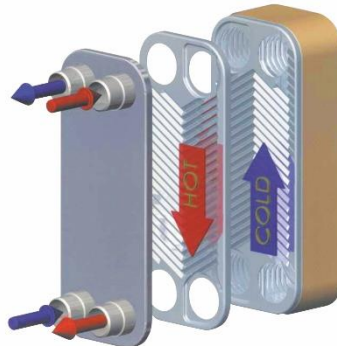


Fig. 3.1-4 - BPHE internal functioning scheme

The specific used exchangers are all produced by the brand *SWEP* and are two different models. The evaporator and condenser are identical and their model is *B80Hx70/1P-SC-S 4x24U*, the sub-cooler model is *B10THx16/1P-SC-M*.

The main characteristics of this exchangers are summarized in the following table:

	<b>CONDENSER AND EVAPORATOR</b>	<b>SUB-COOLER</b>
<b>PRIMARY MEDIA VOLUME [cm<sup>3</sup>]</b>	3942,72	426,88
<b>SECONDARY MEDIA VOLUME [cm<sup>3</sup>]</b>	4059,07	487,84
<b>A [mm]</b>	523,875	292,1
<b>B [mm]</b>	114,3	114,3
<b>MAXIMUM WORKING FLUID TEMPERATURE [°C]</b>	240	240
<b>MAXIMUM WORKING FLUID PRESURE [kPa]</b>	4481,59	4481,59
<b>NUMBER OF PLATES</b>	70	16
<b>PLATE THICKNESS [mm]</b>	0,3	0,3

Table 3.1-3 - *SWEP* model *B80Hx70/1P-SC-S 4x24U* (left) and *B10THx16/1P-SC-M* (right) characteristics



Fig. 3.1-5 - SWEP model B80Hx70/1P-SC-S 4x24U

### 3.2 Overall experimental plant

In the scheme below it is possible to see the experimental plant, constructed by the student Felipe Airoidi during his thesis work *"Experimental characterization of scroll expander for small-scale power generation in an Organic Rankine Cycle"*, which was used as reference to build, first, the map-based and then physical-based components, as a whole.

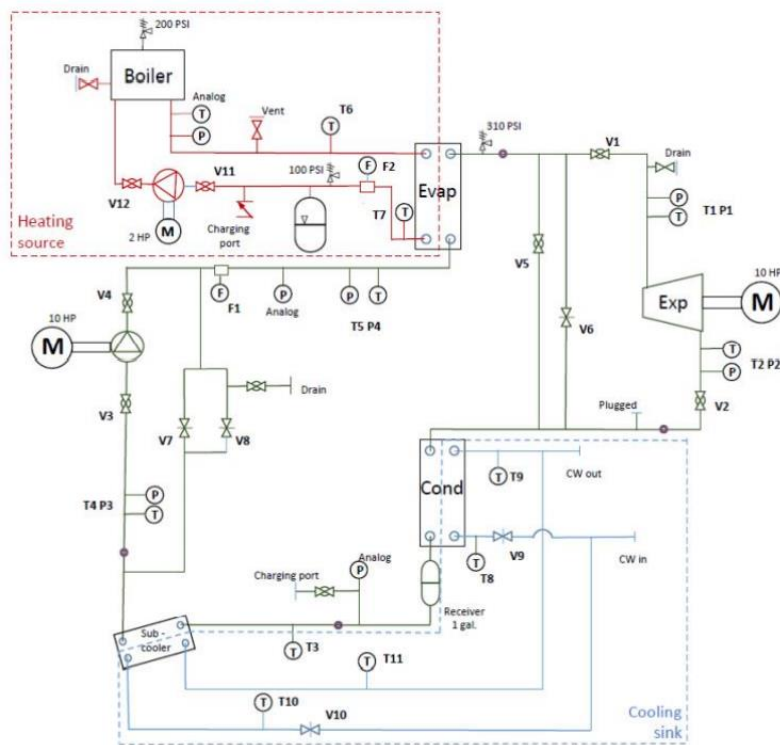


Fig. 3.2-1 - General scheme of the experimental reference plant

### 3.3 Map-based model building

As first step it has been decided to build the model of ORC circuit, using the data collected from experimental plant<sup>8</sup>. This work was made with two different purposes: the first one to familiarize with the principal software used in this thesis work GT-Suite and second one to check and understand all result obtained from the map-based model, to be able to make, in a second time, a correct comparison with the physical-based model, that will be explained in the next chapters. So, thanks this starting work, was possible to understand how all components works, their driving constitution equations and how these components interact with each other.

### 3.4 Single components building process

The model constructed in this phase was a map-based model. This means that the components were built on the basis of their functioning maps, coming from the collected experimental data.

The construction of each component can be divided in two steps.

#### 3.4.1 Step 1

Once the component to build has been selected, as first, it has been looked and analyzed all characteristics of every specific element, thanks the function “*Help*”, which was present for any component, and allowed to understand the function of all these and all inputs necessary for their operation which must be entered. For some fields, in addition to the description, there were the constitution equations that regulate the functioning of the components, for a specific value considered. To complete the “*Help*” function, generally, was given a small example of how the component can be used in a circuit.

---

<sup>8</sup> Values taken from the thesis “Experimental characterization of scroll expander for small-scale power generation in an Organic Rankine Cycle” of Felipe Airoidi.

## Map-based model

It is reported, for example, the case of the *Receiver*:

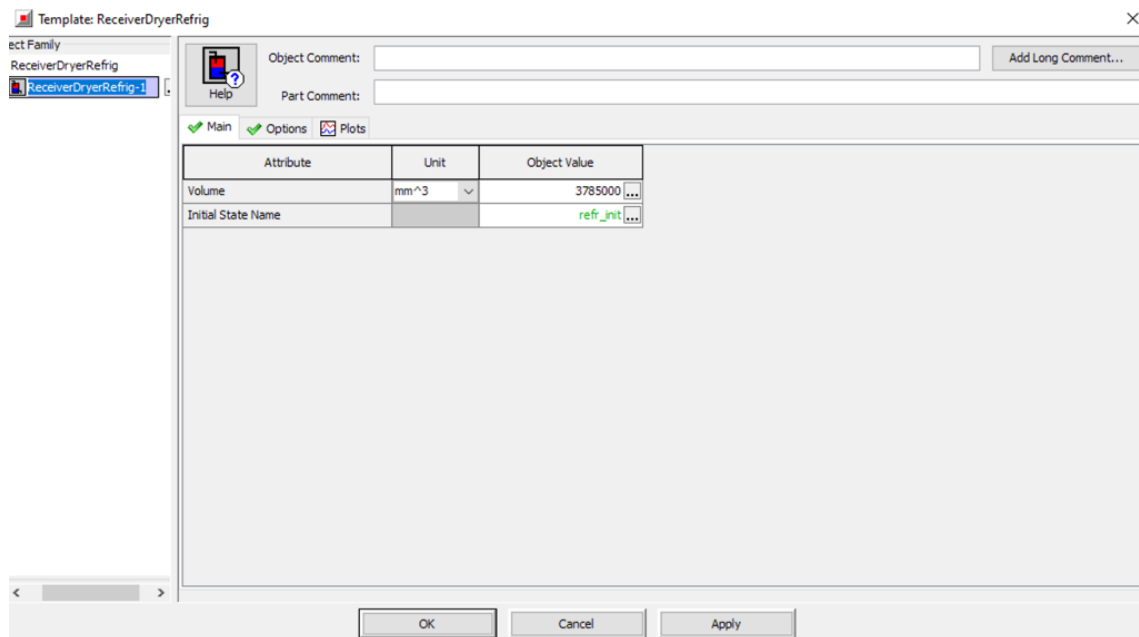


Fig. 3.4-1 - Template of Receiver

### **ReceiverDryerRefrig - Receiver Dryer for Refrigerant Circuit**

This template, representing a receiver/dryer in an air conditioning circuit, is typically used on the high pressure side in air conditioning systems that use a thermal expansion valve, or in on the low side in Rankine cycle systems. The receiver/drier is designed primarily to store excess liquid, or in the case of non-liquid inlet from the condenser, provide saturated liquid at the outlet until the threshold is reached (see mixing threshold attribute below).

It is important to note that even though during normal operation, when the output of this template is liquid (see description of mixing threshold attribute), any pressure losses that occur in downstream volumes **can** cause the fluid to appear to be two phase. This is because only a very small amount of pressure drop is needed for the fluid to drop below the liquid saturation line, and become two phase.

#### **Main**

<b>Volume</b>	'ReceiverDryerRefrig' volume.
<b>Initial State Name</b>	Name of the reference object describing the initial conditions inside the 'ReceiverDryerRefrig'.

#### **Options**

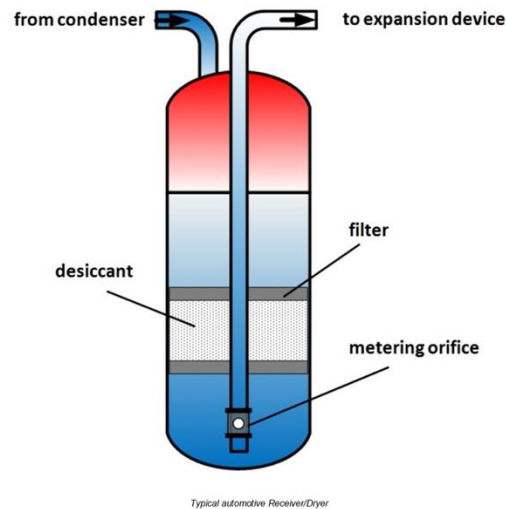
<b>Receiver Dryer Mixing Threshold</b>	Volume fraction limit for mixing in the 'ReceiverDryerRefrig'. When the liquid volume fraction (LVF - this can be thought of as a non-dimensional height of liquid) is above this value, the outlet of the 'ReceiverDryerRefrig' is only liquid phase. When the LVF is below this value, the outlet is a two phase mixture. By default, this value is 10 percent ("def" = 0.1).
--	---

$$LVF = \frac{V_{liquid}}{V_{liquid} + V_{vapor}}$$

where LVF is the liquid volume fraction,  $V_{liquid}$  is the volume of liquid, and  $V_{vapor}$  is the volume of vapor. The LVF may vary from 0 (pure vapor) to 1 (pure liquid).

Fig. 3.4-2 - "Help" function of Receiver, page 1

## Map-based model



**Configuration:**

A flow inlet and outlet is required for this template.

This template can be used without thermal connections, in which case an adiabatic tank is assumed.

To model heat losses, a separate thermal component to represent the wall mass needs to be connected, using typically using a "ThermalMass" or "ThermalNode" component. Heat transfer from the fluid to the wall mass occurs through a "ConvectionConn" connection, where it uses the convection heat transfer coefficient and surface area.

Fig. 3.4-3 - "Help" function of Receiver, page 2

### 3.4.2 Step 2

After understanding the operation of each field of the component, it was necessary to fill them. To do this, it has begun form the experimental data stored in some Microsoft Excel sheets. It has proceeded to find the necessary data for the specific component being rebuilt and to copy and entering them in the required field.

Since, to reconstruct an operating map of all components of the ORC circuit truthful and reliable as possible, it was necessary to acquire 61 operating values for each field to be filled. In order to have greater control on the simulations that were performed, it was decided to insert the different values into a set of cases with the aim of being able to decide, during the simulation phase, to start the simulation for all cases or only for some of them.

# Map-based model

Case Setup - C:\Users\Alessandro\Desktop\Impianto mio ORC\Impianto ORC.gtm

Options Folders

Help Tile 2nd Setup Append Case Insert Case(s) Delete Case(s) Subassembly Parameters Add Parameter(s) Add Super Parameter Delete Parameter Find Parameter Turn On All Turn Off All Show Formula Hide Inactive Propagate Value Change

Parameter	Unit	Description	Case 1	Case 2	Case 3	Case 4	Case 5	Case 6	Case 7	Case 8
Case On/Off		Check Box to Turn Case On	<input checked="" type="checkbox"/>							
Case Label		Unique Text for Plot Legends								
pump_rpm	RPM	Pump speed RPM	80	80	80	80	80	80	80	80
Evap_HT_Mult_1ph		Single Phase Refrigerant Heat Transf...	25	25	25	25	25	25	25	25
Evap_HT_Mult_2ph		Two Phase Refrigerant Heat Transfer...	25	25	25	25	25	25	25	25
Refr_temperature_initial	C	System initial temperature	14.94	14.75	14.77	14.85	14.82	15.07	14.91	14.56
Evap_Water_pressure_init	bar	Pressure (Absolute)	2	2	2	2	2	2	2	2
Evap_Water_pressure_out	bar	Evaporator pressure water outlet	2	2	2	2	2	2	2	2
Evap_Water_temp_initial	C	Evaporator water temperature initial	110.21	110.27	85.13	110.31	110.04	110.3	110.36	110.15
Evap_Water_temp_out	C	Evaporator water temperature outlet	101.09	101.87	77.74	101.32	99.21	99.9	101.84	101.77
Evap_water_inlet_MFR	kg/s	Evaporator water inlet mass flow rate	0.58	0.615	0.624	0.616	0.583	0.617	0.615	0.617
Evap_water_temp_inlet	C	Evaporator water temperature inlet	110.21	110.27	85.13	110.31	110.04	110.3	110.36	110.15
turbine_RPM	RPM	Turbine(expander) outlet angular spe...	800	800	800	800	800	800	1600	1600
Cond_coolant_temp_init	C	Condenser coolant (water) initial tem...	13.81	13.68	13.63	13.81	13.67	13.95	13.9	13.99
Cond_coolant_pressure_init	bar	Condenser coolant (water) initial pres...	2	2	2	2	2	2	2	2
Cond_coolant_temp_out	C	Condenser coolant (water) temperat...	22.11	20.87	21.69	21.88	23.94	22.81	21.18	21.24
Cond_coolant_pressure_out	bar	Condenser coolant (water) pressure ...	2	2	2	2	2	2	2	2
Cond_coolant_inlet_MFR	kg/s	Condenser coolant (water) inlet MFR	0.534	0.62	0.509	0.618	0.536	0.62	0.616	0.627
Cond_coolant_temp_in	C	Condenser coolant (water) temperat...	13.81	13.68	13.63	13.81	13.67	13.95	13.9	13.99
Cond_Ref_1ph_HTCMult		Liquid Phase Heat Transfer Multiplier	25	25	25	25	25	25	25	25
Cond_Ref_2ph_HTCMult		Liquid Phase Heat Transfer Multiplier	25	25	25	25	25	25	25	25
Refrigerant		Refrigerant fluid	R249FA							
Refr_temp_init	C	Refrigerant temperature initial	14.94	14.75	14.77	14.85	14.82	15.07	14.91	14.56
Refr_chargeMass	kg	Refrigerant charge mass	10	10	10	10	10	10	10	10

Fig. 3.4-4 - Case setup for case from 1 to 8

The assembled map-based virtual model is:

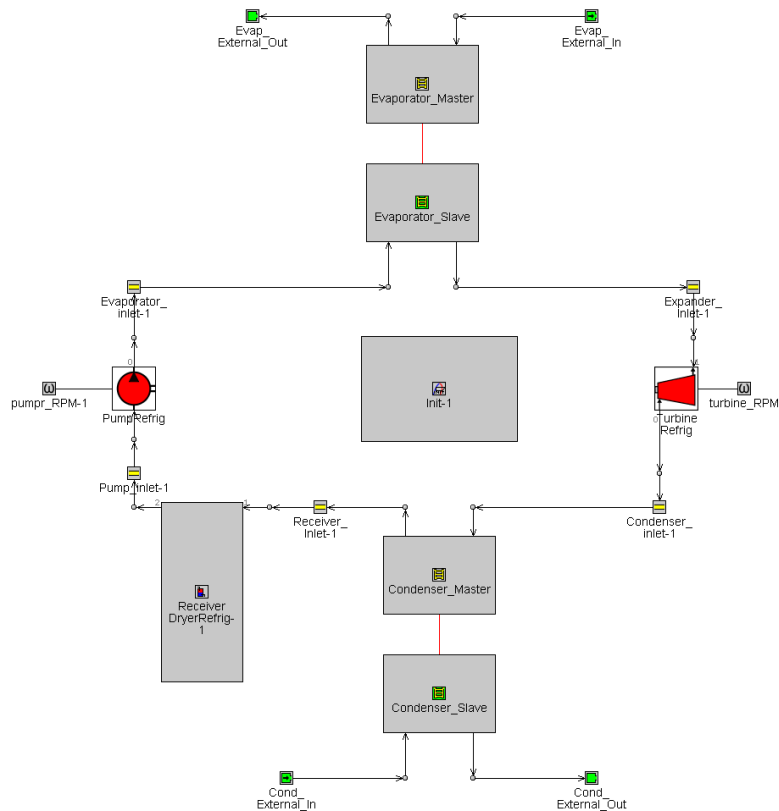


Fig. 3.4-5 – Assembled map-based model

### 3.5 Built model simulation

Once all the individual components have been reconstructed and the fields filled with their experimental operating parameters, they were connected to each other, to build the complete ORC plant. Once this process was also completed, it has moved to the simulation phase. The purpose of this phase was to compare the results obtained from the original experimental model and those obtained from the virtual map-based model. Before launching the simulation, it has proceeded to set all the parameters to carry out the simulation correctly, setting them in the specific window “Run speed”. The two most important parameters in order to obtain a correct simulation, were the “Time control flag” and the “Maximum simulation duration (Time)”.

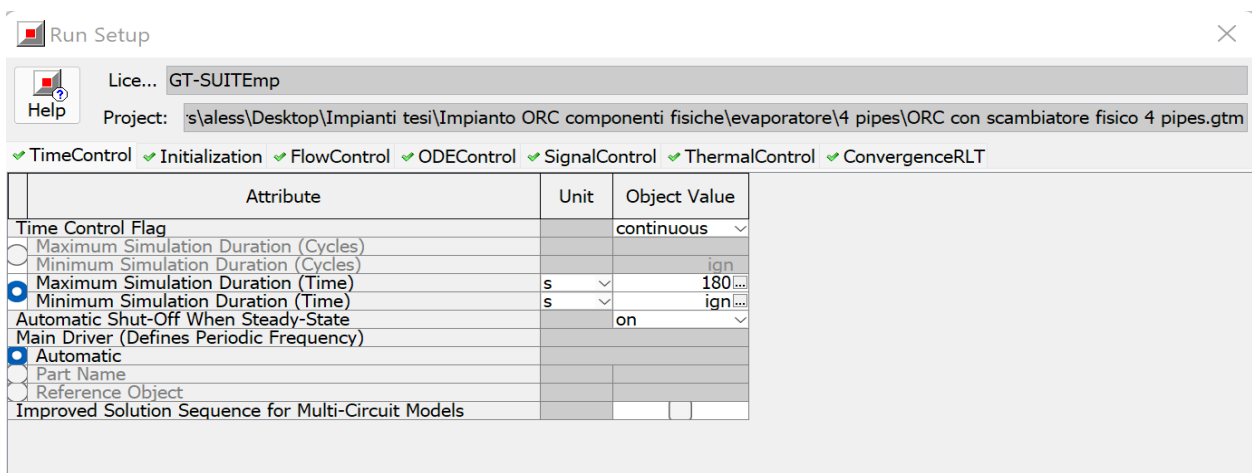


Fig. 3.5-1 – Simulation setting template

### TimeControl

This folder is used to define the simulation duration and time-controlling variables. The attributes in this folder must be defined for all simulations.

#### **Time Control Flag**

Defines the global simulation type with regard to time. One of the following options:

**periodic** indicates that the model contains at least one circuit which contains a periodic event (i.e. engine cylinder "cycle") and therefore requires tracking of results with respect to angle over each cycle. Any model that includes an 'EngineCrankTrain', 'CrankAnalysis', or 'EngineCrankShaft' part should use the periodic option. Note that the simulation duration for a periodic simulation can be specified in cycles or in time, whichever is most convenient.

- **continuous** indicates that the simulation includes no periodic event, and therefore has no need to track results with respect to a cyclic angle. This is the typical setting for models that contain only quasi-steady fluid circuits such as coolant or underhood air. The simulation duration for a continuous simulation is typically specified in time.

*Please note that within the **FlowControl** and **ODEControl** folders, it is possible to override the global Time Control Flag selected here with a different value for a specific circuit. This is possible only when the **Improved Solution Sequence for Multi-Circuit Models** is selected..*

#### **© Maximum Simulation Duration (Cycles)**

Requested maximum number of cycles of the main driver, as defined in the **Main Driver (Provides Periodic Frequency)** attribute below. This option is typically only used for periodic models.

A simulation may stop prior to the maximum number of cycles if the simulation has satisfied all steady state convergence criteria and the **Automatic Shut-off When Steady State** flag is set to **on**.

Fig. 3.5-2 - "Help" for Time Control Flag and Maximum Simulation Duration (Time)

The "Maximum simulation duration" was set at 180 seconds, as in most of cases, the steady-state conditions was reached before the maximum time. Increasing the simulation time would have meant an increasing in simulation duration, without benefits in the accuracy of the results obtained. The "Time control flag" has been set to "continuous", since, as it is possible to read from the figure "Fig. 3.5-2", this type of control is used for "quasi-steady fluid circuit", contrary to the "periodic" control flag, used in cases where there is a periodic event that repeats itself over time.

### 3.6 Map-based simulation results

A more complete treatment of the map-based model of the analyzed ORC power plant, with a more accurate study, and more complete results, can be found in the thesis "Modellazione e calibrazione di un sistema ORC per il recupero del calore dei gas di scarico di un motore a combustione interna" written by the student Michelangelo D'Amborgio.

## Map-based model

The work carried out in this thesis, in fact, focused more on the physical-based model and on the comparison with the map-based model, reason because it had to be constructed.

Therefore, only the most interesting values for this thesis are reported<sup>9</sup>, leaving out any comments or deductions on the results obtained, the latter available in the aforementioned thesis.

The most important results are the temperature, the pressure and the gas fraction at the outlet from the plant exchangers, so from the evaporator and the condenser, and the power produced from the expander. In addition to these values, stored in some Microsoft Excel tables, it is also important to evaluate their relative percentage error with respect to the experimental measured values. Finally, to conclude, the formula for calculating the relative percentage error is now added:

$$error\% = \frac{|experimental\ value - calculated\ value|}{experimental\ value} * 100 \quad \text{Equation 37}$$

### 3.6.1 Temperature, pressure and gas fraction relative percentage error at the evaporator outlet

The first value that is take into account is the temperature. The following table shows the experimental average value, the calculated average value, the average percentage relative error and the maximum percentage relative error:

<b>EXPERIMENTAL AVERAGE TEMPERATURE [°C]</b>	<b>MAP-BASED AVERAGE TEMPERATURE [°C]</b>	<b>MAP-BASED TEMPERATURE AVERAGE PERCENTAGE RELATIVE ERROR</b>	<b>MAP-BASED TEMPERATURE MAXIMUM PERCENTAGE RELATIVE ERROR</b>
101,8	103,5	1,7%	7,3%

Table 3.6-1 – R245fa temperature at the evaporator outlet, full map-based model

---

<sup>9</sup> The values calculated are referred to the initial refrigerant charge in the circuit set equal to 10 kg.

Map-based model

The graph of the error trend of temperature, respect the measured (experimental) one, with a maximum error range of  $\pm 5\%$ , is now reported:

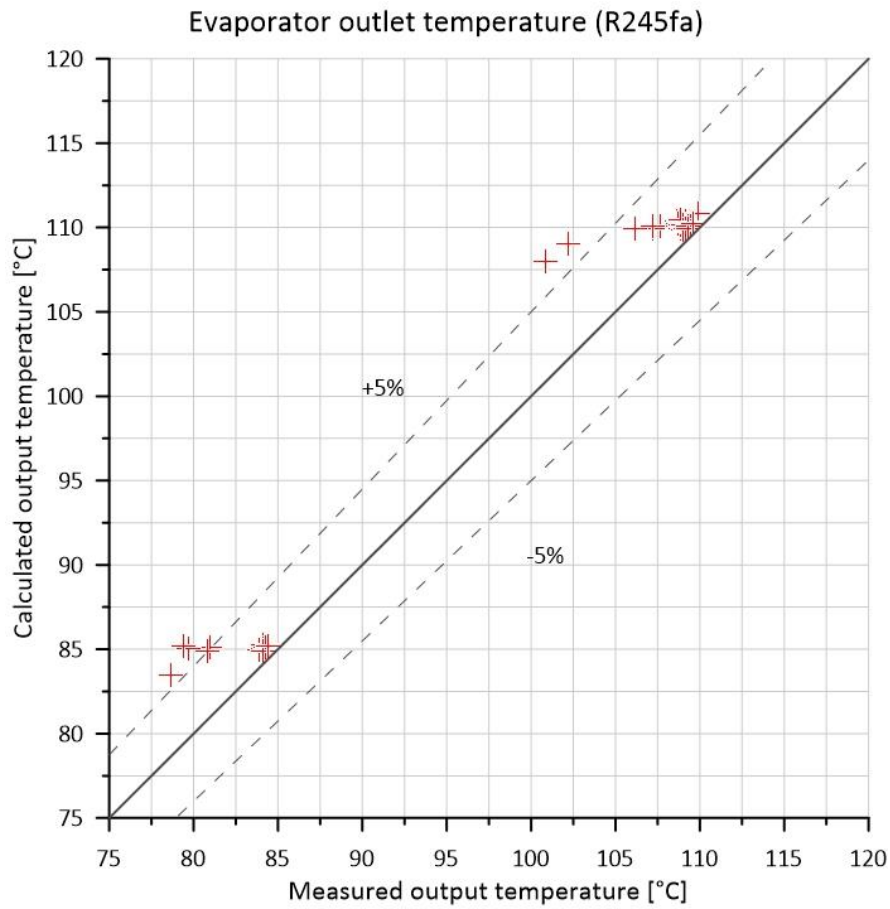


Fig. 3.6-1 – Error trend of R245fa temperature at the evaporator outlet, full map-based model

Now it is possible to move to pressure. The same statements made for the temperature can be applied.

EXPERIMENTAL AVERAGE PRESSURE [bar]	MAP-BASED AVERAGE PRESSURE [bar]	MAP-BASED PRESSURE AVERAGE PERCENTAGE RELATIVE ERROR	MAP-BASED PRESSURE MAXIMUM PERCENTAGE RELATIVE ERROR
8,4	8,3	1,7%	4,4%

Table 3.6-2 - R245fa pressure at the evaporator outlet, full map-based model

Map-based model

The graph of the error trend of pressure, respects the measured (experimental) one, with a maximum error range of  $\pm 5\%$ , is now reported:

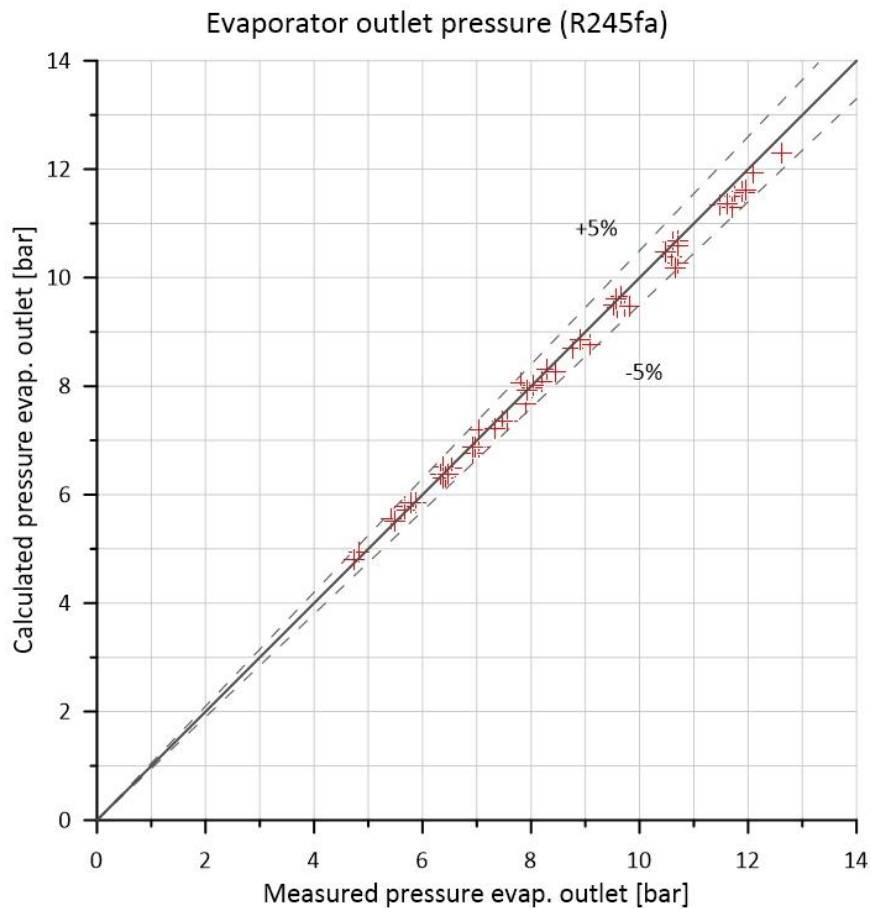


Fig. 3.6-2 – Error trend of R245fa pressure at the evaporator outlet, full map-based model

Finally, the results for the gas fraction of R245fa at the outlet from the evaporator are reported.

EXPERIMENTAL AVERAGE GAS FRACTION	MAP-BASED AVERAGE GAS FRACTION	MAP-BASED GAS FRACTION AVERAGE PERCENTAGE RELATIVE ERROR	MAP-BASED GAS FRACTION MAXIMUM PERCENTAGE RELATIVE ERROR
100 %	100%	0%	0%

Table 3.6-3 – R245fa gas fraction at the evaporator outlet, full map-based model

In this case it is unnecessary to report the error graph because the values measured experimentally and those calculated in the map-based model are identical.

### 3.6.2 Power to the shaft produced by the expander

After the analysis of temperature, pressure and gas fraction, the other parameter fundamental to analyze the correctness of the map-based model and to be able to make a correct comparison with the physical-based model, that will be explained in the following chapters, is the power to the shaft produced by the scroll expander. As for previous values, a comparison is made between the average of the experimental values, the average of the map-based simulation values and the relative percentage errors of the map-based model.

<b>EXPERIMENTAL AVERAGE POWER [kW]</b>	<b>MAP-BASED AVERAGE POWER [kW]</b>	<b>MAP-BASED POWER AVERAGE PERCENTAGE RELATIVE ERROR</b>	<b>MAP-BASED POWER MAXIMUM PERCENTAGE RELATIVE ERROR</b>
1,9	1,9	4,3%	23,1%

*Table 3.6-4 – Power to the shaft produced by the expander, full map-based model*

## Map-based model

The graph of the error trend of power, respect the measured (experimental) one, with a maximum error range of  $\pm 5\%$ , is now reported:

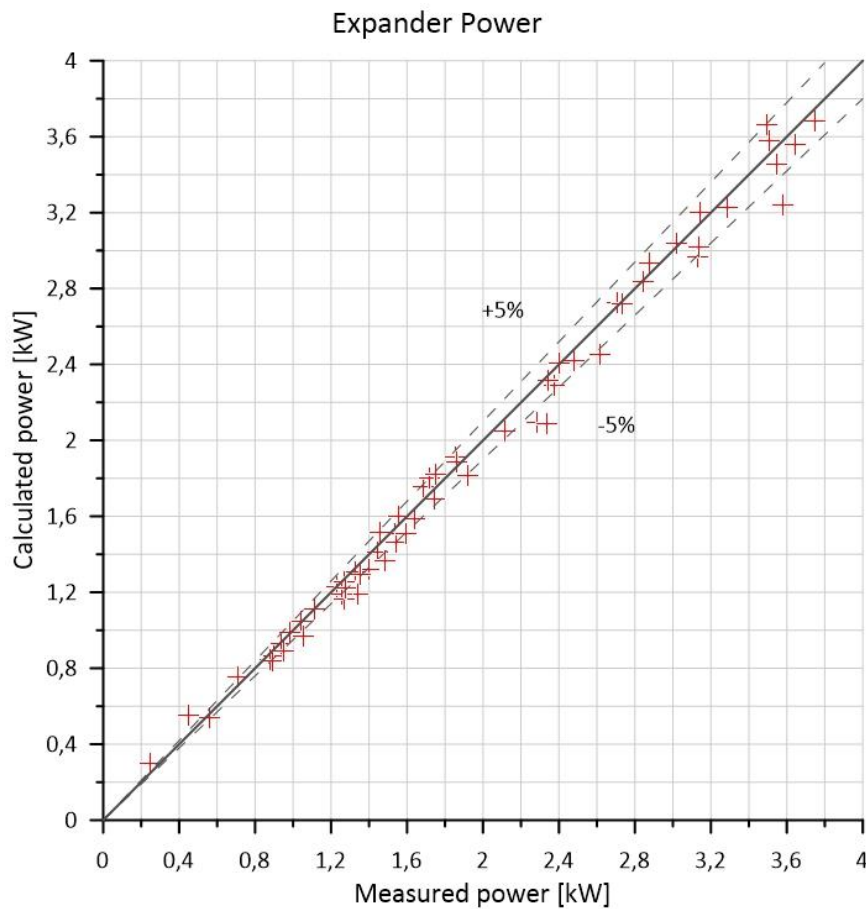


Fig. 3.6-3 – Error trend of produced power to the shaft, full map-based model

### 3.7 Brief conclusions on the results of the map-based model

As can be seen from the tables of the previous paragraph, *Table 3.6-1*, *Table 3.6-2*, *Table 3.6-3* and *Table 3.6-4*, although the maximum relative percentage errors can be very high, these are in isolated cases. What is important is that the mean relative percentage error falls inside the maximum imposed range of  $\pm 5\%$ , range for which the constructed virtual model can be considered reliable and its simulations correctly approximate the experimental plant trend.

## 4 Physical modelling of evaporator

### 4.1 Construction of the first model

As first reconstructed component, moving from the map-based model to the physical-based one, it was decided for the heat exchanger that acts as evaporator in the ORC plant considered. However, on a geometric level, as already described in the *paragraph 3.1.3*, the heat exchangers that acts as the evaporator and the one that acts as the condenser, are identical. The only two differences between them there are on functional level and on the input/output values of fluids on the master and slave sides.

#### 4.1.1 Geometry construction

To reconstruct a physical model that faithfully represent the real exchanger, it was necessary to analyze in detail the geometry of the considered exchanger.

It has been described that it is a Blazed Plate Heat Exchanger (BPHE) composed by 70 channels. By recalling the data already mentioned in the *paragraph 3.1.3*, and integrating them with the technical specification on the produced catalogue for the specific considered model, it has reached all the geometric data necessary for the construction of the physical-based model of the exchanger:

- Plate length: 523,875 mm
- Plate width: 114,3 mm
- Plate thickness: 0,3 mm
- Channel height: 3 mm
- Number of channels (for slave and master part): 70

In addition, it was found the following data relating the material:

- Material: stainless steel – AISI 304
- Total mass of metal: 13,75 kg

# Physical modelling of evaporator

**PRODUCT SHEET**

## B80

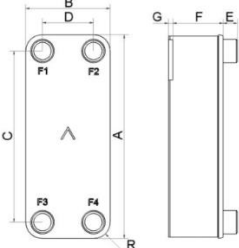
The B80 is our medium-size high-capacity model. It is the perfect choice for most types of low-capacity chiller applications and high-performance heat pumps. It covers a wide capacity range in district heating substations and is a proven oil cooler for compressors and hydraulics.



**Basic specifications**

Maximum number of plates (NoP)	148
Max flow	16.9 m³/h (74.41 gpm)
Channel volume	0.107/0.107 dm³ (0.0038/0.0038 ft³)
Material	316/316L stainless steel plates, copper brazing
Weight excl. connections	2.09+(0.164*NoP) kg 4.61+(0.362*NoP) lb

**Standard dimensions**



#	MM	N
A	526	20.71
B	119	4.69
C	470	18.5
D	63	2.48
F	4.00+2.24*(NoP)	15.75+8.82*(NoP)
G	6	0.24
R	23	0.91
E_1	27	1.06

Fig. 4.1-1 – Extract from the SWEP catalog for the B80Hx70/1P-SC-S 4x24U model

Having found all the necessary data, it has started to think about how to reconstruct the geometry through the functional blocks present in the program used for this thesis.

In the program's section: *Template Library -> Flow -> General flow -> Components*, it was possible to find different types of pipes.

Since the geometry of a BHPE tends to parallelepiped, it was decided to proceed by choosing the *PipeRectangle* block, which allows to build a rectangular shaped duct.

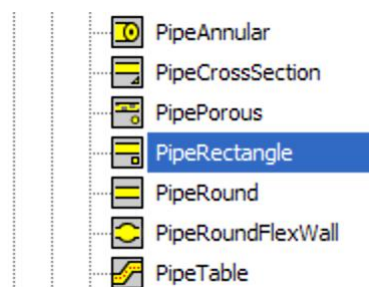


Fig. 4.1-2 - Different types of functional blocks for pipes

As a first attempt, it was decided to approximate the flows of the hot side (water) and the cold side (organic refrigerant R245fa) to two rectangular ducts having the same volume and the same

## Physical modelling of evaporator

exchange surface respect the real exchanger itself.

Moreover, as has already been mentioned several times in the previous paragraph, the exchanger is in countercurrent.

Practically at the end, the result of reconstruction for one channel turned out to be like this:

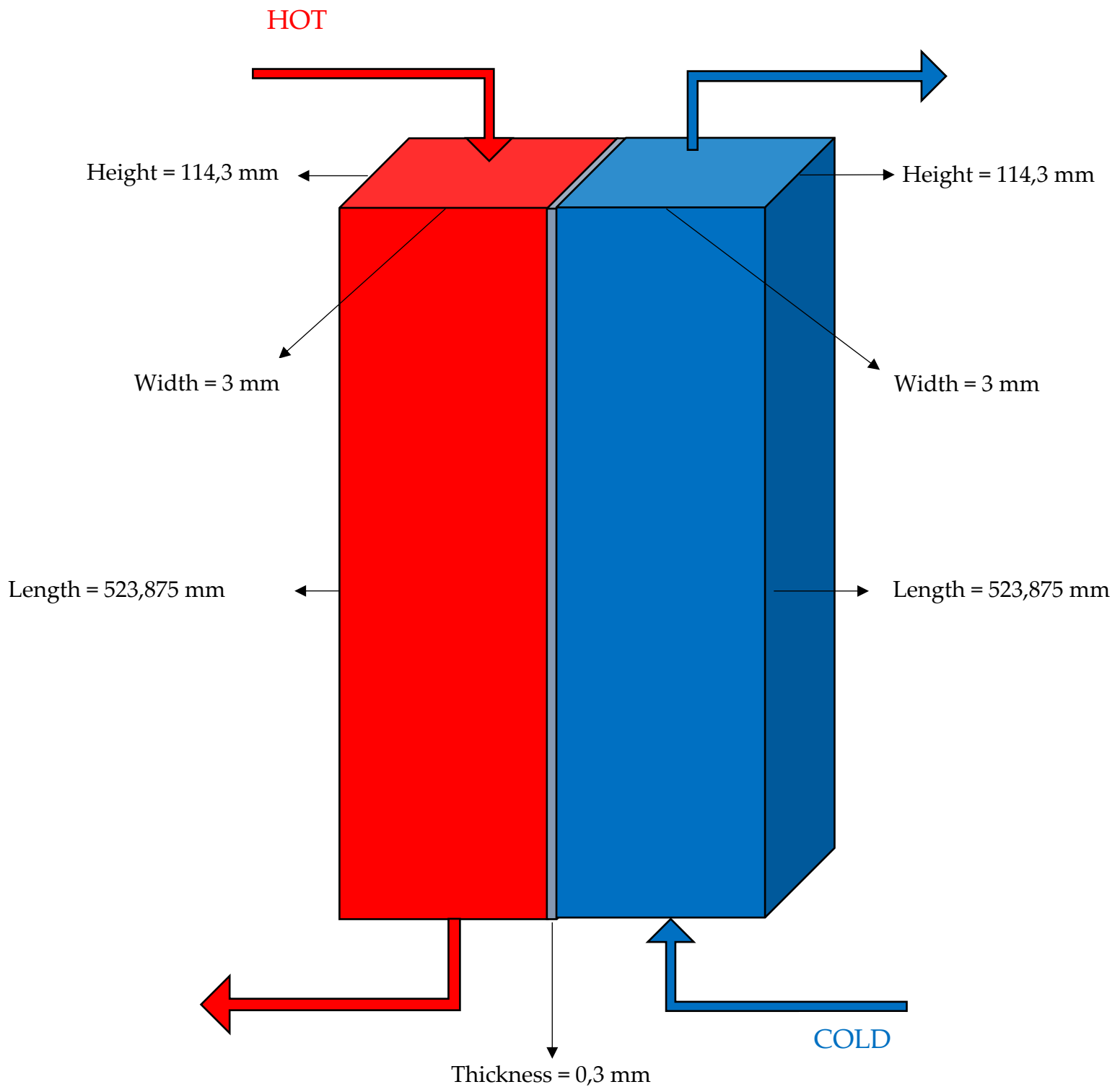


Fig. 4.1-3 - Reconstruction (not to scale) of the exchanger using the PipeRectangle functional blocks

## Physical modelling of evaporator

The total surface of exchange is calculated as follow:

$$\begin{aligned} \text{Total exchange area} &= (\text{length} * \text{number of total channels}) * \text{width} = (523,875 * 70) * 114,3 = \\ &= 4191523,875 \text{ mm}^2 \end{aligned}$$

Equation 38

The value may seem high at first glance, but, practically, it is going to consider the total internal exchange surface of all 70 channel.

The gray part in the figure Fig 4.1-3, represents the total volume of the plate that separates the two flows.

Once the draft of the physical-based model of the evaporator was completed, it was built on the program using the functional blocks mentioned above.

First, all the necessary geometric data have been set in the *Case Setup* section, in order to facilitate their modification if it is decided to consider exchangers with different characteristics:

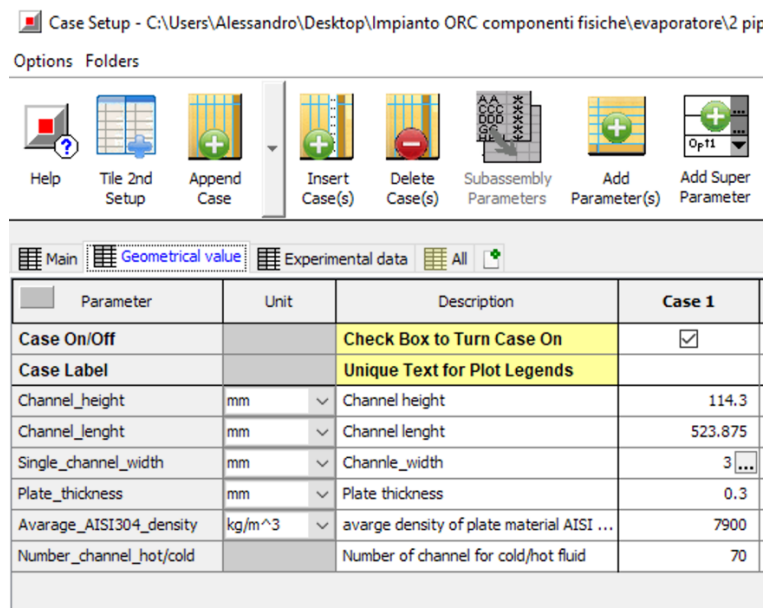


Fig. 4.1-4 - Geometric data set on the program

## Physical modelling of evaporator

Once this operation was completed, it has moved on to fill in the fields required by the functional block *PipeRectangle*:

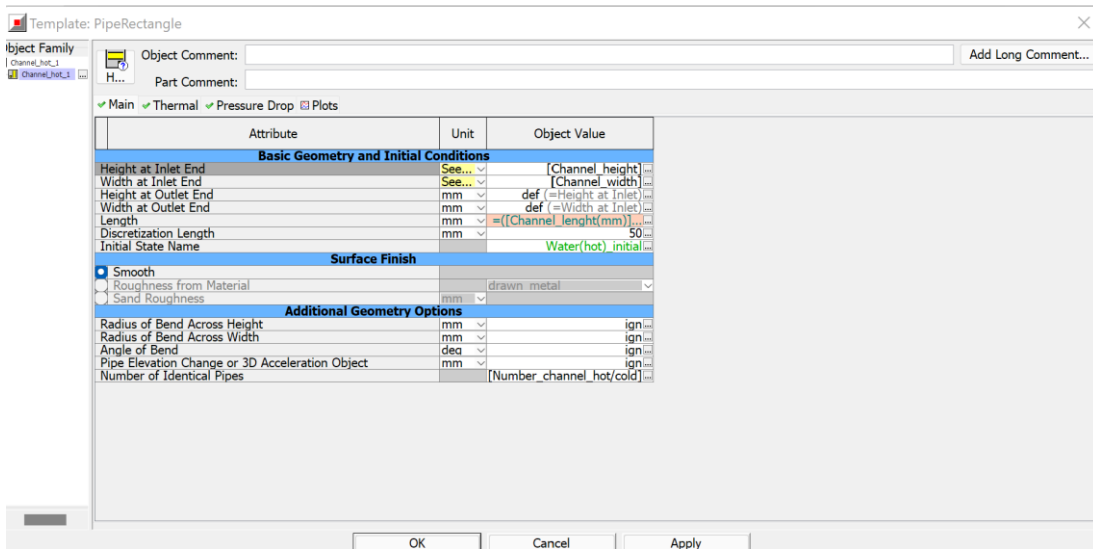


Fig. 4.1-5 – Geometry section of functional block *PipeRectangle*

As is possible to see, the field corresponding to the “*Number of identical pipes*” has been completed by directly entering the *Number channel hot/cold*. In this way it has been imposed 70 identical channel in parallel.

In addition to the section on geometry, it is asked to complete the filed relating to heat exchange in the thermal section. For this one, the item “*Wall Temperature from Connected Thermal Primitive*” has been set, which allows to automatically calculate the thermal flow based on the thermal functional blocks that will be connected to it and which will be examined in the following chapters.

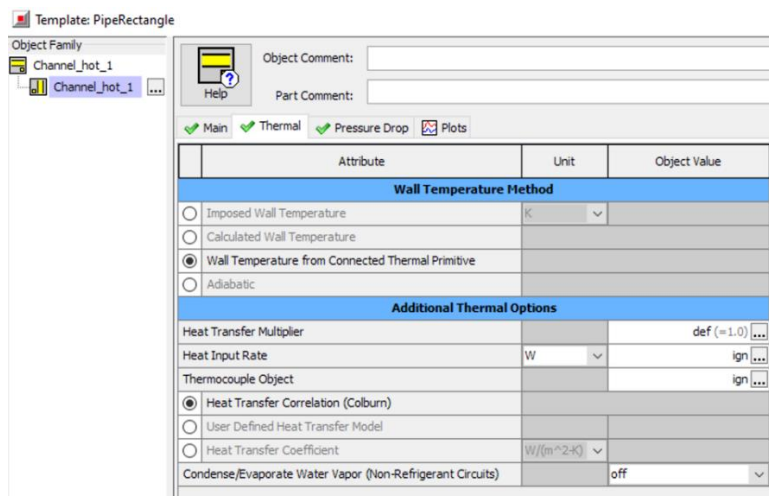


Fig. 4.1-6 - Thermal section of functional block *PipeRectangle*

## Physical modelling of evaporator

An important field, which will subsequently be analyzed in detail, but which for the moment is left as default, equivalent to the value of 1, is the *Heat Transfer Multiplier*, already mentioned in the *paragraph 2.3.1*, which considers the variation on the components which constitute the Convective Heat Transfer Coefficient and consequently influence the heat flow

Given the geometry built considering 70 channels in parallel, it was necessary to add a functional block, called *FlowSplit General* which allowed to divide the flow from a single incoming pipe into the 70 channels placed in parallel and the other way around for the outgoing flow.

### 4.1.2 Construction of the convective heat exchange

Once the geometric construction was completed, the convective heat exchange had to be reconstructed using the functional blocks present in the program.

The specific functional block for the type of heat exchange that occurs in the evaporator is present in: *Template Library -> Thermal -> General Thermal -> Connections -> ConvectionConn*.

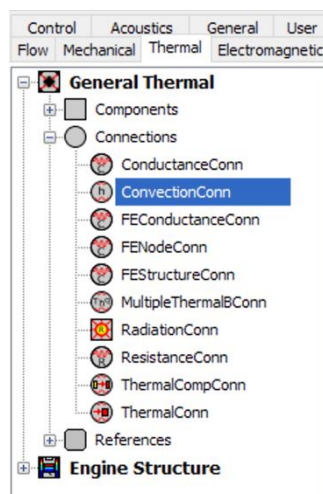


Fig. 4.1-7 - Different functional blocks for thermal connections

The operation of this functional block allows to have the heat exchange between the hot flow and the plate, which construction will be described later, but also between the plate and the cold flow. The two values that could be set are the *Heat Transfer Coefficient*, which however, were left set as default, which implies that it is calculated by the program itself and the *Heat Exchange Area* that was

## Physical modelling of evaporator

also left set as default, but this implies that it is simply considered the same as that set in the functional block of the plate that will be analyzed later.

### 4.1.3 Plate thermal mass

Once the functional block for thermal convection was completed, it moved on, to the construction of the thermal mass of the plate that separates the two flows.

This one was a fundamental part for the heat exchange reconstruction: in fact, until now, the material and the area through which the heat exchange takes place have never been introduced.

Thanks this functional block it was possible to complete the physical modeling of the heat exchange by imposing the mass, the chemical-physical and the geometrical proprieties of exchange surface.

To find the specific functional block is necessary to go to: *Template Library -> Thermal -> General Thermal -> Components -> ThermalMass.*

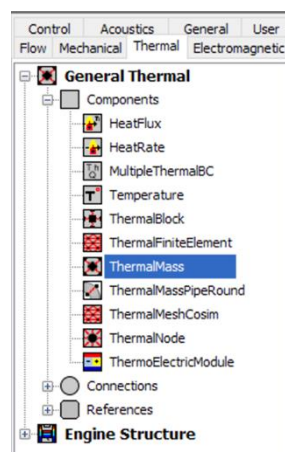


Fig. 4.1-8 - General components for thermal exchange

In the main page of this component, it was possible to set different parameters, as for example, the surface of exchange, which was given by the *Equation 38*. Another set parameter was the material for which it was selected *StainlessSteel* directly form the library of the materials present on the software, which returns the chemical-physical proprieties of an AISI 304 steel, in accordance with the material given by manufacturer's catalog for the chosen exchanger model and, moreover, also used for the map-based model.

The following table summarize the characteristics of AISI 304 steel, directly set in the program:

Temperature [K]	Thermal conductivity $\left[\frac{W}{m * K}\right]$	Density $\left[\frac{kg}{m^3}\right]$	Specific heat $\left[\frac{J}{kg * K}\right]$
100,00	9,2	/	272,0
200,00	12,6	/	402,0
300,00	14,9	7900,00	477,0
400,00	16,6	/	515,0
600,00	19,8	/	557,0
800,00	22,6	/	582,0
1000,00	25,4	/	611,0
1200,00	28,0	/	640,0
1500,00	31,7	/	682,0

Table 4.1-1 – Chemical-physical proprieties for StainlessSteel material presents in the software library

After setting the material, the mass field was filled, value that was already known from the proprieties described in the *paragraph 4.1.1*.

#### 4.1.4 Boundary and initial conditions

Once the geometrical and physical heat exchange reconstruction was completed, the boundary and initial condition of the refrigerant were set.

The boundary conditions of hot water inlet and outlet, as for the map-based model, were set starting from the experimental values collected during the analysis of the experimental plant.

The boundary conditions of the R245fa refrigerant inlet and outlet the evaporator, were also set starting from the experimental data. However, some of the necessary values were not present in the collected data tables, so the missing values were taken from the simulation of the map-based validated model of the complete plant.

The last values to be set were the initial conditions of the R245fa refrigerant fluid. If, in fact, the required composition and proprieties of the gas are automatically set by the program, it is no longer possible to set 10 kg as the initial charge quantity, as for the map-based model, since the only

## Physical modelling of evaporator

evaporator model is being considered, and that quantity cannot physically enter all inside the single component considered. For this reason, it has no longer focused on the initial charge of the R245fa, but on the initial density value. To find the correct value, different simulation, and analyses were necessary, which deserve a dedicated paragraph below.

### 4.1.5 Study of the initial density of refrigerant R245fa

Not being able to consider a random initial charge of refrigerant in the exchanger model alone, as it would imply a random initial phase, it has been concentrated on the initial density.

Going to the “Help” section of the initial conditions of the refrigerant, it is possible to find a part dedicated to setting the density when the charge value is unknown.

**Unknown System Charge:**

When the system charge is not known in the system, it is typically less error-prone to use the average system density attribute instead of guessing the charge. To arrive at a reasonable estimate of the average density, please calculate the saturated liquid density at the estimated condensing pressure, and multiply by these fractions, depending on the application:

HVAC (includes Heat Pump): 20-30%  
Rankine Cycle: 30-40%

The following is a table that summarizes popular refrigerants and their resulting suggested average system densities. Note that the saturated liquid density can be calculated with the Fluid Properties Calculation Utility (Tools -> GT Excel Sheets -> Fluid Properties).

Application	Refrigerant	Condensing Pressure Estimate (bar)	Saturated Liquid Density (kg/m <sup>3</sup> )	Suggested Average System Density (kg/m <sup>3</sup> )
Rankine	Water	1.0	958.6	335.5
Rankine	Ethanol	1.0	736.8	257.9
Rankine	R245FA	3.0	1280.5	448.2
HVAC	R134a	20.0	1011.4	252.9
HVAC	R1234yf	20.0	888.9	222.2

Fig. 4.1-9 - “Help” function for the initial density value of R245fa

As it is possible to read, the recommended value for a Rankine cycle, with R245fa as operating fluid and a condensation pressure of about 3 bar, similar to the one of the plant considered in this thesis, is about  $450 \frac{kg}{m^3}$ .

However, before entering this value, it was wanted to make sure that this suggested value was correct. To do this, various simulations were performed on different cases of the previously validated map-based model of complete plant, setting as the initial value of refrigerant no longer 10 kg of charge, but the initial suggested density of  $450 \frac{kg}{m^3}$  to see how the results obtained from the simulation varied, compared to the original model with 10 kg of initial charge.

Physical modelling of evaporator

The results obtained from the simulations with the set initial density and the one obtained from the set initial charge, for some critical variables, are compared in the following table, in the form of mean relative percentage error (MRPE), which formula is:

$$MRPE = \frac{\sum_{i=1}^N \left( \frac{|calculated\ value_i - experimental\ value_i|}{experimental\ value_i} * 100 \right)}{N} = \frac{\sum_{i=1}^N relative\ percentage\ error_i}{N}$$

Equation 39

With:

- N = total number of cases = 61

	TEMPERATURE AT EVAPORATOR OUTLET	PRESSURE AT EVAPORATOR OUTLET	GAS FRACTION AT EVAPORATOR OUTLET (NO ERROR)	POWER TO THE SHAFT
MAP-BASED MODEL WITH 10 KG INITIAL CHARGE	1,7 %	1,7%	100%	4,3%
MAP-BASED MODEL WITH 450 $\frac{kg}{m^3}$ INITIAL DENSITY	1,6%	1,7%	100%	4,4%

Table 4.1-2 - Comparison between relative percentage error of map-based model with set initial charge and set initial density

As the Table 4.1-2 shows, the errors obtained from the simulation of the 61 cases in the two models, is absolutely superimposable and therefore it is possible to use the value of 450  $\frac{kg}{m^3}$  as initial density refrigerant value in the exchanger physical-based model alone, having the certainty of obtaining correct values.

These results for this initial density value were used for the study of heat exchanger alone.

### 4.1.6 First assembled model

Once the last values have been set, the first physical-based evaporator model was assembled in its entirety.

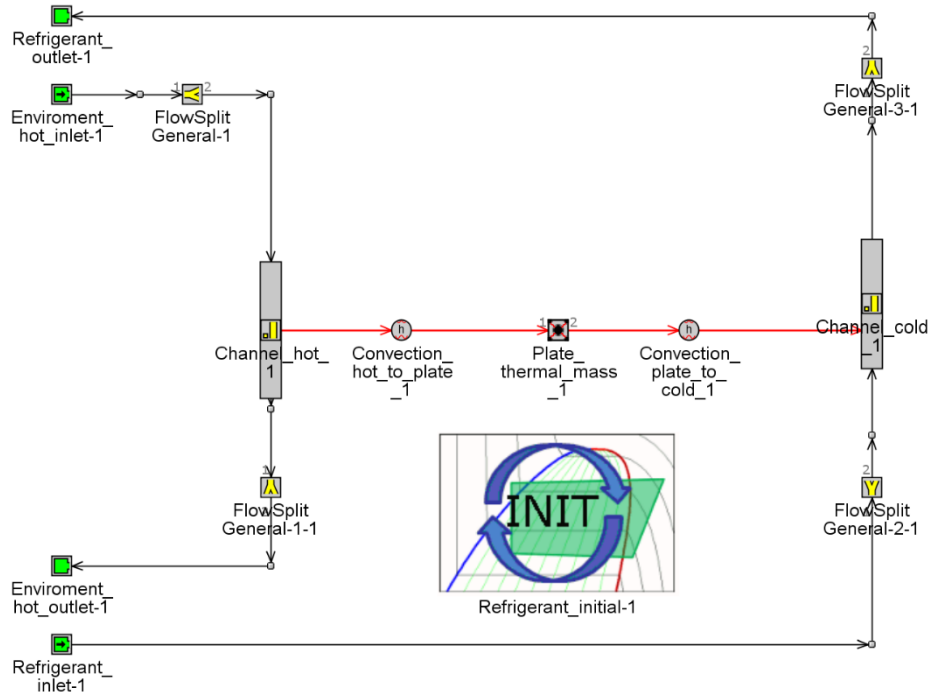


Fig. 4.1-10 -First attempt of physical-based model of evaporator

Before starting the simulation, its proprieties must still be set in the “Run speed” section. The set values were identical to the map-based model, so just refer to *paragraph 3.5*.

### 4.1.7 Conclusion on the first model attempt

This first model was very useful to understand the approach followed to try to create a physical-based model that best approximate the real evaporator trend. However, no simulation has been performed on this model because it did not take into account the phenomenon of countercurrent exchange, which must be implemented with a further step.

## 4.2 Countercurrent exchange implementation

The model built so far did not take into account the countercurrent exchange. The software used, in fact, is not a 3D modeler, but a graphical equation solver. When a model is built and the connection between the different components are created, this allows the software to solve the constitutive equations of the individual components, also based on the parameters set for each of it, in different physic areas such as fluid dynamic, thermodynamic, electric, mechanical, etc., but does not consider the direction of the flow or the direction of exchange.

To be able to implement the heat exchange in countercurrent, it was necessary to think about the physic at the base of this type of heat exchange between flows and to readjust the model to satisfy this physic. Describing at words, in the simplest way as possible, the physic behind the countercurrent exchange: the hot fluid exchange heat with the hottest part of cold fluid and as the hot fluid releases heat it cools, exchanging heat with the colder part of the cold fluid.

Graphically:

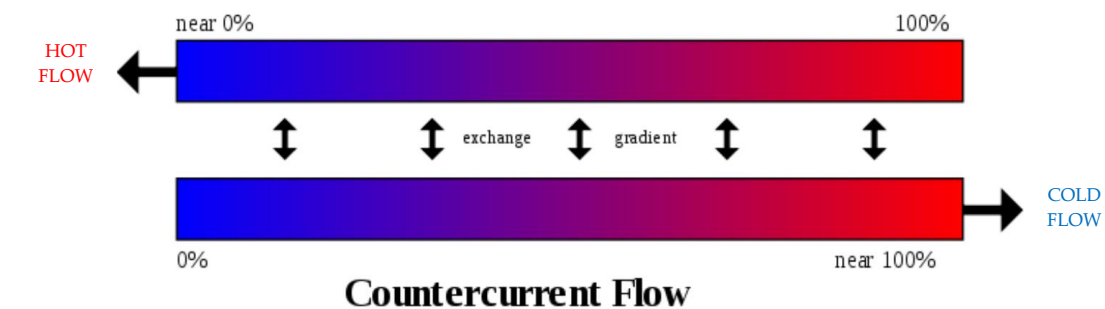


Fig. 4.2-1 - Countercurrent flow

In order to implement this exchange in the physical-based evaporator model, the hot side, where hot water flows, and cold side, where the R245fa refrigerant flows, must be divided into several segments, forcing the cold part of the water to exchange with the cold part of R245fa and the hot part of the water to exchange with the hot part of the R245fa.

In practice, the exchange is forced on different wall temperatures, so as to impose the heat exchange on different temperature gradients and thus approximate the exchange in countercurrent.

Once this type of exchange was also implemented, the model was complete and correctly describes the real behavior and can be simulated.

### 4.3 Two segment physical-based model

The first implementation of the countercurrent case was made by dividing the hot and cold side in two segments each. By dividing into several segments, the quantities relating to the geometry of the channels and the exchange surface also had to be adjusted consequently.

In particular, the length of each side, hot and cold, had to be divided by the number of segments. In the case considered of subdivision in two segments, it is possible to obtain:

$$\begin{aligned} Total\ length_{2\ segments} &= \frac{length\ of\ a\ single\ channel}{number\ of\ segments} = \frac{523,875}{2} = \\ &= 261,937\ mm \end{aligned}$$

Equation 40

The same reasoning had to be made for the exchange surface relating to the functional block representing the plate mass *ThermalMass*, which had to be divided by the number of segments:

$$Exchange\ area_{2\ segments} = \frac{Total\ exchange\ area}{number\ of\ segments} = \frac{4191523,87}{2} = 2095761,93\ mm^2$$

Equation 41

Once the modification that allow the implementation of the countercurrent exchange have been completed, setting the initial density of refrigerant equals to  $450 \frac{kg}{m^3}$  for the considerations made in the *paragraph 4.1.5*, the final model was obtained.

Instead, as regards the other parameters mentioned in the previous paragraphs, including the Heat Transfer Multiplier, they were left identical to the first attempt model.

## Physical modelling of evaporator

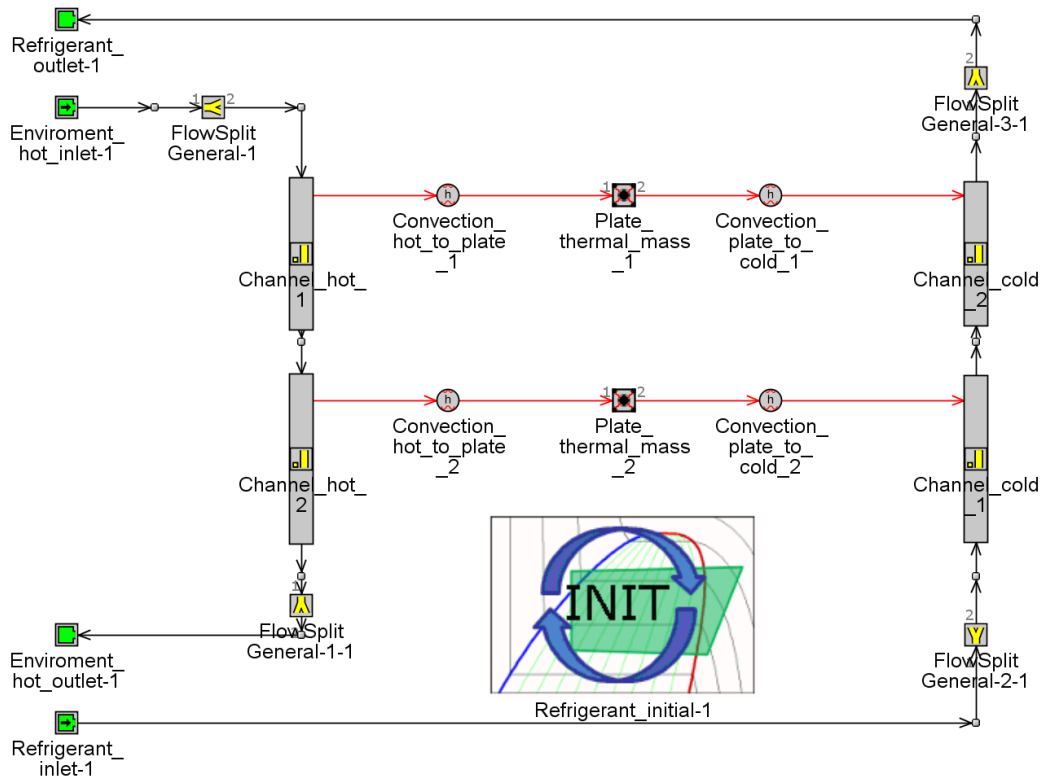


Fig. 4.3-1 – Two segments physical-based evaporator model

### 4.3.1 Simulation and results

It was set a maximum simulation time of 180 seconds, as for the map-based model, because in the most cases the steady state condition was reached before the simulation imposed time limit and increasing this value means a considerable increasing in the overall time simulation, it proceeded to run the simulation of all 61 cases for which the experimental values were known.

Once the simulation was completed, a comparison was made between three significant values at the outlet from the evaporator on the refrigerant R245fa side, which were temperature, pressure and gas fraction, between the newly built physical-based model, the map-based model and the know experimental values.

## Physical modelling of evaporator

- TEMPERATURE

The first value analyzed is the temperature of R245fa at the outlet from the evaporator. It starts with the comparison of the average value:

EXPERIMENTAL [°C]	MAP-BASED [°C]	PHYSICAL-BASED [°C]
101,8	103,5	78,6

Table 4.3-1 - Temperature average comparison, 2 segments evaporator

Graphically, the temperature trend in the three models:

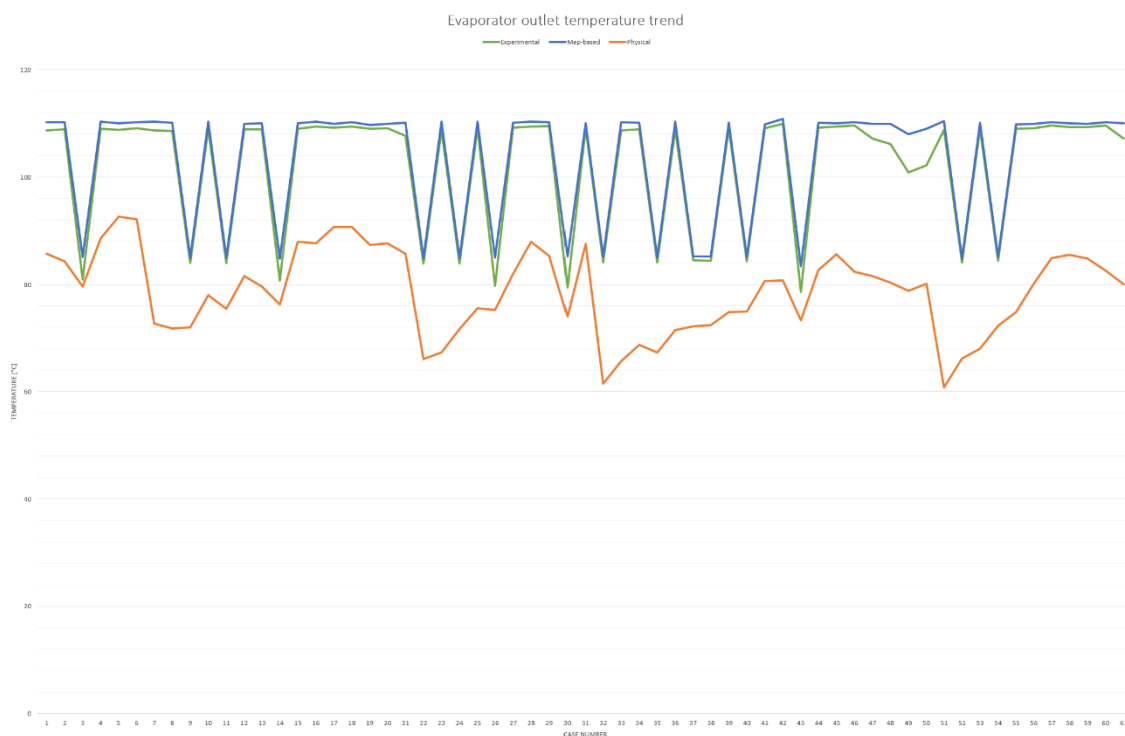


Fig. 4.3-2 - Temperature trend of three models, 2 segments evaporator

However, to have a clear idea of the difference between the various models, it is useful to analyze the mean relative percentage error with respect to the experimental values:

ESPERIMENTAL (REFERENCE)	MAP-BASED	PHYSICAL-BASED
0%	1,7%	22,2 %

Table 4.3-2 – Temperature mean relative percentage error, 2 segments evaporator

## Physical modelling of evaporator

Graphically the error is:

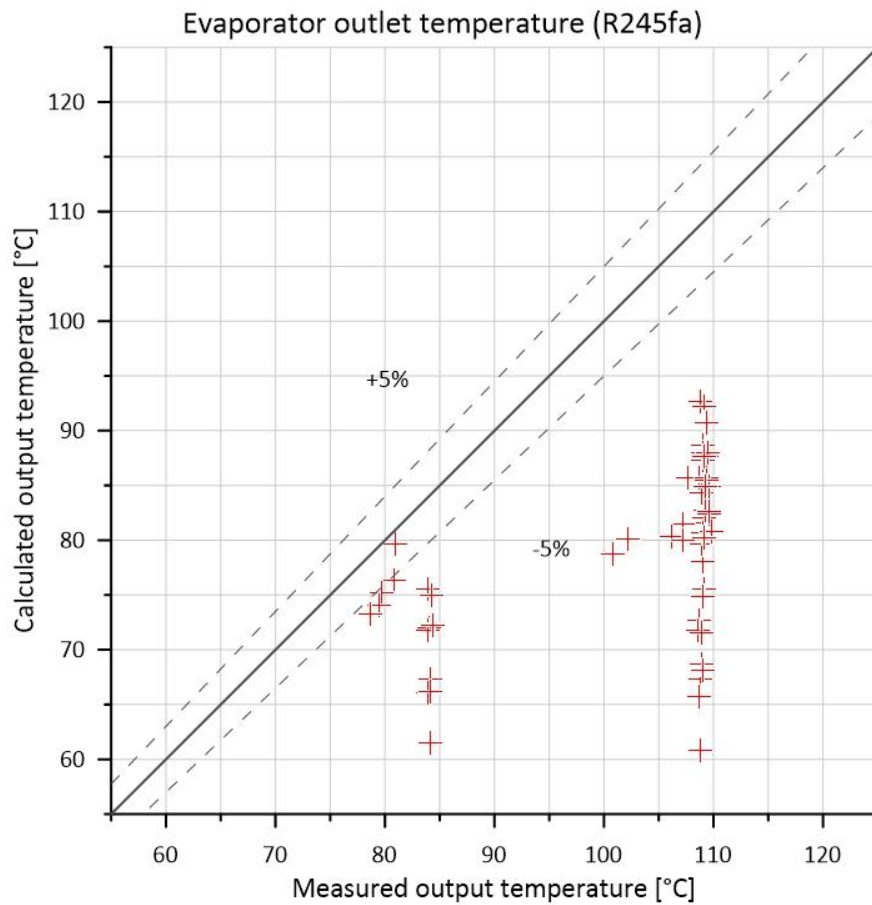


Fig. 4.3-3 – 61 cases temperature error trend, 2 segments evaporator

Through the analysis of the relative error trend, it is possible to see, as taking a maximum range of variation of  $\pm 5\%$ , which allows to affirm that the model well represents the experimental trend, a lot of values are outside this range and also the value average is higher than the imposed range limit.

Therefore, as regards the temperature, the physical-based model of evaporator alone divided in two segments, does not faithfully represent the experimental trend.

## Physical modelling of evaporator

- PRESSURE

The second value analyzed is the pressure of R245fa at the outlet from the evaporator. As for the temperature, it starts with the comparison of the average value:

EXPERIMENTAL [bar]	MAP-BASED [bar]	PHYSICAL-BASED [bar]
8,4	8,3	8,4

Table 4.3-3 - Pressure average comparison, 2 segments evaporator

Graphically, the pressure trend in the three models:

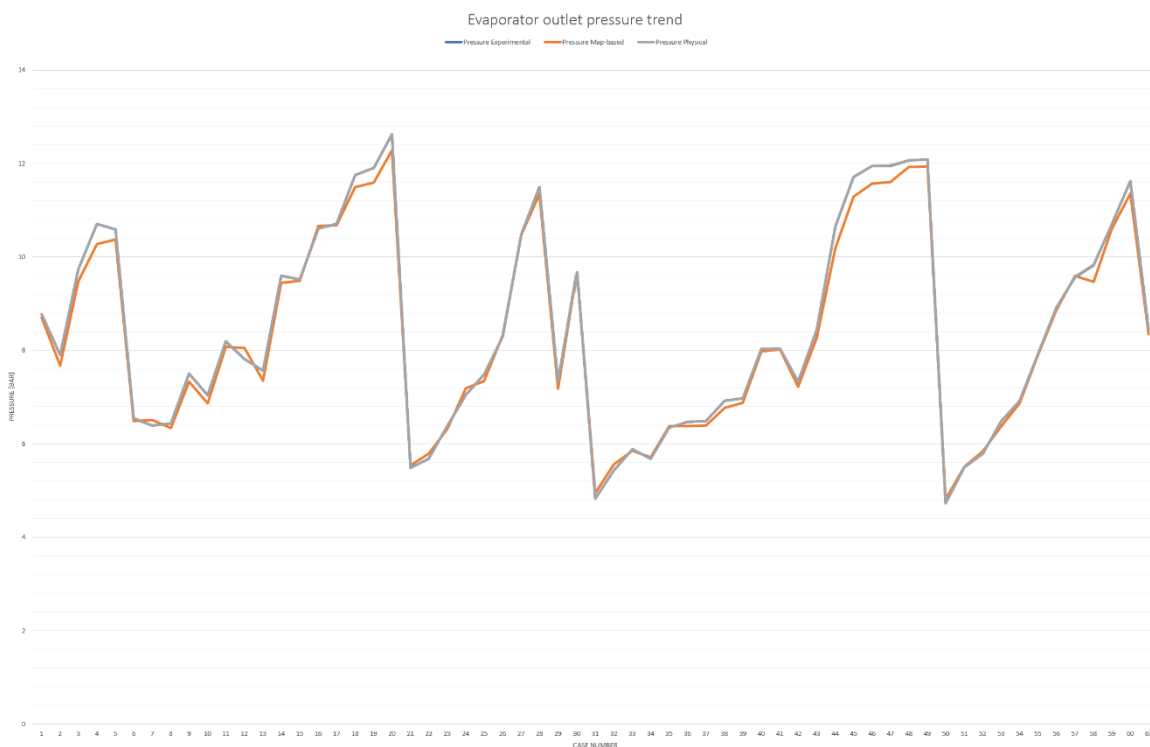


Fig. 4.3-4 - Pressure trend of three models, 2 segments evaporator

As for the temperature, to get a clear idea of the difference between the various models, it is useful to analyze the mean relative percentage error with respect to the experimental values:

ESPERIMENTAL (REFERENCE)	MAP-BASED	PHYSICAL-BASED
0%	1,7%	0,02%

Table 4.3-4 - Pressure mean relative percentage error, 2 segments evaporator

## Physical modelling of evaporator

Graphically the error is:

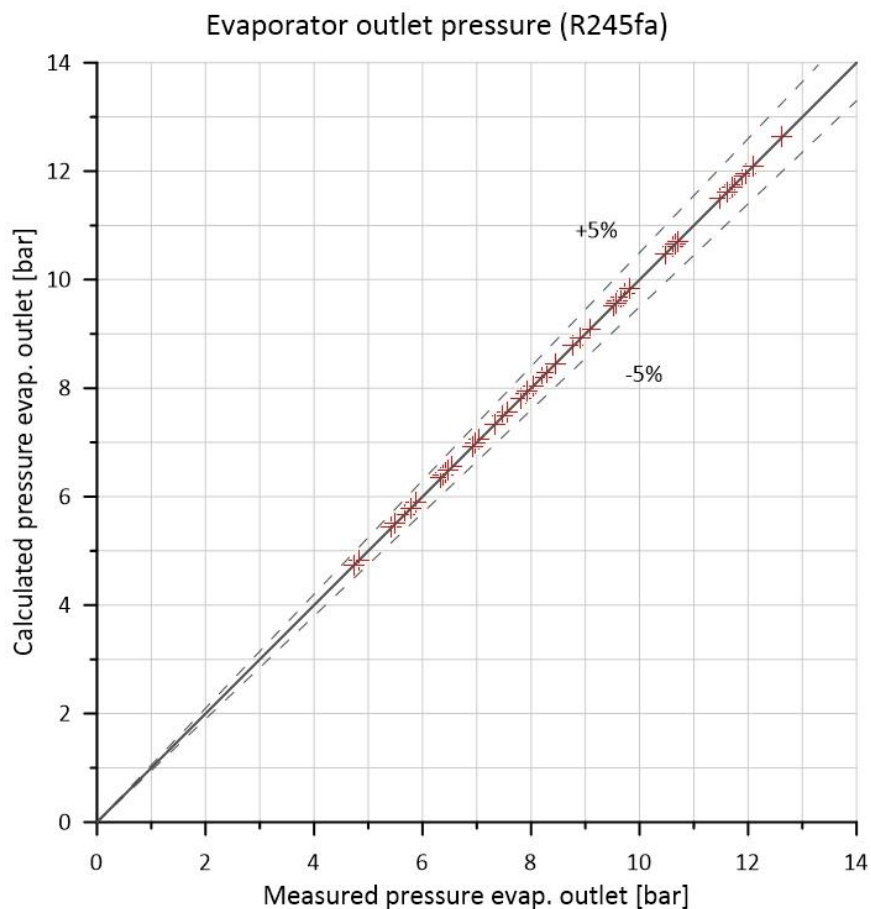


Fig. 4.3-5 - 61 cases pressure error trend, 2 segments evaporator

Through the analysis of the relative error trend, it is possible to see, as taking a maximum range of variation of  $\pm 5\%$ , which allows to have a model that well represents the experimental trend, all pressure error values are inside this range as well as the mean relative percentage error. The pressure trend of the physical-based model truthfully represent the experimental trend, also better than the map-based model.

- GAS FRACTION

The last parameter considered is the percentage of gas at the evaporator outlet for the R245fa refrigerant. The first comparison is between the average percentage of gas:

EXPERIMENTAL	MAP-BASED	PHYSICAL-BASED
100%	100%	14,9%

Table 4.3-5 – Refrigerant gas percentage comparison, 2 segments evaporator

## Physical modelling of evaporator

Graphically the average gas fraction trend is:

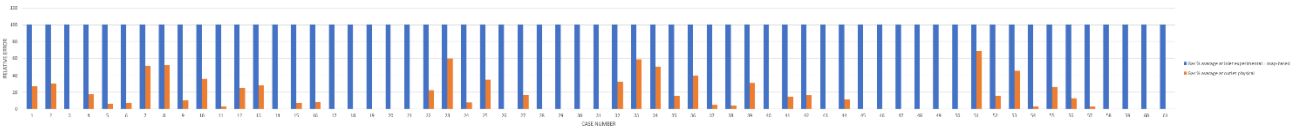


Fig. 4.3-6 – 61 case average gas fraction trend, 2 segments evaporator

As for the two previous parameters is useful to analyze the mean relative percentage error respect the experimental trend:

<b>ESPERIMENTAL (REFERENCE)</b>	<b>MAP-BASED</b>	<b>PHYSICAL-BASED</b>
0%	0%	85,1%

Table 4.3-6 – Refrigerant gas fraction mean relative percentage error, 2 segments evaporator

In this case it does not make sense to draw a graph of the error because it is necessary to obtain a relative percentage error quite near of 0% for gas fraction at the evaporator outlet as it does not allow a liquid phase in the expander, which connection will be analyzed in the next chapters.

### 4.3.2 Conclusions on the two segments model

The pressure is already simulated in an extremely precise way by this model, but the temperature and, above all, the gas fraction, still contain a high mean relative percentage error, which does not allow to state that the model truly represent the experimental behavior.

To refine the model and try to reduce the temperature and gas fraction relative error, it proceeded by further dividing the channels into several segments, thus going to further increase the number of wall temperatures and refining the exchange in countercurrent.

#### 4.4 Three segment physical-based model

For the model divided into three segments it was possible to retract the exact same reasoning made for the model divided into two segments.

The first passage was to add another *PipeRectungal*, *ThermalMass* and the associated *ConvectionConn* functional blocks and to adjust the length and the exchange area:

$$\begin{aligned}
 Total\ length_{3\ segments} &= \frac{length\ of\ a\ single\ channel}{number\ of\ segments} = \frac{523,875}{3} = \\
 &= 174,625\ mm \\
 &Equation\ 42
 \end{aligned}$$

$$\begin{aligned}
 Exchange\ area_{3\ segments} &= \frac{Total\ exchange\ area}{number\ of\ segments} = \frac{4191523,87}{3} = 1397174,623\ mm^2 \\
 &Equation\ 43
 \end{aligned}$$

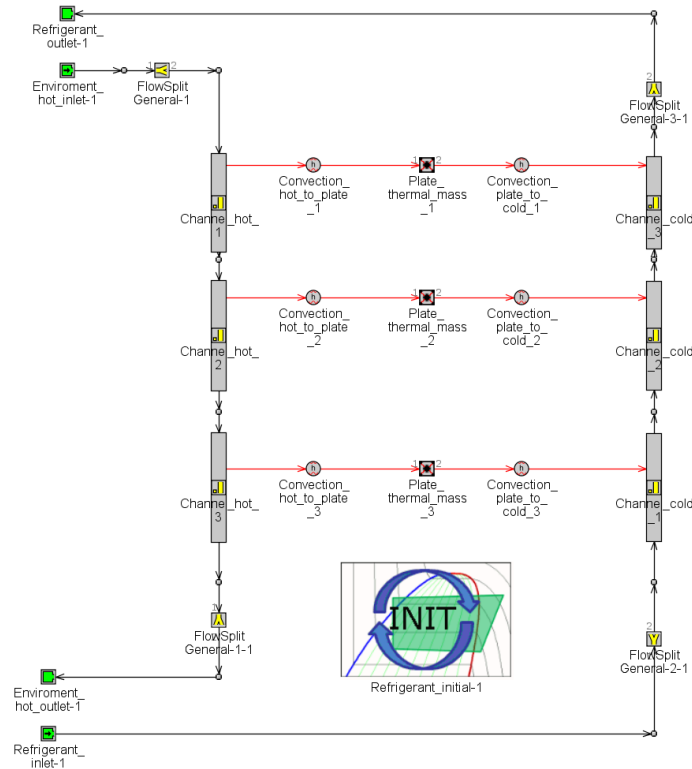


Fig. 4.4-1 - Three segments physical-based evaporator model

All values, except the geometrical ones related to the division in more segments, have been left equals to the two segments model.

### 4.4.1 Simulation and results

As for the two segments case it is useful to analyze the trend of temperature, pressure and gas fraction at the outlet of evaporator of refrigerant R245fa and their associated relative percentage errors.

- TEMPERATURE:

The first value analyzed is the temperature of R245fa at the outlet from the evaporator. It starts with the comparison of the average value:

EXPERIMENTAL [°C]	MAP-BASED [°C]	PHYSICAL-BASED [°C]
101,8	103,5	80,2

Table 4.4-1 - Temperature average comparison, 3 segments evaporator

Graphically the temperature trend is:

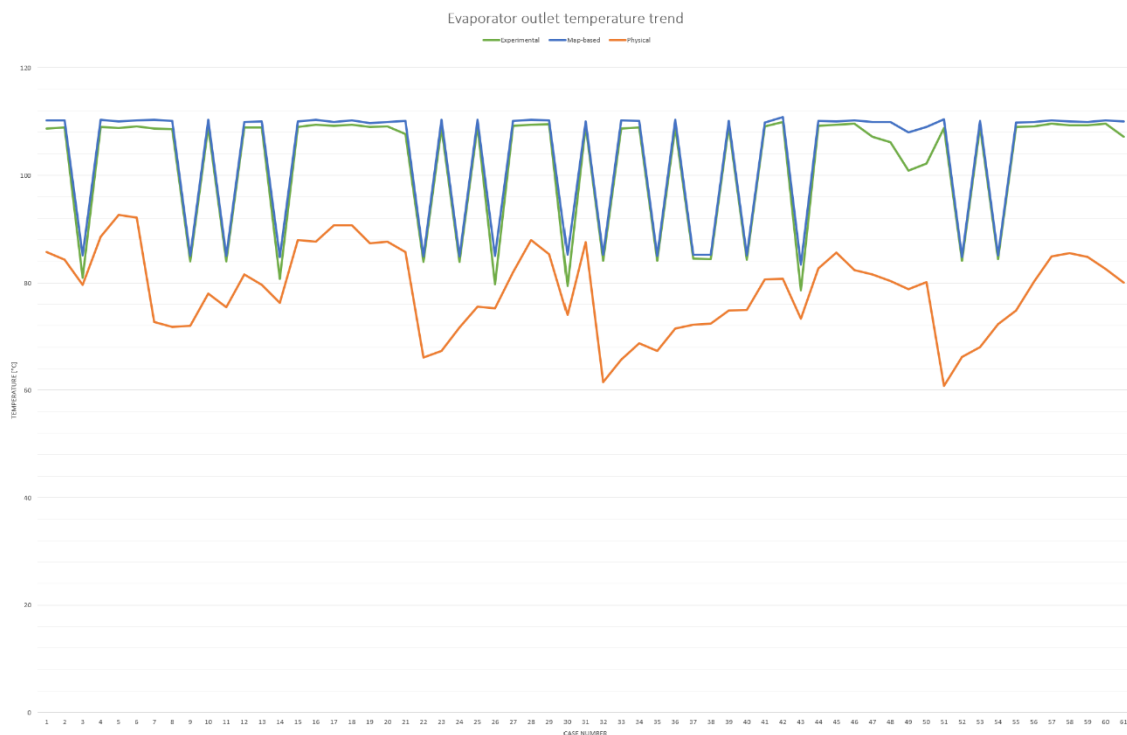


Fig. 4.4-2 - Temperature trend of three models, 3 segments evaporator

## Physical modelling of evaporator

To better compare the trend it is necessary to analyze the mean relative percentage error respect the experimental values:

ESPERIMENTAL (REFERENCE)	MAP-BASED	PHYSICAL-BASED
0%	1,7%	21,8%

Table 4.4-2 - Temperature mean relative percentage error, 3 segments evaporator

Graphically the error is:

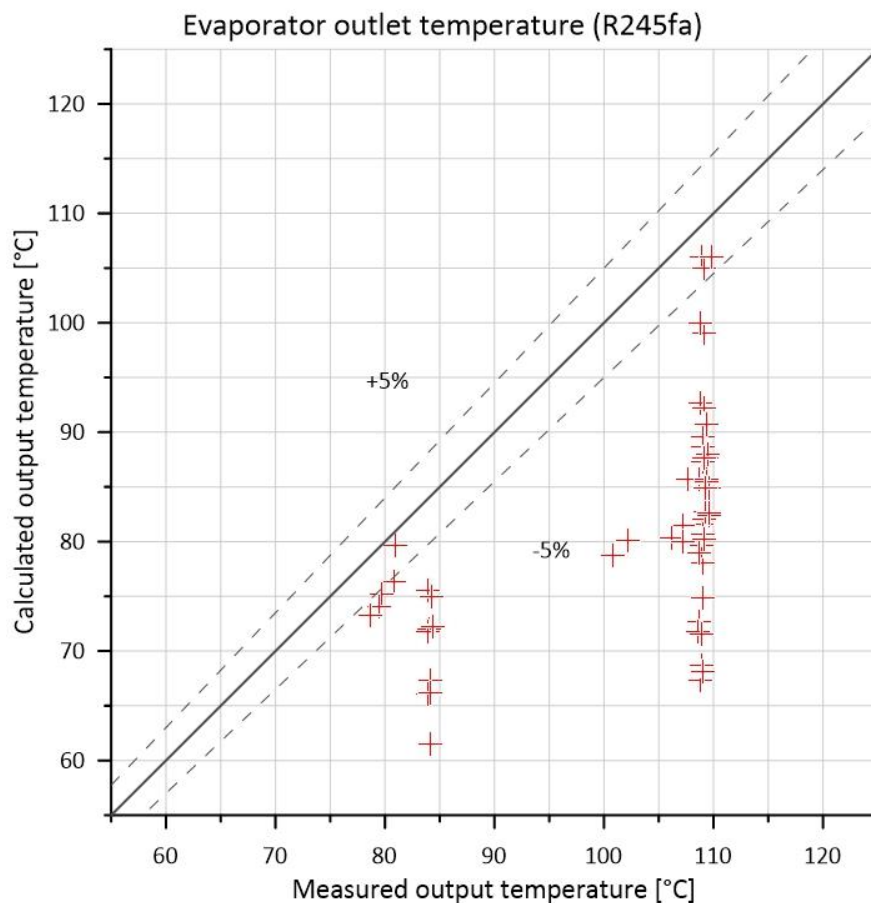


Fig. 4.4-3 - 61 cases temperature error trend, 3 segments evaporator

In this new model, as regards the temperature, it is possible to see that, although many values are outside the maximum range of  $\pm 5\%$ , range which allows to have a model that well represents the experimental trend, the average of the relative percentage errors, unlike the two segments model which was greater than this imposed limit, is higher than  $\pm 5\%$ . Therefore, although it is still

## Physical modelling of evaporator

necessary to improve the model, also if this divided into three segments represent more truthfully the temperature and is more realistic than the two segments model.

- PRESSURE

Now it moves to the analysis of pressure, following the same logical thread of temperature.

It starts with its average value:

EXPERIMENTAL [bar]	MAP-BASED [bar]	PHYSICAL-BASED [bar]
8,4	8,3	8,4

Table 4.4-3 - Pressure average comparison, 3 segments evaporator

Graphically the pressure trend is:

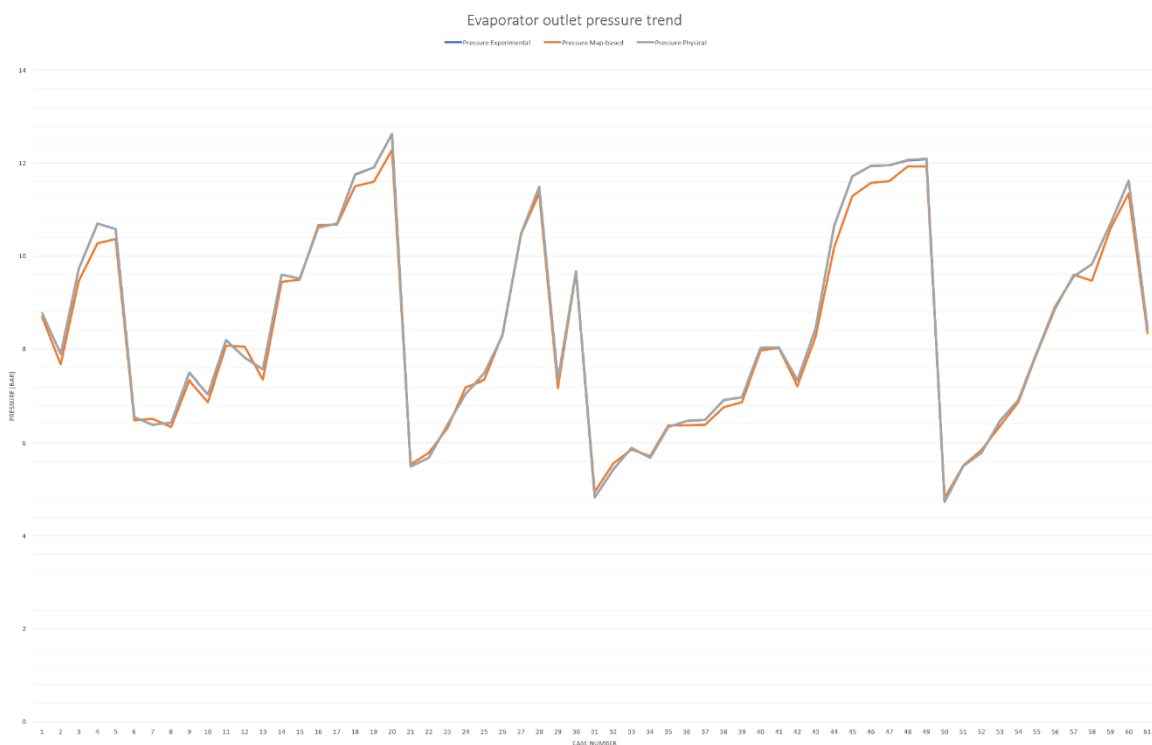


Fig. 4.4-4 - Pressure trend of three models, 3 segments evaporator

## Physical modelling of evaporator

As for the temperature, it is useful to analyze the relative percentage error respect the experimental values:

ESPERIMENTAL (REFERENCE)	MAP-BASED	PHYSICAL-BASED
0%	1,7%	0,02%

Table 4.4-4 – Pressure mean relative percentage error, 3 segments evaporator

Graphically the error is:

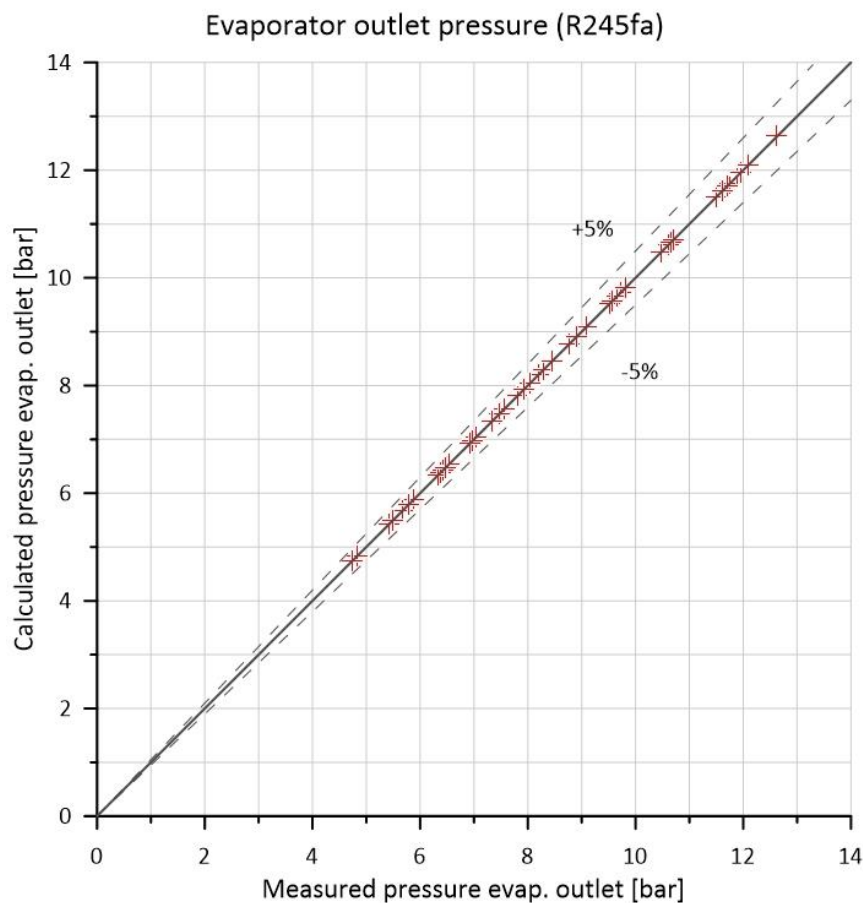


Fig. 4.4-5 - 61 cases pressure error trend, 3 segments evaporator

As for the two segments model, the relative percentage error relating to the experimental pressure values, falls well inside the imposed range of  $\pm 5\%$ , therefore it was possible to affirm that the pressure trend of the three segments physical-based model represent truthfully the experimental trend, and better compared to the map-based model.

Physical modelling of evaporator

- GAS FRACTION

The last parameter that it is possible to analyze is the gas fraction of the refrigerant R245fa at the outlet from the evaporator:

EXPERIMENTAL	MAP-BASED	PHYSICAL-BASED
100%	100%	15,0%

Table 4.4-5 - Refrigerant gas percentage comparison, 3 segments evaporator

Graphically the gas fraction average trend is:

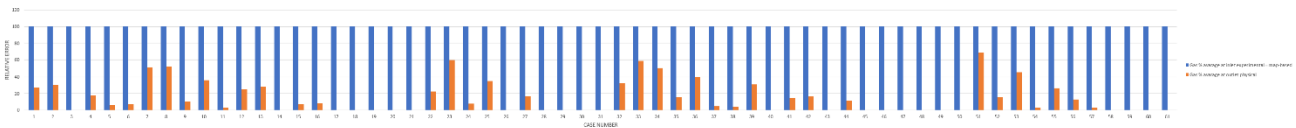


Fig. 4.4-6 - 61 case average gas fraction trend, 3 segments evaporator

As for the two previous parameters is better to analyze the mean relative percentage error respect the experimental trend:

EXPERIMENTAL (REFERENCE)	MAP-BASED	PHYSICAL-BASED
0%	0%	84,8%

Table 4.4-6 - Refrigerant gas fraction mean relative percentage error, 3 segments evaporator

The same conclusions for gas fraction can be made as for 2 segments model.

#### **4.4.2 Conclusions on the three segments model**

To conclude the discussion of the three segments model, it is possible to state that it faithfully represents the pressure trend of the R245fa at the evaporator outlet, while the temperature and gas fraction trend of R245fa at the evaporator outlet, despite a small improvement respect the two segments model, they produce an even greater relative percentage error than the map-based model. It is therefore necessary to further refine the model, which must be divided into four segments, thus going to further increase the number of wall temperatures and refining more the exchange in countercurrent.

### 4.5 Four segments physical-based model

As for previous models, it is possible to calculate the length and the exchange area of each segment:

$$\begin{aligned}
 \text{Total length}_{3 \text{ segments}} &= \frac{\text{length of a single channel}}{\text{number of segments}} = \frac{523,875}{4} = \\
 &= 130,969 \text{ mm}
 \end{aligned}$$

Equation 44

$$\text{Exchange area}_{4 \text{ segments}} = \frac{\text{Total exchange area}}{\text{number of segments}} = \frac{4191523,87}{4} = 1047880,968 \text{ mm}^2$$

Equation 45

The four segments model is:

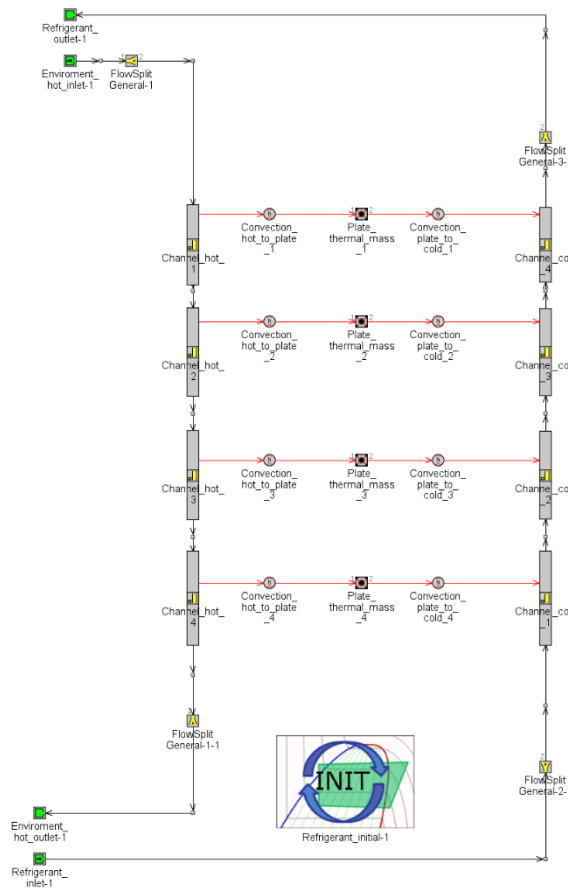


Fig. 4.5-1 - Four segments physical-based evaporator model

All values, except the geometrical ones related to the division in more segments, have been left equals to the three segments model.

## Physical modelling of evaporator

Without specify every single step, the same procedure and observation made for both two-segments and three-segments models can be applied also for the four segments model.

- TEMPERATURE

The average temperature value of R245fa at the evaporator outlet is:

EXPERIMENTAL [°C]	MAP-BASED [°C]	PHYSICAL-BASED [°C]
101,8	103,5	81,0

Table 4.5-1 - Temperature average comparison, 4 segments evaporator

Graphically the temperature trend is:

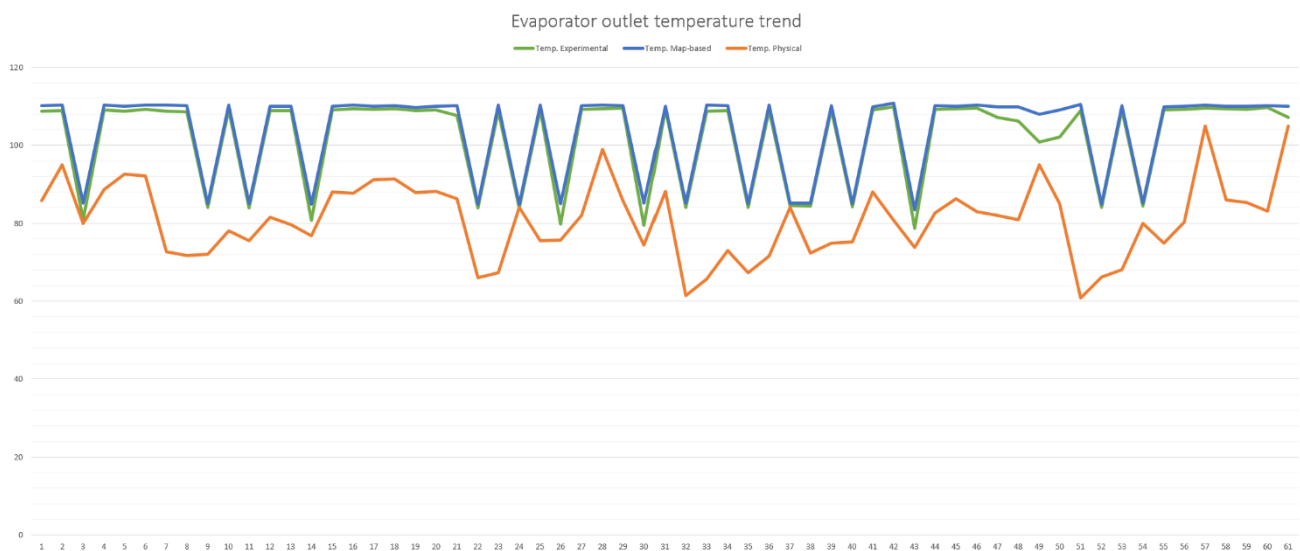


Fig. 4.5-2 - Temperature trend of three models, 4 segments evaporator

The temperature mean relative percentage error is:

ESPERIMENTAL (REFERENCE)	MAP-BASED	PHYSICAL-BASED
0%	1,7%	19,8%

Table 4.5-2 – Temperature mean relative percentage error, 4 segments evaporator

Physical modelling of evaporator

Graphically the error is:

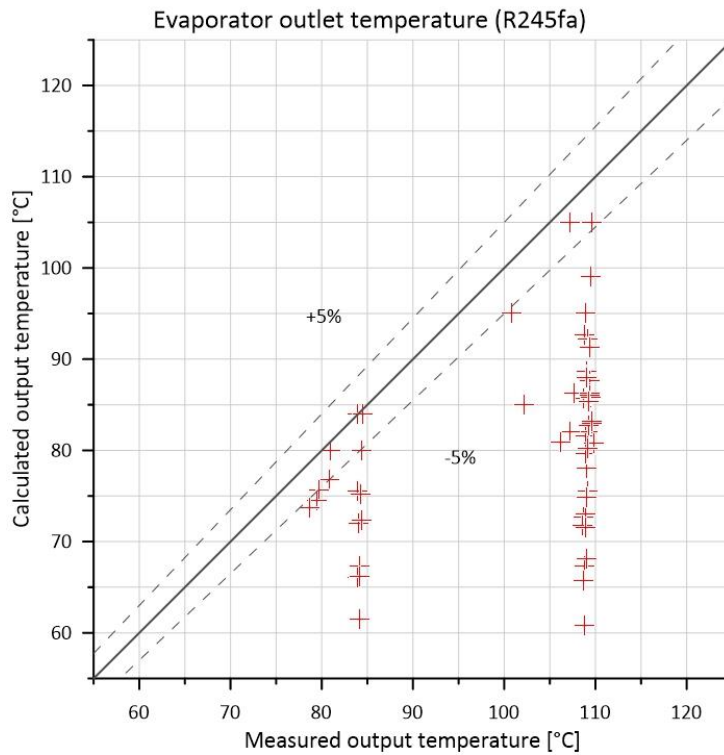


Fig. 4.5-3 - 61 cases temperature error trend, 4 segments evaporator

- PRESSURE

The pressure average of refrigerant R245fa at the evaporator outlet is:

EXPERIMENTAL [bar]	MAP-BASED [bar]	PHYSICAL-BASED [bar]
8,4	8,3	8,4

Table 4.5-3 - Pressure average comparison, 4 segments evaporator

Graphically the pressure trend is:

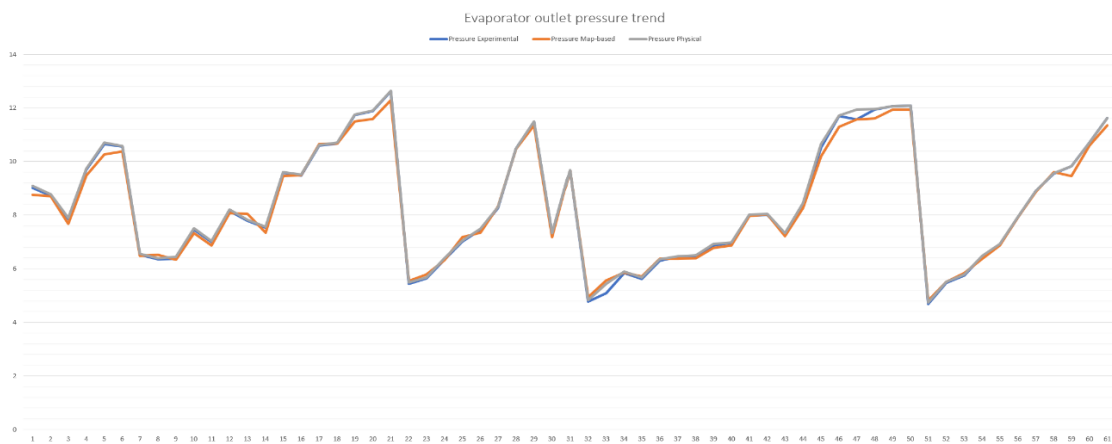


Fig. 4.5-4 - Pressure trend of three models, 4 segments evaporator

Physical modelling of evaporator

The mean pressure relative percentage error is:

ESPERIMENTAL (REFERENCE)	MAP-BASED	PHYSICAL-BASED
0%	1,7%	0,03%

Table 4.5-4 - Pressure mean relative percentage error, 4 segments evaporator

Graphically the relative percentage error is:

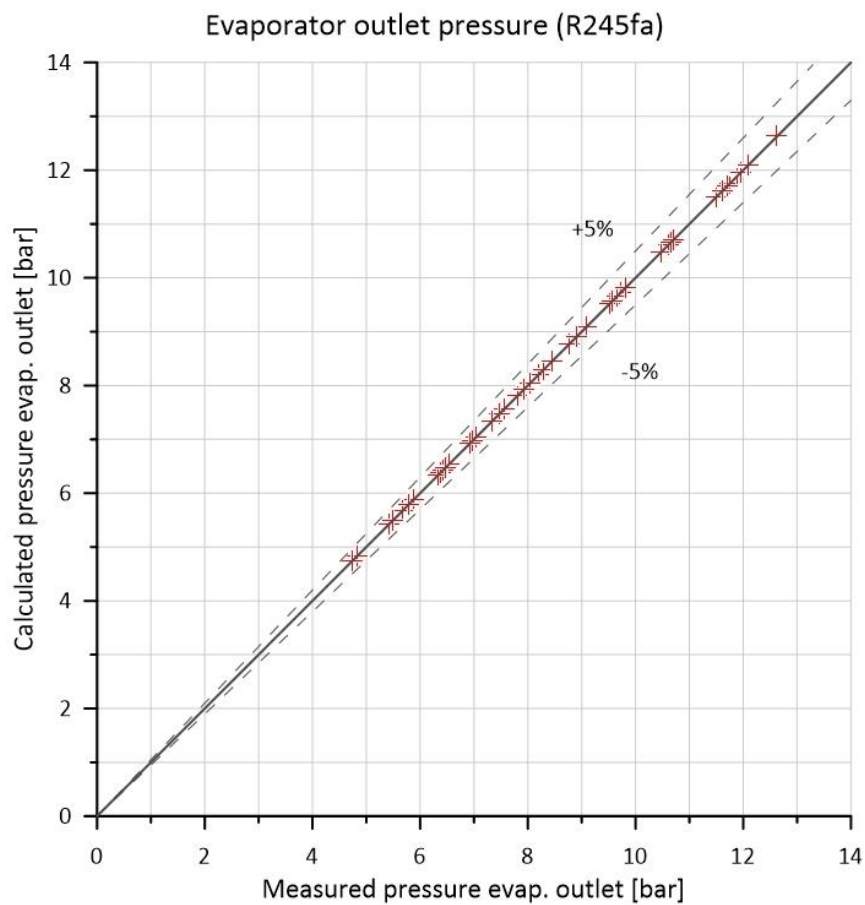


Fig. 4.5-5 - 61 cases pressure error trend, 4 segments evaporator

- GAS FRACTION

The gas fraction of R245fa at the evaporator outlet is:

EXPERIMENTAL	MAP-BASED	PHYSICAL-BASED
100%	100%	17,1%

Table 4.5-5 - Refrigerant gas percentage comparison, 4 segments evaporator

Physical modelling of evaporator

Graphically the gas fraction average trend is:

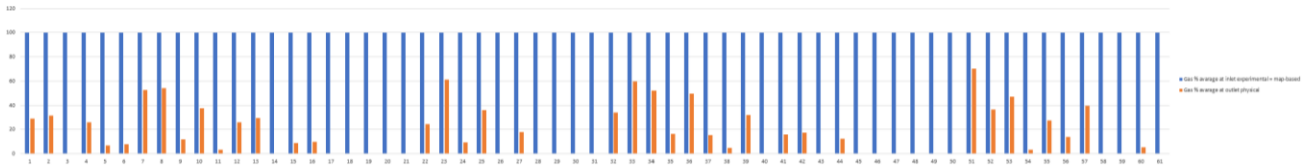


Fig. 4.5-6 - 61 case average gas fraction trend, 4 segments evaporator

The mean relative percentage error is:

EXPERIMENTAL (REFERENCE)	MAP-BASED	PHYSICAL-BASED
0%	0%	82,9%

Table 4.5-6 - Refrigerant gas fraction mean relative percentage error, 4 segments evaporator

**4.5.1 Conclusion on the four segments model**

To conclude the paragraph on the model divided into 4 segments, it is possible to affirm that, as for the two and three segments models, the pressure trend of the R245fa at the evaporator outlet is practically perfectly superimposable to the experimental trend, with a produced mean relative percentage error quite near to zero.

For the temperature of the R245fa at the evaporator outlet, it is possible to observe a further improvement in accuracy compared to the previous three segments model, but not yet sufficient to make fall the mean relative percentage error in the imposed range of  $\pm 5\%$  and even greater than the one produced by the map-based model.

The biggest problem is found on the R245fa gas fraction at the evaporator outlet which produces a still very high mean relative percentage error, with a consequent dual phase presence for R245fa at evaporator outlet in some of the simulated cases and, moreover, outside the desired range of  $\pm 5\%$ .

At this point it would have been possible to proceed with a further division into five segments, but, after an attempt made, a great expansion in simulation time was noted, without a benefit in accuracy so evident to justify the increase in simulation times, so its results are not reported.

To develop a model that is more accurate in the representation of experimental trend, it was necessary to move on the study of the value of *Heat Transfer Multiplier*, saw in the *paragraph 2.3.1*, starting from this four segments model.

## 5 Heat Transfer Multiplier study

As already mentioned in the previous *paragraph 4.5.1*, increasing the number of segments into which the model is divided, in the specific case of evaporator, imposes limits on the computational power and timing.

In order to solve the problem highlighted in the *paragraph 4.5.1*, it was necessary to move to the study of the *Heat Transfer Multiplier (HTM)* value, left up to this moment as the default value equal to one.

Quickly summarizing what it represents, it allows to consider the variation of the coefficients that influence the convective heat transfer coefficient which influence the convective resistance, which influence the heat flow, due to the variation in the type of channel geometry or exchange surface roughness. In the modeled exchanger, the HTM value becomes fundamental since, in addition to having a rectangular and non a cylindrical channel, the exchange surface is rippled to increase the exchange area and therefore the heat power exchanged.



*Figure 5.1 - View of the internal wavy exchange surface of BHPE*

The value of the HTM can therefore reach value of several tens, because the wavy finishing of the internal surfaces is approximated to an extremely rough surface.

### 5.1 Model considered for the HTM study

The model that was used for the study of the HTM was the model of the evaporator alone divided into four segments. This choice was made because, by isolating the evaporator, it was easier to compare the results with the experimental values and, in particular, to use the four segments model

because, despite it is the one with the longest simulation times, it was the one that had the best approximation of the experimental trend.

The values compared between the physical-based four segments model of the evaporator with different HMT values, the map-based model and the experimental data were temperature, pressure and gas fraction, with the respective relative percentage errors, of the refrigerant fluid R245fa at the evaporator outlet.

The simulation was carried out only changing, respect the 4 segments model view in the *paragraph 4.5*, the HMT value, maintaining an initial refrigerant density of  $450 \frac{kg}{m^3}$  and simulating all 61 known cases.

## 5.2 First attempt with HMT = 2

The implementation scheme that is shown, follows the same passages used for the implementation of the countercurrent exchange of the two, three and four segments model. The three parameters considered, with the reference relative percentage errors, were, as told in the paragraph above, temperature, pressure and gas fraction of R245fa at the outlet of evaporator, studied alone. Obviously for the study of HMT, only this was varied, leaving all other parameters unchanged compared to the 4 segments model, the design is identical to that seen in figure *Fig. 4.5-1*.

- TEMPERATURE

The first value analyzed is the average temperature of R245fa at the outlet of evaporator and it has been possible to compare with the value of the 4 segments model with default value equal to 1, obtained from simulation of model of *paragraph 4.5*, with the value obtained from the map-based model<sup>10</sup> and with the experimental value<sup>11</sup>:

	EXPERIMENTAL [°C]	MAP-BASED [°C]	PHYSICAL-BASED [°C]
<b>HTM = def = 1</b>	101,8	103,5	81,0
<b>HTM = 2</b>	101,8	103,5	81,7

*Table 5.2-1 – Temperature average, 4 segments evaporator, HMT = 2*

<sup>10</sup> The value of HMT in the exchanger in the map-based model is always the same, automatically calculated by the program.

<sup>11</sup> Experimental values are independent from the HMT value.

## Heat Transfer Multiplier study

The mean relative percentage errors respect the experimental value are:

	EXPERIMENTAL (REFERENCE)	MAP-BASED	PHYSICAL-BASED AVERAGE	PHYSICAL-BASED MAXIMUM
HTM= def = 1	0%	1,7%	19,8%	44,1%
HTM = 2	0%	1,7%	19,1%	39,5%

Table 5.2-2 – Temperature mean relative percentage error, 4 segments evaporator, HTM = 2

Graphically the error trend for the 61 known cases is:

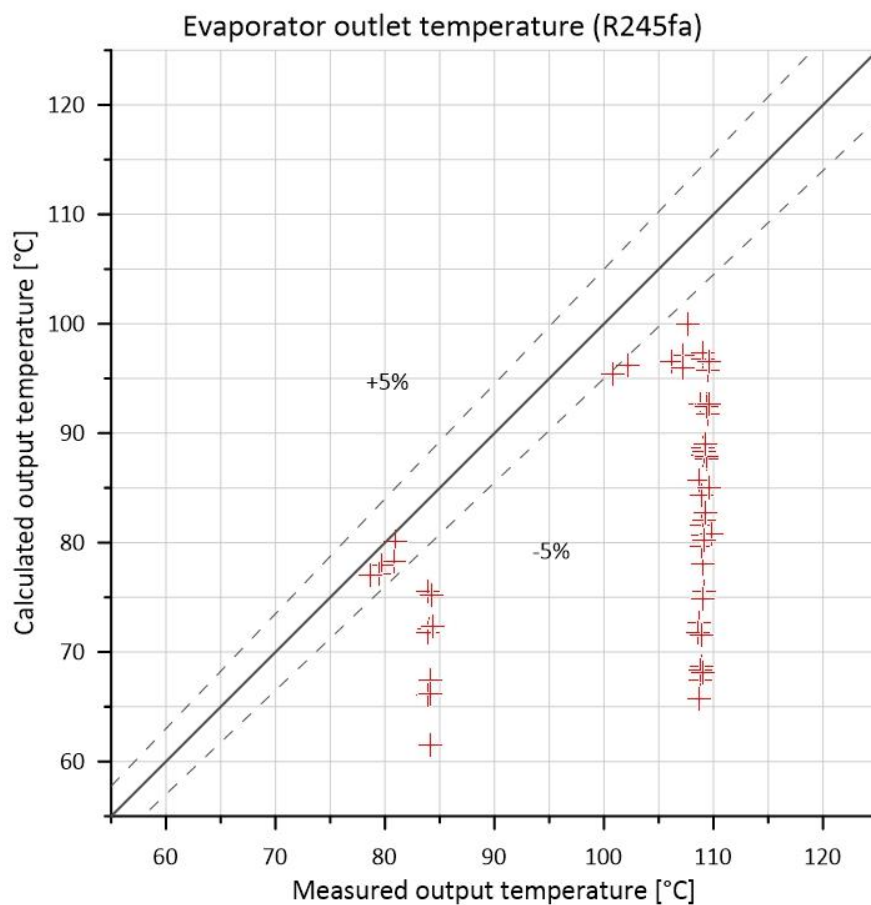


Fig. 5.2-1 – 61 cases temperature error trend, 4 segments evaporator, HTM = 2

Already passing from HTM = default = 1 to an HTM = 2, the error trend of the temperature improve, not fully falling within the imposed range of  $\pm 5\%$ , but being better than the trend obtained from the default model. However, the temperature trend is not even better than the map-based model trend and lot of cases' errors are out from the imposed range.

## Heat Transfer Multiplier study

- PRESSURE

The second compared value is the pressure of R245fa at the outlet from the evaporator. As for the temperature it is possible to compare with the value of the 4 segments model with default value equal to 1, with the value obtained from the map-based model<sup>12</sup> and with the experimental value<sup>13</sup>:

	EXPERIMENTAL [bar]	MAP-BASED [bar]	PHYSICAL-BASED [bar]
<b>HTM = def = 1</b>	8,4	8,3	8,4
<b>HTM = 2</b>	8,4	8,3	8,4

*Table 5.2-3 - Pressure average, 4 segments evaporator, HTM = 2*

The mean relative percentage errors respect the experimental value are:

	EXPERIMENTAL (REFERENCE)	MAP-BASED	PHYSICAL-BASED AVERAGE	PHYSICAL-BASED MAXIMUM
<b>HTM= def = 1</b>	0%	1,7%	0,03%	0,1%
<b>HTM = 2</b>	0%	1,7%	0,05%	0,2%

*Table 5.2-4 – Pressure mean relative percentage error, 4 segments evaporator, HTM = 2*

---

<sup>12</sup> The value of HTM in the exchanger in the map-based model is always the same, automatically calculated by the program.

<sup>13</sup> Experimental values are independent from the HTM value.

## Heat Transfer Multiplier study

Graphically the error trend for the 61 known cases is:

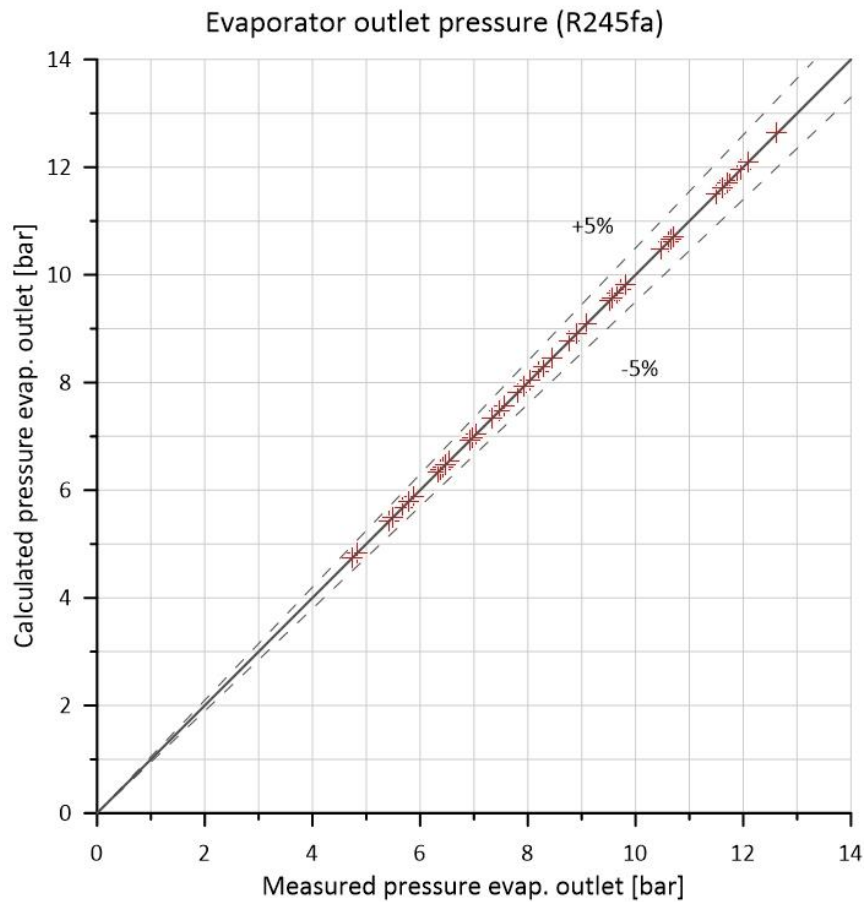


Fig. 5.2-2 - 61 cases pressure error trend, 4 segments evaporator, HTM = 2

As for the models with HTM = default = 1, analyzed in the previous paragraphs, the pressure trend is practically perfectly superposable to the experimental trend.

- GAS FRACTION

The last parameter analyzed is the R245fa gas fraction at the evaporator outlet. It is possible to begin to analyze the average value, comparing the values of the map-based model<sup>14</sup> and the experimental value<sup>15</sup>:

	EXPERIMENTAL	MAP-BASED	PHYSICAL-BASED
HTM = def = 1	100%	100%	17,1%
HTM = 2	100%	100%	38,0%

Table 5.2-5 – Gas fraction average, 4 segments evaporator, HTM = 2

Now it is possible to analyze the mean relative percentage error:

	EXPERIMENTAL	MAP-BASED	PHYSICAL-BASED AVERAGE	PHYSICAL-BASED MAXIMUM
HTM= def = 1	0%	0%	82,9%	100%
HTM = 2	0%	0%	62,0%	100%

Table 5.2-6 – Gas fraction mean relative percentage error, 4 segments evaporator, HTM = 2

The average error on the gas fraction has a notable improvement, but not an improvement in terms of maximum error. However, it is still far from the perfect desired error value quite neat to 0%, obtained even with the map-based model, with still a dual-phase coexistence in some cases.

### 5.2.1 Conclusions on the first attempt of HTM = 2

Although noticeable improvements can be appreciated on the temperature and gas fraction trend respect the 4 segments model with default value of Heat Transfer Multiplier, it was necessary to perform further tests with different HTM values to try to obtain a validated model that had the trends of the three considered variables as similar as possible to the experimental trends.

---

<sup>14</sup> The value of HTM in the exchanger in the map-based model is always the same, automatically calculated by the program.

<sup>15</sup> Experimental values are independent from the HTM value.

### 5.3 Parametric analysis of the HTM

Once the influence of the HTM on the heat exchange and consequently on the three variables considered of temperature, pressure and gas fraction has been demonstrated, a parametric analysis was carried out to obtain the HTM value that allows to have a more similar trend of the physical-based model as possible to the trend of experimental model.

The parametric analysis consists in keeping all the parameters fixed except for the Heat Transfer Multiplier, analyzing how it affect the three variables considered. Without repeating all parameters made previously, the result obtained are grouped by the influence value, to avoid the treatment becoming overly repetitive.

The model considered is the evaporator alone model, divided in 4 segments with an initial refrigerant R245fa density of  $450 \frac{kg}{m^3}$ .

#### 5.3.1 Temperature

The average temperature trend is:

	EXPERIMENTAL [°C]	MAP-BASED [°C]	PHYSICAL-BASED [°C]
HTM = def = 1	101,8	103,5	81,0
HTM = 2	101,8	103,5	81,7
HTM = 5	101,8	103,5	88,8
HTM = 10	101,8	103,5	95,9
HTM = 25	101,8	103,5	100,7
HTM = 50	101,8	103,5	101,8

Table 5.3-1 – Temperature average, 4 segments evaporator, HTM parametric analysis

The mean relative percentage error is:

	EXPERIMENTAL (REFERENCE)	MAP-BASED	PHYSICAL-BASED AVERAGE	PHYSICAL-BASED MAXIMUM
HTM= def = 1	0%	1,7%	19,8%	44,1%
HTM = 2	0%	1,7%	19,1%	39,5%
HTM = 5	0%	1,7%	12,6%	26,5%
HTM = 10	0%	1,7%	6,5%	19,0%
HTM = 25	0%	1,7%	2,3%	11,8%
HTM = 50	0%	1,7%	1,5%	7,2%

Table 5.3-2 – Temperature mean relative percentage error, 4 segments evaporator, HTM parametric analysis

### 5.3.2 Pressure

The average pressure trend is:

	EXPERIMENTAL [bar]	MAP-BASED [bar]	PHYSICAL-BASED [bar]
HTM = def = 1	8,4	8,3	8,4
HTM = 2	8,4	8,3	8,4
HTM = 5	8,4	8,3	8,5
HTM = 10	8,4	8,3	8,5
HTM = 25	8,4	8,3	8,5
HTM = 50	8,4	8,3	8,5

Table 5.3-3 - Pressure average, 4 segments evaporator, HTM parametric analysis

The mean relative percentage error is:

	EXPERIMENTAL (REFERENCE)	MAP-BASED	PHYSICAL-BASED AVERAGE	PHYSICAL-BASED MAXIMUM
HTM= def = 1	0%	1,7%	0,03%	0,1%
HTM = 2	0%	1,7%	0,05%	0,2%
HTM = 5	0%	1,7%	0,09%	0,2%
HTM = 10	0%	1,7%	0,1%	0,2%
HTM = 25	0%	1,7%	0,1%	0,2%
HTM = 50	0%	1,7%	0,1%	0,2%

Table 5.3-4 – Pressure mean relative percentage error, 4 segments evaporator, HTM parametric analysis

### 5.3.3 Gas fraction

The average gas fraction trend is:

	EXPERIMENTAL	MAP-BASED	PHYSICAL-BASED
HTM = def = 1	100%	100%	17,1%
HTM = 2	100%	100%	38,0%
HTM = 5	100%	100%	70,3%
HTM = 10	100%	100%	86,4%
HTM = 25	100%	100%	96,2%
HTM = 50	100%	100%	99,2%

Table 5.3-5 – Gas fraction average, 4 segments evaporator, HTM parametric analysis

The mean relative percentage error is:

	EXPERIMENTAL (REFERENCE)	MAP-BASED	PHYSICAL-BASED AVERAGE	PHYSICAL-BASED MAXIMUM
HTM= def = 1	0%	0%	82,9%	100%
HTM = 2	0%	0%	62,0%	100%
HTM = 5	0%	0%	29,7 %	78,4%
HTM = 10	0%	0%	13,6%	55,0%
HTM = 25	0%	0%	3,7%	25,0%
HTM = 50	0%	0%	0,8%	9,2%

Table 5.3-6 – Gas fraction mean relative percentage error, 4 segments evaporator, HTM parametric analysis

## 5.4 Results and graphs

In order to understand which HTM value best approximates the experimental trend, considering the three variables of temperature, pressure and gas fraction of R245fa at the evaporator outlet, it is useful to calculate the average of the mean relative percentage error of these ones, which, although not having a real physical meaning, but it is extremely useful for understanding how many difference there is between the studied physical-based model and the experimental plant.

The formula to evaluate the average of the mean relative percentage error (MRPE) is:

$$avarage_{MRPE} = \frac{MRPE_{temperature} + MRPE_{pressure} + MRPE_{gas\ fraction}}{3}$$

Equation 46

## Heat Transfer Multiplier study

The following table summarized the  $avarage_{MRPE}$  for the physical-based model for the different chosen HTM values, compared with the map-based  $avarage_{MRPE}$ <sup>16</sup>, for simulations on all 61 known cases:

	<b><math>avarage_{MRPE}</math> MAP – BASED</b>	<b><math>avarage_{MRPE}</math> PHYSICAL – BASED</b>
<b>HTM = 1</b>	1,1%	35,5%
<b>HTM = 2</b>	1,1%	27,1%
<b>HTM = 5</b>	1,1%	14,1%
<b>HTM = 10</b>	1,1%	6,7%
<b>HTM = 25</b>	1,1%	2,0%
<b>HTM = 50</b>	1,1%	0,8%

Table 5.4-1 – Comparison between map-based and physical-based evaporator 4 segments model for the  $avarage_{MRPE}$

As it is possible to observe, at the value of HTM = 10, there is the trade-off for which the  $avarage_{MRPE}$  of the physical-based model exceed the precision of the map-based model, but continue to increasing the HTM, it is possible arrive to have a very small  $avarage_{MRPE}$  of physical-based model, plenty inside the range considered in all previous studies of  $\pm 5\%$ , which represent an evolution of the model very similar to the experimental one.

The value that withstands the trend closest to the experimental one is that of HTM = 50.

This value could be further increased, however, this is not done for three reasons: first because the value would no longer be physically realistic; second because the simulation time increase a lot due to the more complex heat transfer phenomena; third because the error on the pressure increases a lot until it reaches a point where the pressure trend, from being extremely precise, would be incorrect.

The graphical trends of the temperature and pressure error and the trend of the gas fraction are now shown for the selected value of HTM = 50, which best approximates the real model, of R245fa at the physical-based four segments evaporator alone outlet.

<sup>16</sup> The value of HTM in the exchanger in the map-based model is always the same, automatically calculated by the program, so also the  $avarage_{MRPE}$  is always the same value.

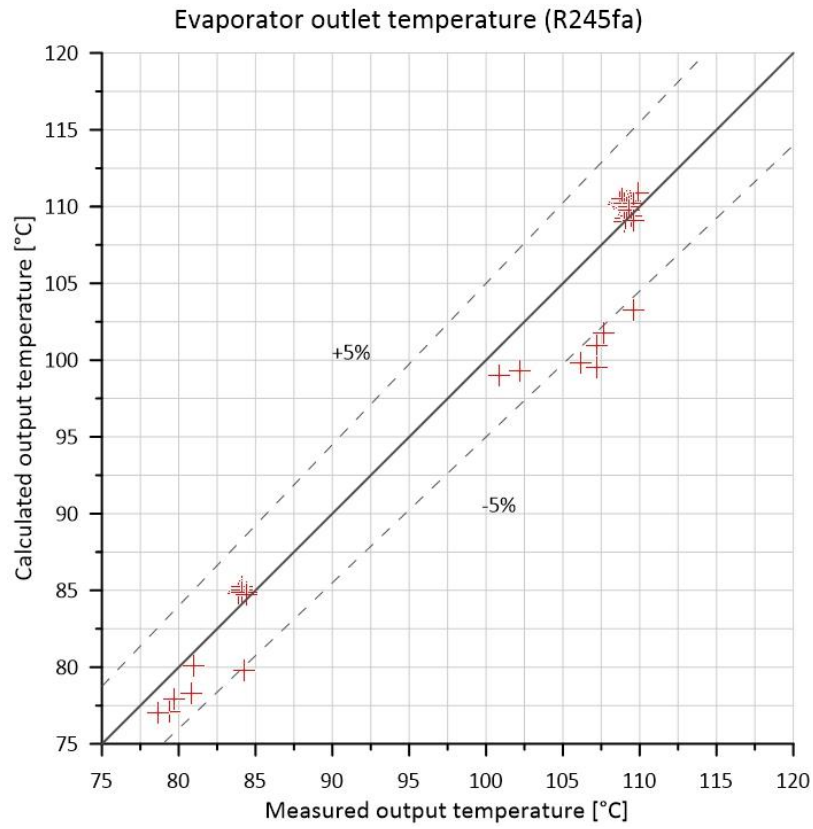


Fig. 5.4-1 - 61 cases temperature error trend, 4 segments evaporator, HTM = 50

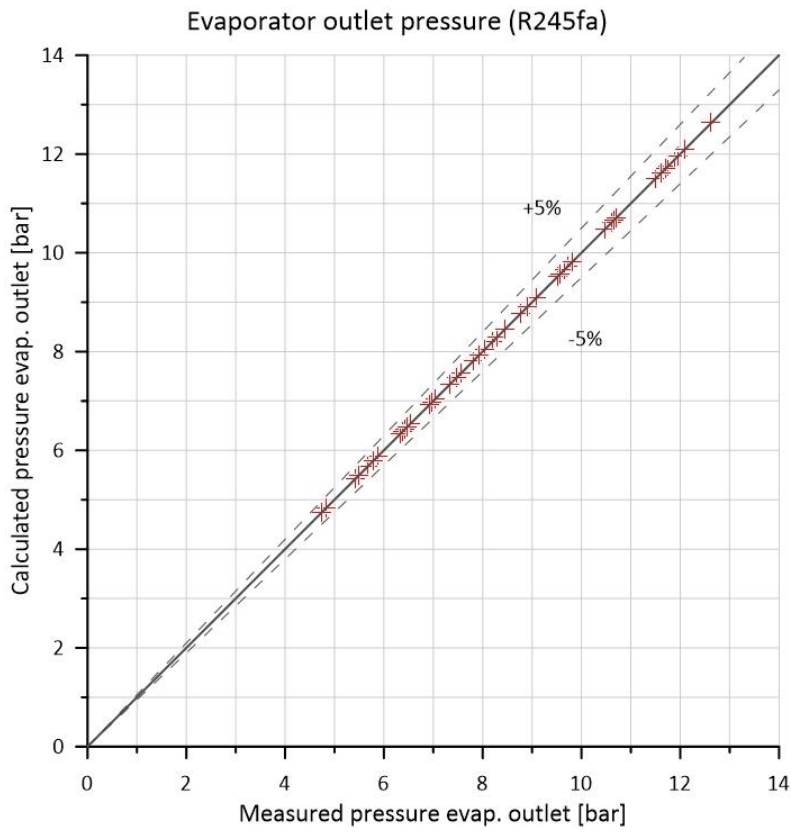


Fig. 5.4-2 - 61 cases pressure error trend, 4 segments evaporator, HTM = 50

## Heat Transfer Multiplier study

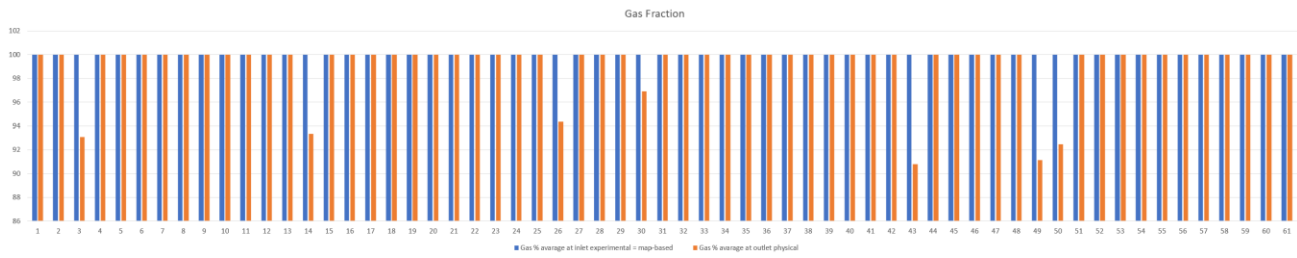


Fig. 5.4-3 – Gas fraction for 61 cases, 4 segments evaporator, HTM = 50

The four segments physical-based model of the evaporator with HTM = 50 can be considered validated and it is possible to affirm that its trend is superimposable to the experimental plant trend, and, moreover, it is possible to pass to the next step of insertion into the complete virtual plant.

## 6 Hybrid plant: physical-based evaporator in map-based plant

The results obtained until now, have allowed to arrive at a validated evaporator model, but the goal is to be able to validate the entire model of the plant. To achieve this, it was necessary to replace the newly validated physical-based evaporator at the old map-based evaporator inside the virtual plant map-based model plant described in the *Chapter 3*. In this way it was possible to get a system that can be nicknamed “hybrid”, because all its components inside were based on a map operation, while the evaporator was based on the physical operation.

### 6.1 Preparation of the model for simulation

The first step was to assemble the hybrid plant. The evaporator model chosen was the four segments one, because, as described in *paragraph 4.5*, this was the one that best approximates the experimental trend, already leaving the value of Heat Transfer Multiplier equals to default. Once the evaporator model was chosen, it was replaced in the map-based system:

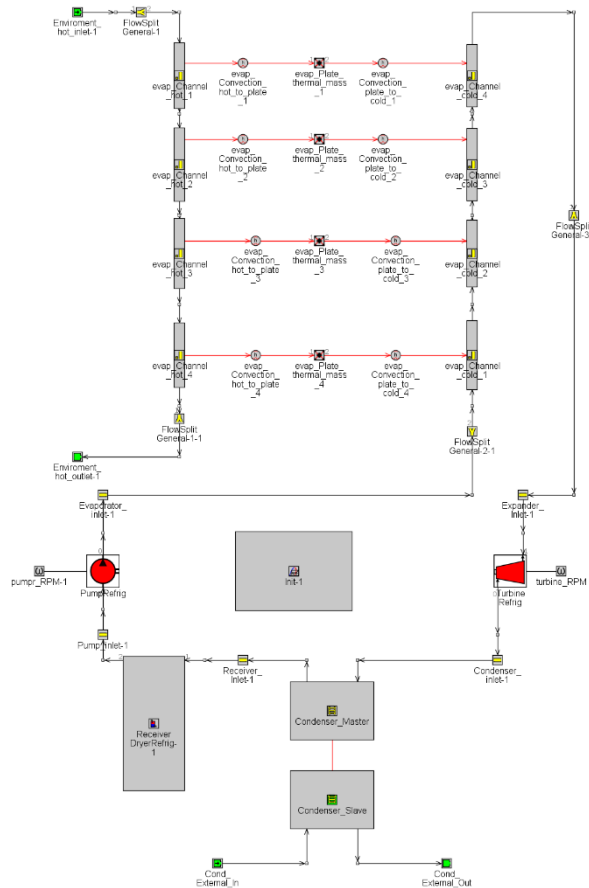


Fig. 6.1-1 – Hybrid plant with physical-based 4 segments evaporator

Hybrid plant: physical-based evaporator in map-based plant

The inlet and outlet conditions of the hot fluid (water), in master side, have been left unchanged with respect to the evaporator model studied alone, while the inlet values of the refrigerant R245fa no longer depends on the imposed boundary conditions, but as the evolution of the entire system returns the refrigerant to the inlet of evaporator itself.

In fact, by studying the evaporator alone, some variables cannot be taken into account, such as velocity of the fluid, mass flow rate or R245fa gas fraction at the inlet of evaporator, which depend on the evolution of the entire plant. It was for this reason that it was necessary to make a new study of the Heat Transfer Multiplier value for the new hybrid plant with physical-based evaporator, because first it was necessary to understand how this HTM value influence the heat transfer in the evaporator taking into account all the variable not considered until now and to make a comparison between the results found in the evaporator alone model and when it is inserted inside the complete plant.

The only value that is changed, compared to the model of the physical-based four segments evaporator alone, is the initial density of refrigerant R245fa: it is no longer set to an initial density of  $450 \frac{kg}{m^3}$ , but to the initial charge of 10 kg, as for the full map-based model, because the system now is closed, so it is more correct to use the initial charge value.

The simulations are performed on all 61 known cases.

## 6.2 Study of the Heat Transfer Multiplier value

As for all the models of the physical-based evaporator alone studied in the previous paragraphs, was necessary to make some attempts with different HTM values to find the trend of virtual model that best approximates the trend of the experimental plant. To satisfy this, in addition to the three variables considered in previous paragraphs of temperature, pressure and gas fraction of refrigerant R245fa at the evaporator outlet, a further variable was necessary to consider the functioning of the plant as a whole, that was the power to the shaft produced by the expander. To avoid that the discussion became repetitive, the result obtained are grouped by the influence value for different HTM values. It is good to specify, for a correct interpretation of the results, that experimental values are independent from the HTM value and the value of HTM in the exchangers of the full map-based model is always the same, automatically calculated by the program, so the results in this model don't change.

### 6.2.1 Temperature

The first analyzed value is the temperature average at the evaporator outlet:

	EXPERIMENTAL PLANT [°C]	MAP-BASED PLANT [°C]	HYBRID PLANT WITH PHYSICAL-BASED EVAPORATOR [°C]
HTM = def = 1	101,8	103,5	57,1
HTM = 2	101,8	103,5	66,4
HTM = 5	101,8	103,5	84,0
HTM = 10	101,8	103,5	95,2
HTM = 25	101,8	103,5	101,9
HTM = 50	101,8	103,5	103,2

Table 6.2-1 - Temperature average, hybrid plant with physical-based evaporator, HTM analysis

It is useful to analyze the mean relative percentage error and the maximum error produced by temperature for different HTM values:

	EXPERIMENTAL PLANT (REFERENCE)	MAP-BASED PLANT	HYBRID PLANT WITH PHYSICAL- BASED EVAPORATOR AVERAGE	HYBRID PLANT WITH PHYSICAL- BASED EVAPORATOR MAXIMUM
HTM= def = 1	0%	1,7%	43,7%	51,7%
HTM = 2	0%	1,7%	34,5%	42,9%
HTM = 5	0%	1,7%	17,6%	28,5%
HTM = 10	0%	1,7%	7,1%	20,6%
HTM = 25	0%	1,7%	1,6%	8,9%
HTM = 50	0%	1,7%	1,5%	7,6%

Table 6.2-2 - Temperature mean relative percentage error, hybrid plant with physical-based evaporator, HTM analysis

The temperature trend is very precise already for values of HTM = 25 and the mean relative percentage error is then quite stable even for higher values of HTM. It can be said that the temperature trend in the hybrid model with physical-based evaporator reflects the experimental trend well.

## 6.2.2 Pressure

The second analyzed value is the pressure average at the evaporator outlet:

	<b>EXPERIMENTAL PLANT</b> [bar]	<b>MAP-BASED PLANT</b> [bar]	<b>HYBRID PLANT WITH PHYSICAL-BASED EVAPORATOR</b> [bar]
<b>HTM = def = 1</b>	8,4	8,3	4,3
<b>HTM = 2</b>	8,4	8,3	5,5
<b>HTM = 5</b>	8,4	8,3	7,0
<b>HTM = 10</b>	8,4	8,3	7,8
<b>HTM = 25</b>	8,4	8,3	8,2
<b>HTM = 50</b>	8,4	8,3	8,3

Table 6.2-3 - Pressure average, hybrid plant with physical-based evaporator, HTM analysis

Also for pressure, it is useful to analyze the mean relative percentage error and the maximum error produced for temperature for different HTM values:

	<b>EXPERIMENTAL PLANT (REFERENCE)</b>	<b>MAP-BASED PLANT</b>	<b>HYBRID PLANT WITH PHYSICAL-BASED EVAPORATOR AVERAGE</b>	<b>HYBRID PLANT WITH PHYSICAL-BASED EVAPORATOR MAXIMUM</b>
<b>HTM= def = 1</b>	0%	1,7%	47,2%	62,4%
<b>HTM = 2</b>	0%	1,7%	32,2%	48,8%
<b>HTM = 5</b>	0%	1,7%	14,7%	31,7%
<b>HTM = 10</b>	0%	1,7%	6,8%	19,4%
<b>HTM = 25</b>	0%	1,7%	3,2%	8,1%
<b>HTM = 50</b>	0%	1,7%	2,1%	6,0%

Table 6.2-4 - Pressure mean relative percentage error, hybrid plant with physical-based evaporator, HTM analysis

For what concern the pressure, although the average value of the mean relative percentage error is in the imposed range for validation of  $\pm 5\%$ , the results of the full map-based plant are better than the hybrid plant with physical-based evaporator. However, it is possible to state that the trend of the pressure is anyway representative in a good way of the trend of the experimental plant.

### 6.2.3 Gas Fraction

At this point it possible to analyze the gas fraction percentage average:

	EXPERIMENTAL PLANT	MAP-BASED PLANT	HYBRID PLANT WITH PHYSICAL-BASED EVAPORATOR
HTM = def = 1	100%	100%	50,9%
HTM = 2	100%	100%	70,1%
HTM = 5	100%	100%	90,3%
HTM = 10	100%	100%	97,0%
HTM = 25	100%	100%	99,8%
HTM = 50	100%	100%	100%

Table 6.2-5 – Gas fraction average, hybrid plant with physical-based evaporator, HTM analysis

The mean relative percentage errors and maximum errors are:

	EXPERIMENTAL PLANT (REFERENCE)	MAP-BASED PLANT	HYBRID PLANT WITH PHYSICAL-BASED EVAPORATOR AVERAGE	HYBRID PLANT WITH PHYSICAL-BASED EVAPORATOR MAXIMUM
HTM= def = 1	0%	0%	49,2%	53,0%
HTM = 2	0%	0%	29,8%	49,8%
HTM = 5	0%	0%	9,7%	29,8%
HTM = 10	0%	0%	2,9%	17,5%
HTM = 25	0%	0%	0,2%	9,4%
HTM = 50	0%	0%	0%	0%

Table 6.2-6 – Gas fraction mean relative percentage error, hybrid plant with physical-based evaporator, HTM analysis

In this case in which the evaporator is insert inside the plant, it is possible to see that only for HTM equals to 50, there is at the outlet a single gaseous phase and therefore it is possible to affirm that the phase trend of virtual model of hybrid plant with physical-based evaporator is perfectly overlapped with the trend of the full map-based and experimental plants for this HTM value.

Hybrid plant: physical-based evaporator in map-based plant

### 6.2.4 Power

In addition to the three variables analyzed, in this case, it is useful to analyze the trend of the power to the shaft produced by the scroll expander, in order to have a reference parameter of how the plant is influenced by the evaporator HTM in its entirety.

It is possible to start analyzing the average power:

	EXPERIMENTAL PLANT [kW]	MAP-BASED PLANT [kW]	HYBRID PLANT WITH PHYSICAL-BASED EVAPORATOR [kW]
HTM = def = 1	1,9	1,9	0,1
HTM = 2	1,9	1,9	0,5
HTM = 5	1,9	1,9	1,2
HTM = 10	1,9	1,9	1,6
HTM = 25	1,9	1,9	1,8
HTM = 50	1,9	1,9	1,8

Table 6.2-7 - Power average, hybrid plant with physical-based evaporator, HTM analysis

Now it is possible to move to the mean relative percentage and maximum errors study:

	EXPERIMENTAL PLANT (REFERENCE)	MAP-BASED PLANT	HYBRID PLANT WITH PHYSICAL-BASED EVAPORATOR AVERAGE	HYBRID PLANT WITH PHYSICAL-BASED EVAPORATOR MAXIMUM
HTM= def = 1	0%	4,3%	98,3%	154,1%
HTM = 2	0%	4,3%	69,8%	130,1%
HTM = 5	0%	4,3%	32,6%	74,0%
HTM = 10	0%	4,3%	15,3%	50,9%
HTM = 25	0%	4,3%	6,7%	28,5%
HTM = 50	0%	4,3%	5,0%	25,5%

Table 6.2-8 – Power mean relative percentage error, hybrid plant with physical-based evaporator, HTM analysis

For the power to the shaft, it is possible to see that only the value of HTM = 50 allows to have a mean relative percentage error inside the range of  $\pm 5\%$ . The full map-based plant is, for this variable, better for the representation of the experimental trend.

### 6.3 Results and graphs

As for the HTM study of evaporator alone, it is useful to introduce the  $avarage_{MRPE}$ , as view in the paragraph 5.3.4.

In this case the formula includes also the mean relative error of power and became:

$$avarage_{MRPE} = \frac{MRPE_{temperature} + MRPE_{pressure} + MRPE_{gas\ fraction} + MRPE_{power}}{4}$$

Equation 47

	<b><math>avarage_{MRPE}</math> MAP – BASED</b>	<b><math>avarage_{MRPE}</math> HYBRID PLANT WITH PHYSICAL – BASED EVAPORATOR</b>
HTM = 1	2,7%	72,5%
HTM = 2	2,7%	51,0%
HTM = 5	2,7%	23,3%
HTM = 10	2,7%	10,5%
HTM = 25	2,7%	4,2%
HTM = 50	2,7%	3,1%

Table 6.3-1 - Comparison between full map-based plant and hybrid plant with physical-based evaporator for the  $avarage_{MRPE}$

The value that best approximates the experimental trend turns out to be HTM = 50.

However, the full map-based plant produces a lower overall error than the hybrid plant with physical-based evaporator and therefore better represents the trend of the experimental plant. For this reason, it was necessary to further implement the hybrid system by also replacing the exchanger that acts as the condenser.

Before proceeding to explain this implementation, the graphs of temperature<sup>17</sup>, pressure<sup>17</sup> and power errors and of the gas fraction trend<sup>17</sup> of hybrid plant with physical-based evaporator with HTM = 50 for the 61 cases considered are inserted.

---

<sup>17</sup> Referred to the refrigerant R245fa at the evaporator outlet.

# Hybrid plant: physical-based evaporator in map-based plant

Temperature error trend:

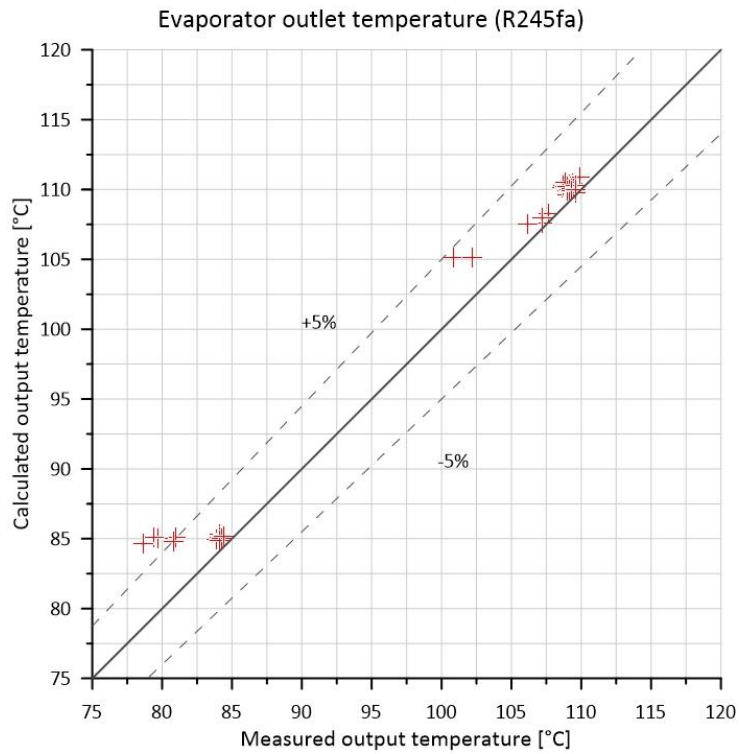


Fig. 6.3-1 - 61 cases temperature error trend, hybrid plant with physical-based evaporator, HTM = 50

Pressure error trend:

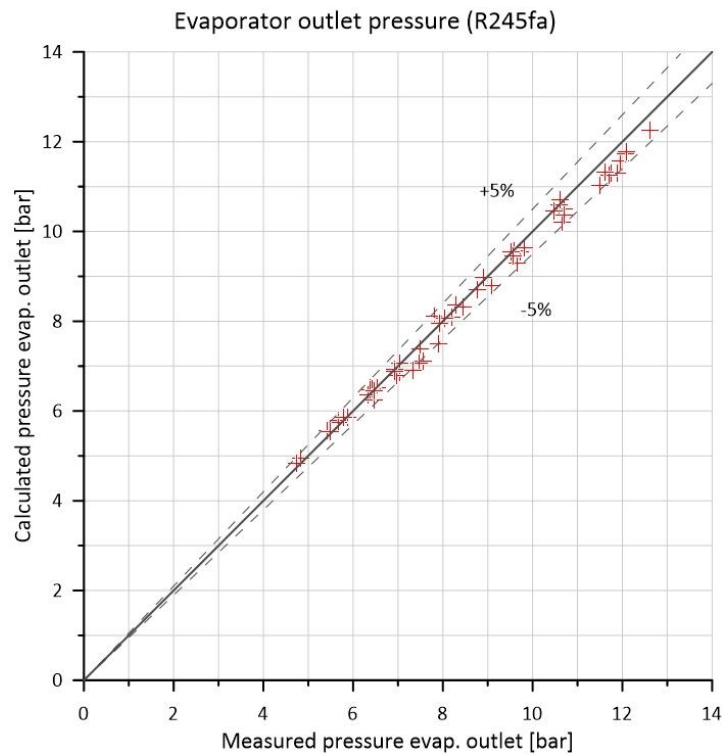


Fig. 6.3-2 - 61 cases pressure error trend, hybrid plant with physical-based evaporator, HTM = 50

# Hybrid plant: physical-based evaporator in map-based plant

Power error trend:

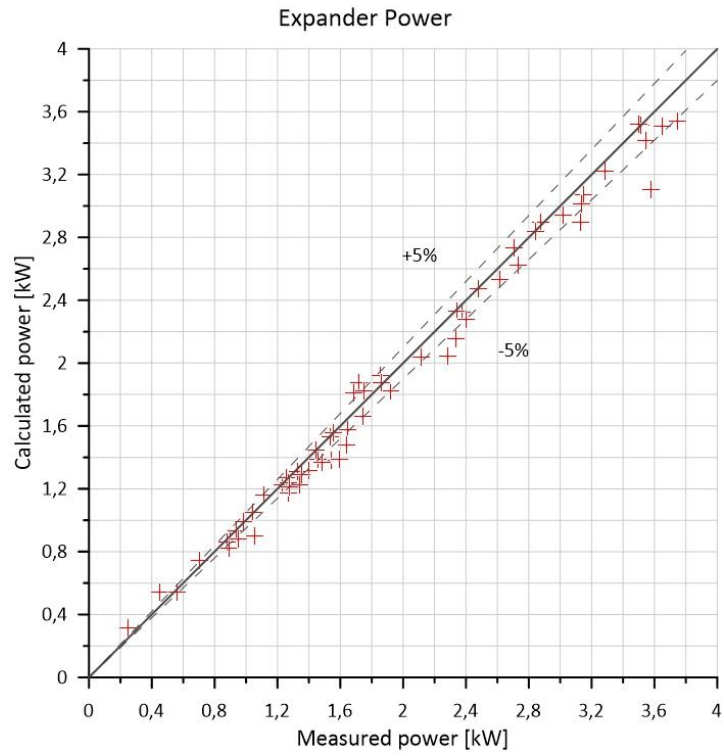


Fig. 6.3-3 – 61 cases power error trend, hybrid plant with physical-based evaporator, HTM = 50

Gas fraction trend:

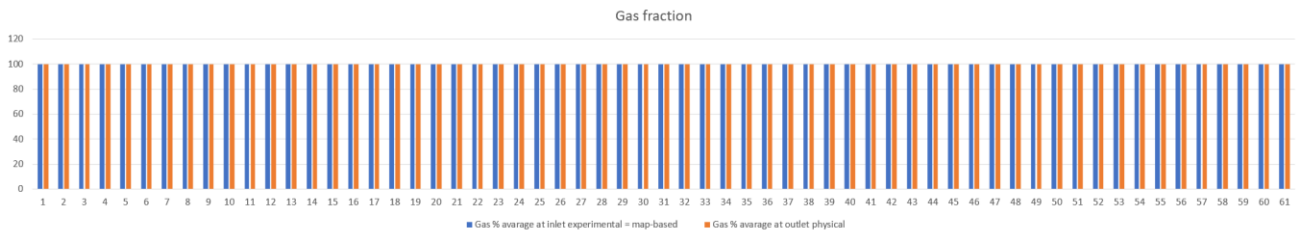


Fig. 6.3-4 - 61 cases gas fraction trend, hybrid plant with physical-based evaporator, HTM = 50

## **7 Hybrid plant: physical-based evaporator and condenser in map-based plant**

To complete the study of how physical-based heat exchangers behave inside the map-based plant, it was also necessary to replace the physical-based condenser, in addition to the evaporator already analyzed in the previous paragraph, at the map-based one.

### **7.1 Physical-based condenser**

The model of heat exchanger that acts as the condenser is exactly identical to the one that acts as an evaporator. For this reason, a separated study of this component alone was not necessary, but was sufficient to replicate the four segments evaporator model, replacing the inlet and outlet conditions for the hot and cold side and inverting them, and to insert it directly into the map-based plant.

However, it was decided to separate the study of Heat Transfer Multiplier between the evaporator and condenser, because the boundary conditions of the two components were different, such as temperature and pressure, so a study of both multipliers individually was more correct.

For this case, given the complexity of the model and the separation of the HTM values study, hence the increase of the number of variables that can be modified, it has been opted for an automated study that will be described in the next paragraphs, called multi-object multi-objective optimization. Before proceeding with this automated study, it was necessary to verify that the HTM values of physical-based evaporator and condenser inserted in the map-based plant, influenced the operation of this hybrid plant. For this reason, one attempt, before the optimization, was made comparing the results of two simulations of all 61 cases with two different HTM values for evaporator and condenser, analyzing four parameters that affected the operation of the plant, of which the correspondent experimental data are known, to verify the influence of HTM on those ones. This chosen parameters were temperature of R245fa at the outlet from evaporator, gas fraction of the R245 at the inlet of expander, temperature of R245fa at the outlet from condenser and power to the shaft produced by the expander.

# Hybrid plant: physical-based evaporator and condenser in map-based plant

The hybrid map-based plant with physical-based condenser and evaporator as a whole is now illustrated:

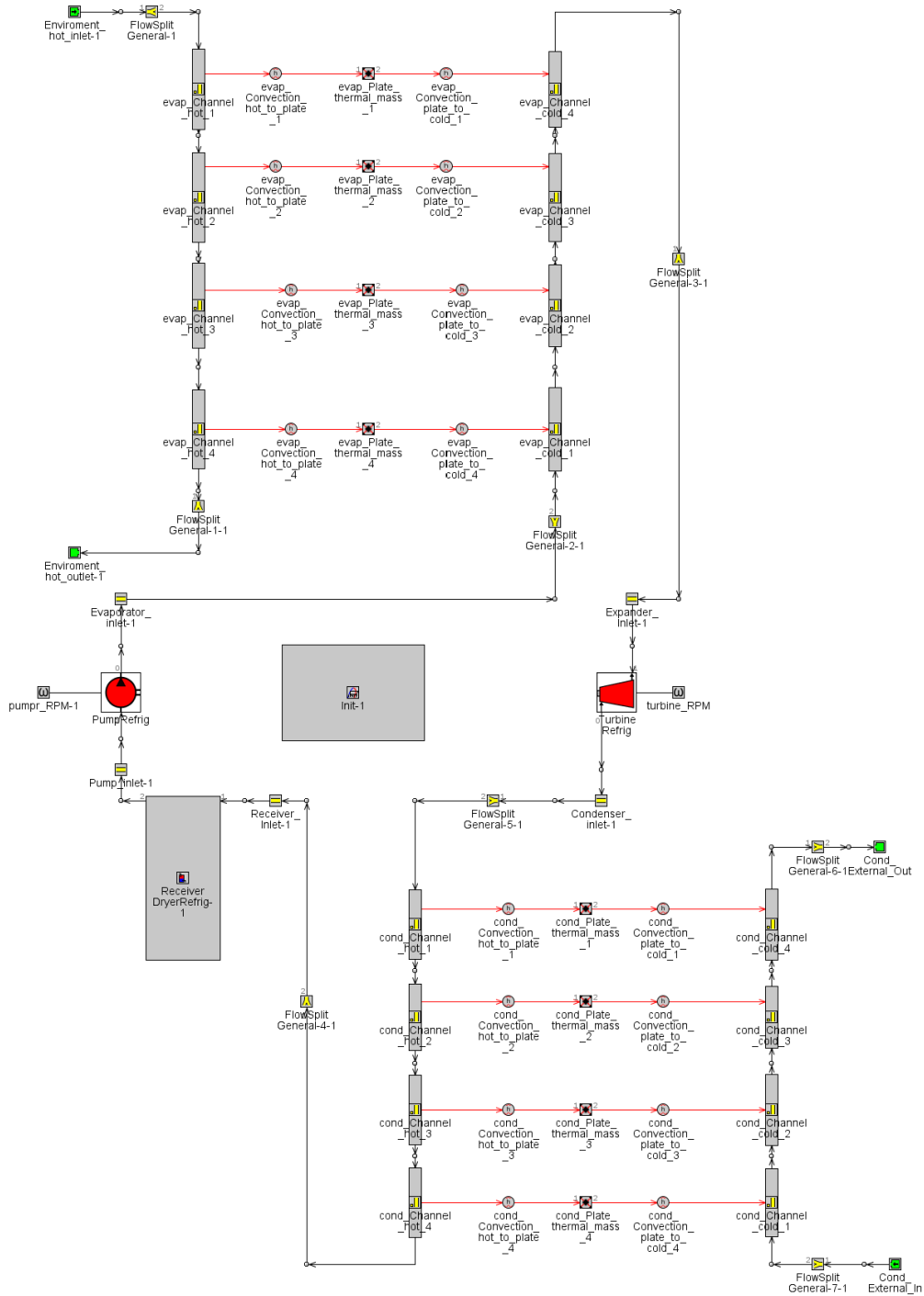


Fig. 7.1-1 – Hybrid map-based plant with physical-based condenser and evaporator

Hybrid plant: physical-based evaporator and condenser in map-based plant

### 7.1.1 Result of verification of the HTMs of evaporator and condenser influence

The values chosen to perform the simulation of all 61 known cases and to make the comparison of the results are the value following values:

	HTM evaporator	HTM condenser
<b>SIMULATION 1</b>	1	1
<b>SIMULATION 2</b>	5	5

Table 7.1-1 - Chosen value for verification of HTM values influence

The results of the average values of the four variables used are grouped in the following table:

	TEMPERATURE OF R245fa AT THE EVAPORATOR OUTLET [°C]	TEMPERATURE OF R245fa AT THE CONDENSER OUTLET [°C]	GAS FRACTION OF R245fa AT EVPORATOR OUTLET	POWER PRODUCED BY EXPANDER [kW]
<b>EXPERIMENTAL PLANT</b>	101,8	16,8	100%	1,9
<b>FULL MAP-BASED PLANT</b>	103,4	19,3	100%	1,9
<b>HYBDRID PLANT WITH PHYSICAL-BASED EVAPORATOR AND CONDENSER WITH <math>HTM_{evaporator} = HTM_{condenser} = 1</math></b>	61,2	55,2	52,5%	-0,6
<b>HYBDRID PLANT WITH PHYSICAL-BASED EVAPORATOR AND CONDENSER WITH <math>HTM_{evaporator} = HTM_{condenser} = 5</math></b>	85,3	40,0	90,8%	0,6

Table 7.1-2 – Values average, hybrid plant with physical-based evaporator and condenser, HTM analysis

Hybrid plant: physical-based evaporator and condenser in map-based plant

It is now possible to move to the study of the mean relative percentage error (MRPE) for the four chosen variables:

	<b>MRPE TEMPERATURE OF R245fa AT THE EVAPORATOR OUTLET</b>	<b>MRPE TEMPERATURE OF R245fa AT THE CONDENSER OUTLET</b>	<b>MRPE GAS FRACTION OF R245fa AT EVPORATOR OUTLET</b>	<b>MRPE POWER PRODUCED BY EXPANDER</b>
<b>EXPERIMENTAL PLANT (REFERENCE)</b>	0%	0%	0%	0%
<b>FULL MAP-BASED PLANT</b>	1,7%	15,8%	0%	4,3%
<b>HYBDRID PLANT WITH PHYSICAL-BASED EVAPORATOR AND CONDENSER WITH <math>HTM_{evaporator} = HTM_{condenser} = 1</math></b>	39,5%	236,7%	47,5%	156,7%
<b>HYBDRID PLANT WITH PHYSICAL-BASED EVAPORATOR AND CONDENSER WITH <math>HTM_{evaporator} = HTM_{condenser} = 5</math></b>	16,4%	141,5%	9,2%	72,7%

Table 7.1-3 – Mean relative percentage error, hybrid plant with physical-based evaporator and condenser, HTM analysis

Despite the values appear very far from the experimental or full map-based plant and, consequently, also the mean relative percentage errors are very large and far from the  $\pm 5\%$  range to be able to consider the plant as validated, it is possible to arrive at the conclusion that HTM values of condenser and evaporator influence the selected variables and, consequently, the functioning of overall plant. Up to now it has been considered the HTM values of condenser and evaporator to be equal, but in practice, due to the different use and operation with fluids at different temperature, pressure and thermodynamical conditions, the HTM values, that allow to have a representation as realistic as possible of experimental trend, could be different between the two components. For this reason the two values of HTM of condenser and evaporator should be studied independently, but due this manually can be very long and complex, so a multi-object multi-objective analysis

Hybrid plant: physical-based evaporator and condenser in map-based plant

was opted to find the HTM that best approximates the power experimental trend, but at the same time trying to maintain a good temperatures trend of R245fa at condenser and evaporator outlet and a good trend of R245 gas fraction at evaporator outlet.

## 7.2 Multi-object multi-objective optimization

The multi-object multi-objective optimization allows to find the HTM value of condenser and evaporator that best approximates the experimental trend of some known quantities that were selected.

To do this optimization was used the software *modeFRONTIER* which allows to use the hybrid map-based virtual plant with physical-based condenser and evaporator built on the software GT-Suite and, setting the various input and output parameters for optimization, to perform it autonomously.

### 7.2.1 Input parameters

The input parameters were those that the software had to optimize. In the case considered, they were the Heat Transfer Multiplier of the condenser and evaporator. It is necessary to make a clarification because there is a division of the model of exchangers between the hot side and cold side, so it was necessary to set four parameters to be studied in the program: HTM of the evaporator for exchange from hot side (hot water) to the division flow plate, HTM of evaporator for exchange from the division flow plate to the cold side (R245fa), HTM of condenser for exchange from the hot side (R245fa) to the division flow plate and HTM of condenser for exchange from the division flow plate to the cold side (cold water).

### 7.2.2 Output parameters

The output parameters are the value that the program uses to find the HTM values that best approximate their trend. In the case considered, given that the study of this thesis focuses on the analysis of the heat exchanger which act as condenser and evaporator, the chosen parameters were: inlet and outlet temperatures of R245fa for the evaporator, inlet and outlet temperatures of R245fa for condenser and the power produced by the expander, in order to also have an optimization of the plant as a whole.

## Hybrid plant: physical-based evaporator and condenser in map-based plant

In particular, the program works on the relative percentage error calculated with respect to the experimental correspondent values, calculated with *Equation 37*.

This type of optimization requires a lot of computing power and even a lot of time, so for this reason it was decided not to perform it on all 61 known cases, but only on 14 cases, selected so that they can be representative of different plant operating conditions.

### 7.2.3 Optimization model

The following figure represents the complete constructed model for optimization:



Fig. 7.2-1 – modeFRONTIER optimization model

Hybrid plant: physical-based evaporator and condenser in map-based plant

#### 7.2.4 Optimization settings

The optimization algorithm set was MOGA II (Multi Objective Genetic Algorithm), which bases its function on the theory of Pareto Front.

The Pareto front is a set of optimal solutions, made up of all non-dominated points, which means that the chosen point not prefers one solution respect others, but is the best at the same time for all objectives considered in the optimization function. In general, this type of solution is largely used in engineering solution, where the designers need to evaluate a multitude of several possible optimal solutions.

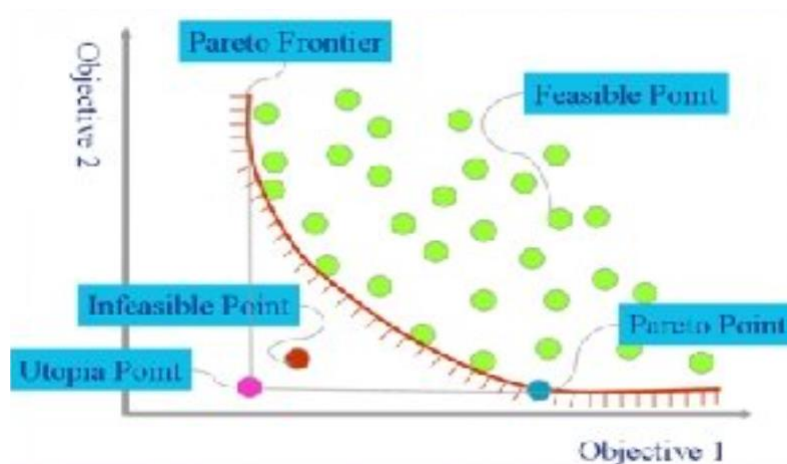


Fig. 7.2-2 – Pareto Front example curve

Once the optimization algorithm has been chosen, its first attempt values have been set. The *SpaceFiller* used were:

- Random
- SOBOL
- Latin Hypercube – Monte Carlo

For each *SpaceFiller* were defined 10 starting families of the plant.

As already mentioned, 14 cases have been chosen, for each of which 5 output variables have been set. Considering a number of generations for the MOGA II set to 100, about 3000 combinations are obtained.

### 7.3 Optimization results

Having set up a genetic algorithm based on the Pareto Front solution, in order to evaluate the solution given by the optimization, that best approximates the experimental trend of the hybrid model with physical-based condenser and evaporator, was taken the solution that provides the shortest distance with respect the origin of the  $n$ -dimensional error graph.  $n$  is evaluated as follows:

$$\begin{aligned}
 n &= \text{number of optimization function} = \text{number of considered case} * \text{number of output paramters} = \\
 &= 14 * 5 = 70 \\
 &\text{Equation 48}
 \end{aligned}$$

The formula for evaluating the minimum distance from the origin, considering the calculated values of percentage errors, is the following:

$$\text{distance}_{min} = \sqrt{\sum_{i=1}^n \text{percentage error}_i^2}$$

Equation 49

In this case, therefore, it is not useful to use the mean percentage relative errors as there would be a risk of having a solution which, despite the mean relative percentage error is small, it contains some very low errors, but others very large. In this way an optimization of all objective functions would not have been made, but only some of them. Considering, instead, the  $\text{distance}_{min}$ , it is possible to be sure to find the value that optimizes all the objective function in an impartial way, even if the mean relative percentage error can be greater respect other cases. It is sure to have and optimization that does not prefer some objective functions respect others, finding the correlated HTM values that best describe the experimental trend of the plant as a whole.

Hybrid plant: physical-based evaporator and condenser in map-based plant

At the end of all optimization simulation, the values of HTM that best approximate the trend of experimental plant were obtained, using the  $distance_{min}$  value as selection criteria:

<b>HTM EVAPORATOR, EXCHANGE FROM HOT TO PLATE</b>	24,6
<b>HTM EVAPORATOR, EXCHANGE FROM PLATE TO COLD</b>	23,0
<b>HTM CONDENSER, EXCHANGE FROM HOT TO PLATE</b>	42,7
<b>HTM CONDENSER, EXCHANGE FROM PLATE TO COLD</b>	27,1
<b>TEMPERATURE MEAN RELATIVE PERCENTAGE ERROR FOR 14 SELECTED CASES OF R245FA AT THE EVAPORATOR INLET</b>	19,5%
<b>TEMPERATURE MEAN RELATIVE PERCENTAGE ERROR FOR 14 SELECTED CASES OF R245FA AT THE EVAPORATOR OULET</b>	0,4%
<b>TEMPERATURE MEAN RELATIVE PERCENTAGE ERROR FOR 14 SELECTED CASES OF R245FA AT THE CONDENSER INLET</b>	10,2%
<b>TEMPERATURE MEAN RELATIVE PERCENTAGE ERROR FOR 14 SELECTED CASES OF R245FA AT THE CONDENSER OUTLET</b>	2,2%
<b>POWER MEAN RELATIVE PERCENTAGE ERROR FOR 14 SELECTED CASES PRODUCED BY THE EXPANDER</b>	5,7%
<b>AVERAGE OF MEAN RELATIVE PERCENTAGE ERRORS</b>	7,6%
<b>ERROR <math>distance_{min}</math></b>	87,2%

Table 7.3-1 – Hybrid map-mased plant with physical-based condenser and evaporator optimization results

To obtain results that allow to highlight the usefulness of optimization, it was decided to introduce a comparison between the hybrid map-based plant with physical-based condenser and evaporator not optimized, so with the HTM values left as default = 1, with the one with optimized HTM values. In order to make this comparison, a complete simulation on all 61 known cases was carried out with the optimized HTM values, comparing the mean relative percentage error with respect the known experimental data, of some selected variables.

Hybrid plant: physical-based evaporator and condenser in map-based plant

- TEMPERATURE OF R245FA AT THE EVAPORATOR INLET

EXPERIMENTAL (REFERENCE)	FULL MAP-BASED	HYBRID NOT OPTIMIZED	HYBRID OPTIMIZED
0%	23,9%	282,0%	25,3%

Table 7.3-2 – Temperature evaporator inlet comparison between experimental, map-based, hybrid not optimized and hybrid optimized plants

Graphically the error comparison between the hybrid not optimized and the optimized plants is:

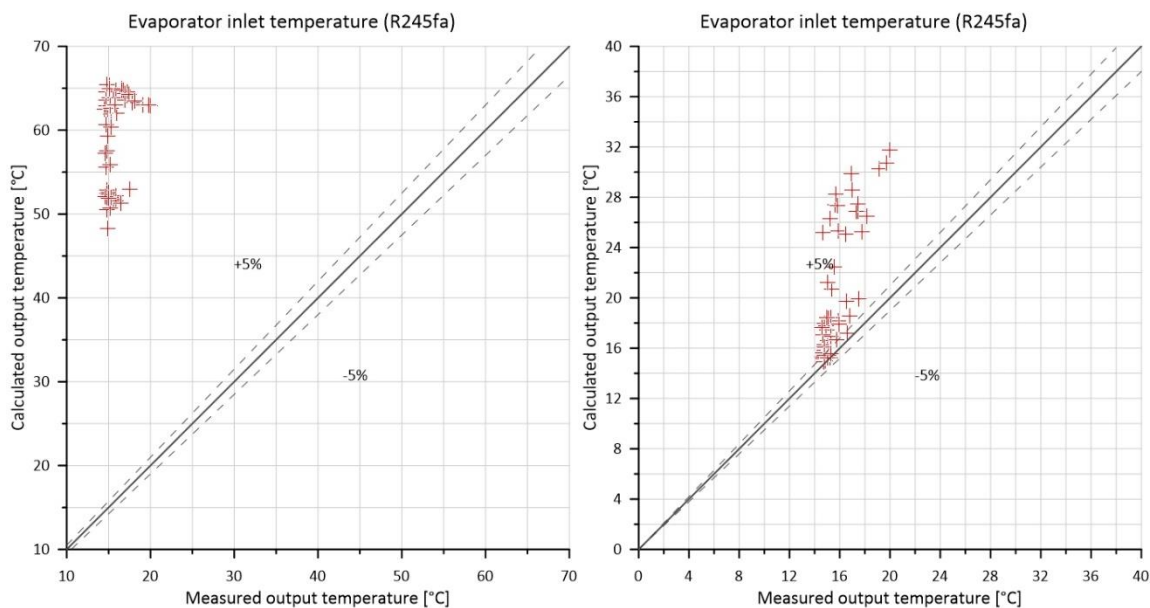


Fig. 7.3-1 - Temperature evaporator inlet hybrid plant error trend: left->not optimized , right->optimized

- TEMPERATURE OF R245FA AT THE EVAPORATOR OULET

EXPERIMENTAL (REFERENCE)	FULL MAP-BASED	HYBRID NOT OPTIMIZED	HYBRID OPTIMIZED
0%	1,7%	39,5%	1,3%

Table 7.3-3 - Temperature evaporator outlet comparison between experimental, map-based, hybrid not optimized and hybrid optimized plants

Hybrid plant: physical-based evaporator and condenser in map-based plant

Graphically the error comparison between the hybrid not optimized and the optimized plants is:

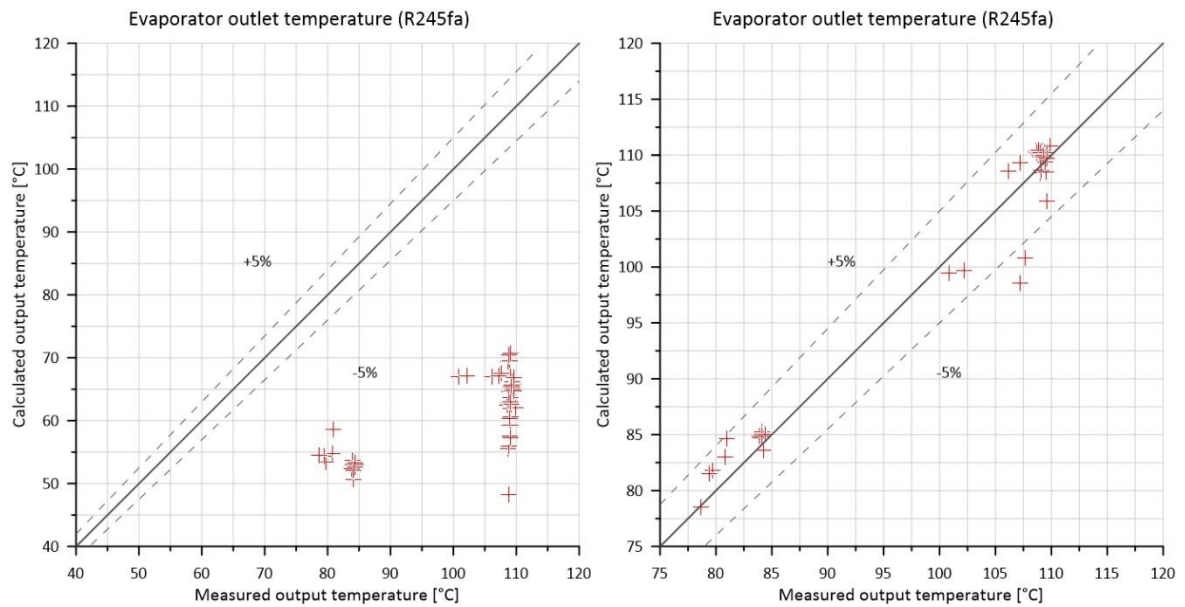


Fig. 7.3-2 - Temperature evaporator outlet hybrid plant error trend: left->not optimized , right->optimized

- PRESSURE OF R245FA AT THE EVAPORATOR OUTLET

EXPERIMENTAL (REFERENCE)	FULL MAP-BASED	HYBRID NOT OPTIMIZED	HYBRID OPTIMIZED
0%	1,7%	40,8%	3,1%

Table 7.3-4 - Pressure evaporator outlet comparison between experimental, map-based, hybrid not optimized and hybrid optimized plants

## Hybrid plant: physical-based evaporator and condenser in map-based plant

Graphically the error comparison between the hybrid not optimized and the optimized plants is:

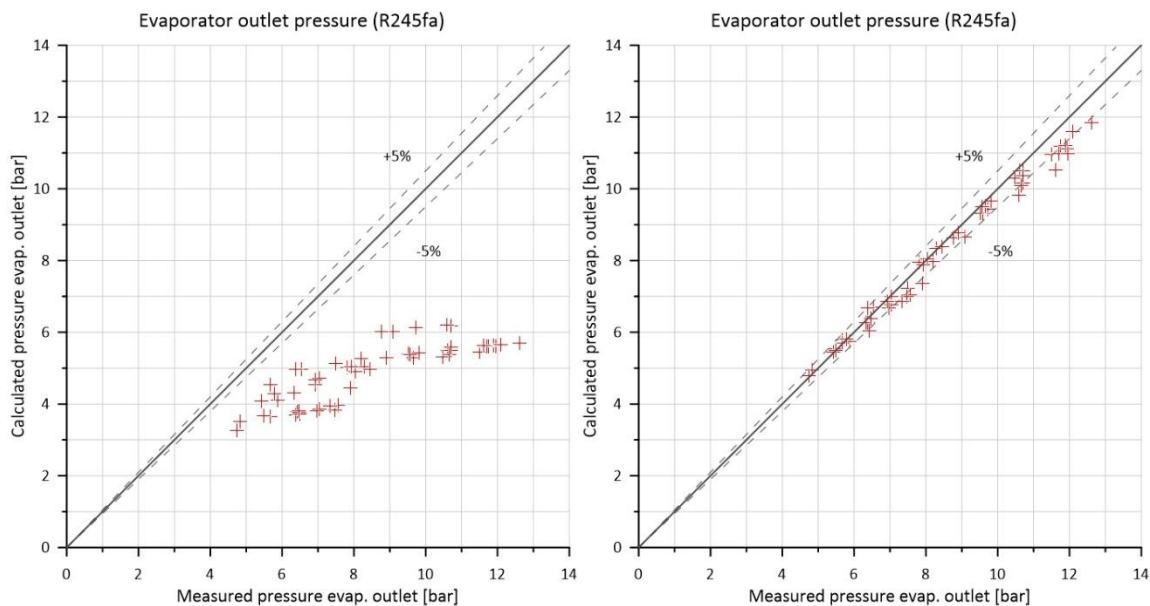


Fig. 7.3-3 - Pressure evaporator outlet hybrid plant error trend: left->not optimized , right->optimized

- GAS FRACTION OF R245FA AT THE EVAPORATOR OUTLET**

EXPERIMENTAL (REFERENCE)	FULL MAP-BASED	HYBRID NOT OPTIMIZED	HYBRID OPTIMIZED
0%	0%	47,5%	0%

Table 7.3-5 – Gas fraction evaporator outlet comparison between experimental, map-based, hybrid not optimized and hybrid optimized plants

Graphically the trend comparison between the hybrid not optimized and the optimized plants is:

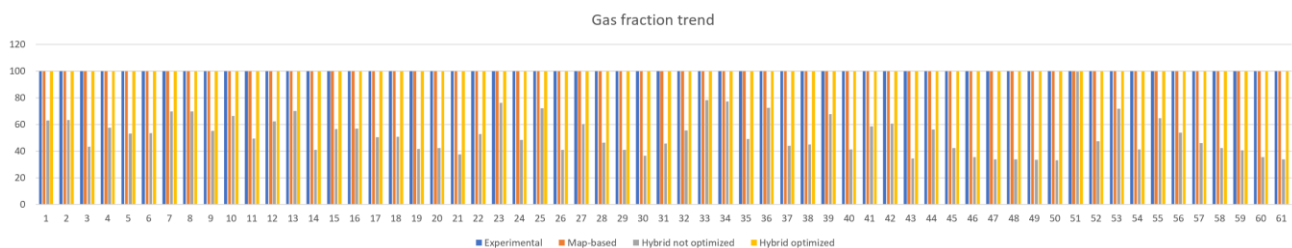


Fig. 7.3-4 – Gas fraction comparison between experimental, full map-based, hybrid not optimized and hybrid optimized

Hybrid plant: physical-based evaporator and condenser in map-based plant

- TEMPERATURE OF R245FA AT THE CONDENSER INLET

EXPERIMENTAL (REFERENCE)	FULL MAP-BASED	HYBRID NOT OPTIMIZED	HYBRID OPTIMIZED
0%	3,0%	20,0%	2,5%

Table 7.3-6 – Temperature condenser inlet comparison between experimental, map-based, hybrid not optimized and hybrid optimized plants

Graphically the error comparison between the hybrid not optimized and the optimized plants is:

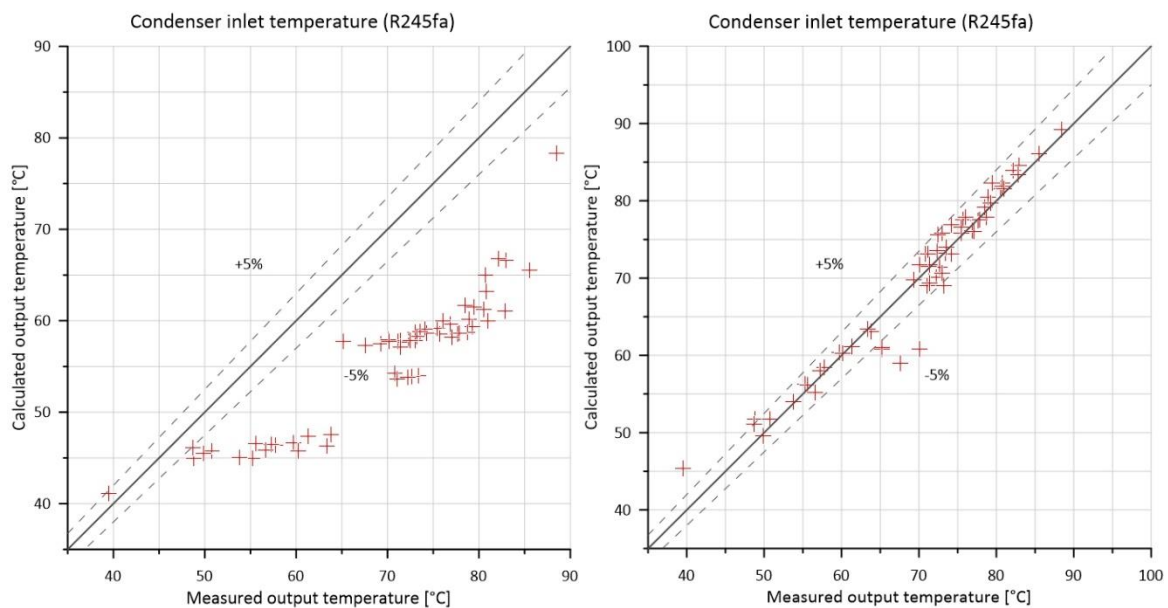


Fig. 7.3-5 - Temperature condenser inlet hybrid plant error trend: left->not optimized , right->optimized

- TEMPERATURE OF R245 AT THE CONDENSER OUTLET

EXPERIMENTAL (REFERENCE)	FULL MAP-BASED	HYBRID NOT OPTIMIZED	HYBRID OPTIMIZED
0%	15,8%	236,7%	15,7%

Table 7.3-7 - Temperature condenser outlet comparison between experimental, map-based, hybrid not optimized and hybrid optimized plants

# Hybrid plant: physical-based evaporator and condenser in map-based plant

Graphically the error comparison between the hybrid not optimized and the optimized plants is:

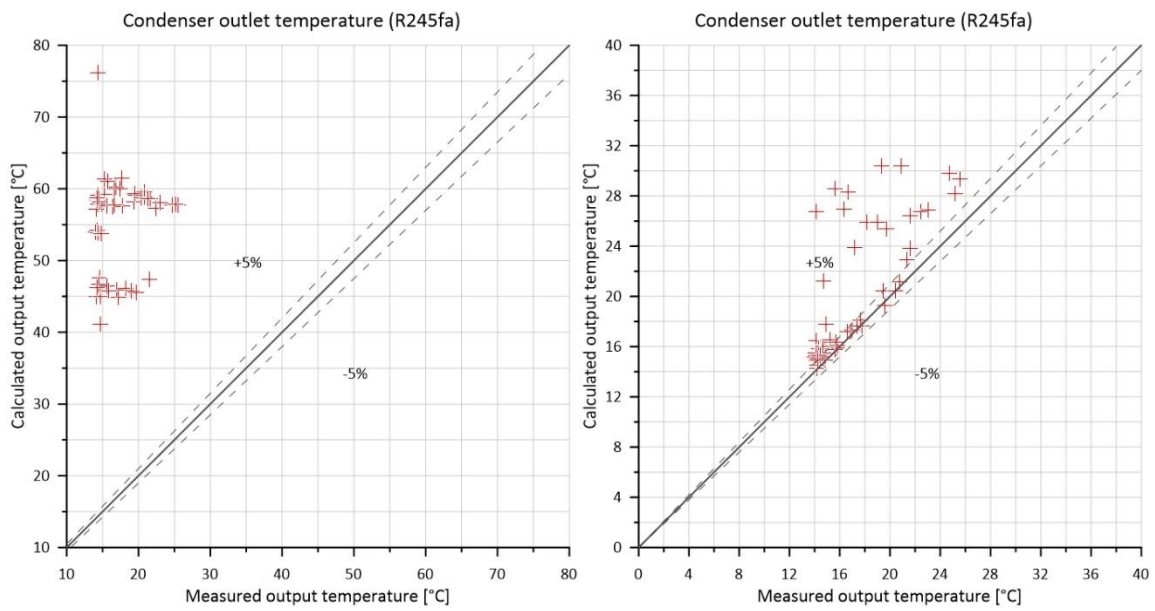


Fig. 7.3-6 - Temperature condenser outlet hybrid plant error trend: left->not optimized , right->optimized

Hybrid plant: physical-based evaporator and condenser in map-based plant

- POWER PRODUCED BY THE EXPANDER

EXPERIMENTAL (REFERENCE)	FULL MAP-BASED	HYBRID NOT OPTIMIZED	HYBRID OPTIMIZED
0%	4,3%	156,7%	4,9%

Table 7.3-8 – Power produced by the expander comparison between experimental, map-based, hybrid not optimized and hybrid optimized plants

Graphically the error comparison between the hybrid not optimized and the optimized plants is:

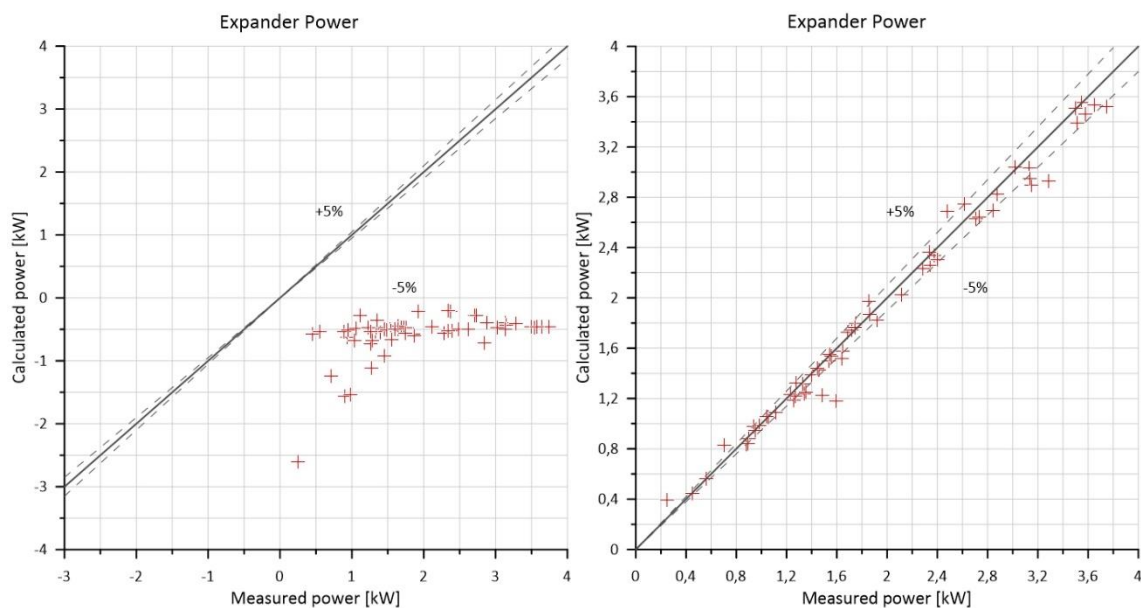


Fig. 7.3-7 – Power produced by expander hybrid plant error trend: left->not optimized , right->optimized

- AVERAGE MEAN RELATIVE PERCENTAE ERROR

The formula for its calculation is:

$$average_{MRPE} = \frac{\sum \text{all MRPE view in previous points}}{7}$$

Equation 50

<i>average</i> <sub>MRPE</sub> EXPERIMENTAL (REFERENCE)	<i>average</i> <sub>MRPE</sub> FULL MAP-BASED	<i>average</i> <sub>MRPE</sub> HYBRID NOT- OPTIMIZED	<i>average</i> <sub>MRPE</sub> HYBRID OPTIMIZED
0%	7,2%	117,6%	7,5%

Table 7.3-9 - *average*<sub>MRPE</sub> comparison between experimental, map-based, hybrid not optimized and hybrid optimized plants

## 7.4 Conclusions about optimization

The first consideration that can be made is to note how the mean relative percentage errors and the average of the mean relative percentage errors decrease drastically thanks to the optimization, passing, for some parameters, from values above 100% to values close to, or inside, the validation range. As it is possible to see, the hybrid map-based with physical-based condenser and evaporator has a quite identical  $average_{MRPE}$  value respect to the full-map based plant value.

The two values of the hybrid optimized plant that most differ from the validation range of  $\pm 5\%$ , are the temperature of R245fa at the output of the condenser and the temperature of R245fa at the inlet of the evaporator. However, going into a more in-depth analysis, it can be observed how the deviation occurs due to a restricted group of parameters that cause very high errors, a group quite identical for both parameters, influencing and significantly increasing the final value for the two temperatures' mean relative percentage errors. Furthermore, the same problem occurs identically even in the case of the full-map based plant, for the same parameters. In fact, trying to eliminate this group of parameters, it was possible to observe a significant decrease in the both mean relative percentage errors of the two variables and the, consequently, on the final  $average_{MRPE}$  one.

The deduction that it was possible to arrive at, was that probably there was an error in the measurements of the experimental values belonging to that group, which went to have a chain effect on the calculation of all errors.

For the remaining considered parameters, it is possible to note how their improvement thanks to the optimization, makes them fall inside the validation range of  $\pm 5\%$ .

Despite therefore, some mean percentage relative errors do not fall inside the validation range, as well as the  $average_{MRPE}$ , it is possible to state, as for the full map-based plant, that the hybrid map-based with physical-based condenser and evaporator optimized plant is calibrated and validated, because the error outside the range is due to an experimental measurement error and not a simulation of the virtual model one.

## 8 Final conclusions and future implementations

The work carried out in this thesis has made to implement and calibrate, also thanks to the final multi-object multi-objective optimization, a virtual condenser and evaporator models that can be considered validated, that means that represent, in a sufficiently accurate way, the trend of the respective real brazed plate heat exchangers inside the considered ORC power plant.

The obtained results, in fact, considering all the approximations made, especially for the one-dimensional model, can be considered more than satisfactory, however the hybrid model of map-based plant with physical-based condenser and evaporator still has ample room for improvement and possible implementations.

Recalling what was said in the introduction, the ultimate purpose of develop a validated physical-based virtual models of heat exchangers, was to have a virtual models that were independent from the geometry, in order to be able to couple the ORC plant within they are used, with an internal combustion engine, to increase its efficiency, of various size and powers, adapting only the geometry and characteristics, but being able to have a model whose simulations resulted in sufficiently accurate results of a possible real application.

The first possible implementation can be to build the remaining components of the ORC plant in which the just constructed physical-based heat exchanger are inserted as condenser and evaporator, from a map-based models to a physical-based models. In fact, for the moment, the plant that was defended as hybrid and it is still bonded to the geometry and power constrains, due to the rest of components based on map construction. An eventually, full physical-based plant model, which corresponds to all components based on a physical construction, would allow to achieve the final purpose mentioned above.

The second possible future development, once the full physical-based ORC plant has been completed, calibrated and validated, can be to couple it to a calibrated and validated model of internal combustion engine to study the power produced by the expander and so analyze the achievable efficiency increasing. To this development can be added the study of the power produced and the increase in efficiency for some automotive homologation cycles as WLTP or NEDC.

Possibly the coupling could be also made, in addition to the one with internal combustion engine for private cars or heavy load transport, with internal combustion engine used on large ships,

## Final conclusions and future implementations

appropriately scaling the various components of the plant, once that this one has been released from the geometric and power constraints present in the map-based virtual model.

The last possible implementation is the construction and validation of the model from one-dimensional to three-dimensional physics, which can be done, for example, as a last development once a specific application has been found and has obtained satisfactory results from the simulations of one-dimensional model, in order to have more accurate simulations that take into account thermodynamic and fluidodynamic aspects impossible to consider in one-dimensional analysis, such as the turbulence of the operating fluids during their flow inside the components or radiation heat transfer phenomena.

As just described, the implementation possibilities are many and the developed physical-based heat exchanger virtual models can be used as the beginning of a line of research on the implementation of recovery systems based on the Organic Rankine Cycle.

## 9 Appendix

	HTM EVAP. HOT TO PLATE	HTM EVAP. PLATE TO COLD	HTM COND. HOT TO PLATE	HTM COND. PLATE TO COLD
<b>SOBOL</b>	1,0000000000000	1,0000000000000	1,0000000000000	1,0000000000000
<b>SOBOL</b>	37,7500000000000	37,7500000000000	13,2500000000000	37,7500000000000
<b>SOBOL</b>	13,2500000000000	13,2500000000000	37,7500000000000	13,2500000000000
<b>SOBOL</b>	7,1250000000000	19,3750000000000	43,8750000000000	43,8750000000000
<b>SOBOL</b>	31,6250000000000	43,8750000000000	19,3750000000000	19,3750000000000
<b>SOBOL</b>	19,3750000000000	7,1250000000000	7,1250000000000	31,6250000000000
<b>SOBOL</b>	43,8750000000000	31,6250000000000	31,6250000000000	7,1250000000000
<b>SOBOL</b>	22,4375000000000	46,9375000000000	34,6875000000000	40,8125000000000
<b>SOBOL</b>	46,9375000000000	22,4375000000000	10,1875000000000	16,3125000000000
<b>SOBOL</b>	10,1875000000000	34,6875000000000	22,4375000000000	28,5625000000000
<b>LHMC</b>	1,6778174902090	26,7819312795083	18,4746425318871	30,6792281475585
<b>LHMC</b>	1,8317010544940	24,5519215516791	5,6521651819394	27,1761577768758
<b>LHMC</b>	1,5048757584434	31,4246977524986	16,7249879037322	48,5144654470916
<b>LHMC</b>	1,3580872780910	22,4865992768405	10,4664009985686	35,2134490333604
<b>LHMC</b>	1,5602989992253	38,8057504371513	17,0542063676303	14,2049711269484
<b>LHMC</b>	1,6045868071777	1,1811526884669	21,3255076008595	24,3933734381132
<b>LHMC</b>	1,4072708034051	19,6704811940572	13,6728287543145	21,2911975520584
<b>LHMC</b>	1,4729417660305	15,4875697411897	14,8473415508688	17,9096676230278
<b>LHMC</b>	1,0404772775302	28,6210273247592	23,1123366250605	28,8710002361415
<b>LHMC</b>	1,4491583595074	33,9609717566624	12,6898395526566	20,7119205109968
<b>RNDDOE</b>	11,1780272241761	17,3031357420160	36,8130313444613	21,0939597631179
<b>RNDDOE</b>	48,2215350541372	47,0534040503136	48,4200395617819	1,2997419310223
<b>RNDDOE</b>	20,4615427670506	18,0283834309524	47,4125509654965	46,9170252959025
<b>RNDDOE</b>	6,6823873136002	38,7562581238797	15,4087945681978	25,8176977389855
<b>RNDDOE</b>	19,5319002207317	7,8483714622838	33,3347427259776	8,6805976379225
<b>RNDDOE</b>	1,2462336236302	26,6336226336283	35,0524510005221	40,4561608022120
<b>RNDDOE</b>	24,6046867772043	27,6831856357900	37,4552398256285	7,9591124575804
<b>RNDDOE</b>	31,5448267209516	10,0506474236195	29,2779128073395	11,0407637421695
<b>RNDDOE</b>	9,7246874852216	27,4794561744060	1,5235361381292	8,8911228452134
<b>RNDDOE</b>	20,3315244084169	11,6625041204766	48,7178664860163	13,0259011254835

*Table 9-1 – SpaceFiller multi-objective multi-object optimization*

Appendix

	TEMP. R245FA EVAPORATOR INLET [°C]	TEMP. R245FA EVAPORATOR OUTLET [°C]	PRESS. R245FA EVAPORATOR OUTLET [KPA]	GAS FRACTION % R245FA EVAPORATOR OUTLET	TEMP. R245FA CONDENSER INLET [°C]	TEMP. R245FA CONDENSER OUTLET [°C]	POWER PRODUCED BY EXPANDER [KW]
1	14,94	108,72	901,39	100	70,82	14,21	1,398
2	14,75	108,9	872,81	100	73,41	14,06	1,33
3	14,77	80,97	785,23	100	39,53	14,74	1,055
4	14,85	108,99	969,02	100	72,7	14,3	1,536
5	14,82	108,78	1064,09	100	71,09	14,79	1,689
6	15,07	109,14	1054,95	100	72,26	14,82	1,718
7	14,91	108,67	651,85	100	75,7	14,23	1,339
8	14,56	108,6	634,42	100	77,65	13,98	1,233
9	14,76	84,04	637,96	100	55,27	14,12	1,114
10	14,76	109,06	745,07	100	74,24	14,12	1,649
11	14,83	83,97	699,65	100	53,81	14,68	1,352
12	14,68	108,89	815,9	100	73,01	14,3	1,92
13	14,7	108,89	778,34	100	75,53	14,38	1,751
14	15,56	80,79	753,29	100	48,82	17,21	1,543
15	15,08	109,06	957,51	100	71,17	15,76	2,374
16	14,81	109,39	947,11	100	72,32	14,3	2,342
17	15,86	109,24	1058,52	100	71,29	17,77	2,709
18	15,12	109,42	1067,51	100	71,42	14,89	2,734
19	14,66	108,98	1173,46	100	71,43	14,16	2,874
20	15,63	109,09	1187,16	100	69,28	16,35	3,132
21	17,79	107,66	1261,26	100	67,59	22,43	3,286
22	14,74	83,94	543,66	100	57,73	14,08	0,938
23	14,85	108,81	563,65	100	80,51	14,22	1,041
24	14,99	83,88	633,49	100	55,59	14,7	1,257
25	14,67	109,13	701,05	100	78,48	14,45	1,558
26	15,9	79,72	745,57	100	48,73	18,18	1,642
27	14,74	109,2	826,73	100	75,48	15,25	2,113
28	16,56	109,45	1048,2	100	74,14	19,58	2,844
29	17,43	109,5	1147,98	100	72,99	21,6	3,146
30	15,83	79,42	731,44	100	50,73	18,99	1,458
31	16,77	109,18	965,6	100	76,85	20,79	2,4
32	15,22	84,1	477,12	100	63,83	14,58	0,448
33	14,71	108,73	507,69	100	82,91	14,16	0,901
34	15,24	108,88	584,66	100	82,18	14,63	0,984
35	14,77	84,14	562,63	100	59,7	14,44	0,877
36	14,79	108,92	630,48	100	80,76	14,48	1,27
37	17,53	84,51	643,94	100	61,33	21,58	0,89
38	15,03	84,39	645,7	100	57,28	15,61	1,267
39	14,94	109,13	687,51	100	80,77	15,26	1,448
40	15,34	84,29	695,73	100	56,62	17,02	1,487
41	15,31	109,07	798,72	100	78,95	16,86	1,854

Appendix

42	15,94	109,88	800,68	100	79,43	17,65	1,864
43	16,5	78,64	730,54	100	49,87	19,73	1,597
44	15,31	109,25	838,78	100	76,03	16,6	2,283
45	17,29	109,43	1052,82	100	73,56	20,88	3,134
46	16,91	109,59	1170,04	100	73,19	19,32	3,545
47	19,11	107,22	1156,17	100	70,12	24,72	3,647
48	15,24	106,2	1194,33	100	70,13	15,6	3,511
49	15,72	100,85	1206,79	100	65,22	16,68	3,498
50	19,97	102,17	1207,75	100	65,2	25,55	3,746
51	14,95	108,85	469,09	100	88,47	14,32	0,248
52	14,62	84,13	547,26	100	63,38	14,29	0,559
53	14,58	109,03	575,12	100	85,57	14,26	0,707
54	15,03	84,39	645,79	100	60,2	15,83	0,949
55	15,28	109,02	688,88	100	82,85	15,71	1,279
56	15,77	109,16	792,15	100	80,95	17,39	1,744
57	16,61	109,6	889,59	100	79,27	19,48	2,337
58	16,98	109,33	954,26	100	78,77	20,44	2,482
59	17,46	109,29	982,99	100	77,89	21,33	2,617
60	18,17	109,64	1070,36	100	77,06	23,04	3,022
61	19,75	107,22	1162,64	100	72,48	25,17	3,578

Table 9-2 – Experimental collected data

## Bibliography

- [1] F. Millo, «Lezioni di Propulsori Termici,» Torino, A.A. 2019-2020.
- [2] C. D. Charles Sprouse III, «Review of organic Rankine cycles for internal combustion engine» *Applied Thermal Engineering*, vol. 51, pp. 711-722, 2013.
- [3] «Wikipedia» [Online]: Rankine Cycle. Available: [https://en.wikipedia.org/wiki/Rankine\\_Cycle](https://en.wikipedia.org/wiki/Rankine_Cycle).
- [4] «Wikipedia» [Online]: Organic Rankine Cycle. Available: [https://en.wikipedia.org/wiki/Organic\\_Rankine\\_cycle](https://en.wikipedia.org/wiki/Organic_Rankine_cycle).
- [5] «Wikipedia» [Online]: Heat Transfer Coefficient. Available: [https://en.wikipedia.org/wiki/Heat\\_transfer\\_coefficient](https://en.wikipedia.org/wiki/Heat_transfer_coefficient).
- [6] «Wikipedia» [Online]: Ottimo paretiano. Available: [https://it.wikipedia.org/wiki/Ottimo\\_paretiano](https://it.wikipedia.org/wiki/Ottimo_paretiano).
- [7] B. F. Tchanche, G. Lambrinos, A. Frangoudakis, G. Papadakis Low-grade heat conversion into power using organic Rankine cycles - A review of various applications., *Renewable and Sustainable Energy Reviews*, 15: 3963-3979, 2011.
- [8] J. Bao and L. Zhao, "A review of working fluid and expander selections for organic Rankine cycle," *Renew. Sustain. Energy Rev.*, vol. 24, pp. 325– 342, 2013.
- [9] «techweb.rohm.com» [Online]: Fundamentals of Thermal Resistance and Heat Dissipation: Thermal Resistance in Convection. Available: <https://techweb.rohm.com/knowledge/thermal-design/s-thermal-design/01-s-thermal-design/9554>
- [10] «web.mit.edu» [Online]: 17.2 Combined conduction and Convection. Available: <https://web.mit.edu/16.unified/www/FALL/thermodynamics/notes/node123.html>
- [11] «sciencedirect.com» [Online]: design and testing of the Organic Rankine Cycle. Available: <https://www.sciencedirect.com/science/article/abs/pii/S0360544200000633>
- [12] «sciencedirect.com» [Online]: Experimental Study of R245fa Condensation Heat Transfer Properties in Horizontal Tube. Available: <https://www.sciencedirect.com/science/article/pii/S1876610216316290>
- [13] «researchgate.net» [Online]: Properties of HFC-245fa. Available: [https://www.researchgate.net/figure/R245fa-properties-11\\_tbl1\\_260791538](https://www.researchgate.net/figure/R245fa-properties-11_tbl1_260791538)
- [14] «caeconference.com» [Online]: Implementazione di una metodologia di ottimizzazione per la riduzione delle perdite nelle reti di distribuzione idrica. Available: [https://www.caeconference.com/proceedings/abstract/abstract\\_07/uni\\_roma.html](https://www.caeconference.com/proceedings/abstract/abstract_07/uni_roma.html)